A DISCONTINUOUS GALERKIN METHOD FOR STRAIN GRADIENT PLASTICITY

by

Jakob T. Ostien

A dissertation submitted in partial fulfillment
of the requirements for the degree of
Doctor of Philosophy
(Mechanical Engineering and Scientific Computing)
in The University of Michigan
2009

Doctoral Committee:

Associate Professor Krishnakumar R. Garikipati, Chair
Professor Gregory M. Hulbert
Professor Peter S. Smereka
Assistant Professor Samantha H. Daly

"As far as the laws of mathematics refer to reality, they are not certain, and as far as they are certain, they do not refer to reality."

— Albert Einstein

" 'cuz I did!"

— Diego Sy

ACKNOWLEDGEMENTS

As I began the search for an advisor, colleagues of mine at Sandia National Labs "highly recommended" Professor Krishna Garikipati, due in part to his knowledge of mathematics and mechanics, but also to his generally personable disposition. Even so, my interaction with Krishna far surpassed any expectations, and for that reason I must devote my most sincere thanks to him for his patience and willingness to take on the hard timeline associated with my Sandia funded Doctoral Studies Program. I fully expect constructive collaboration moving forward.

Motivation for the attempt to return to school, family in tow, can be attributed to Dr. Doug Bammann, who opened my eyes to not only plasticity, but the love for the mathematics behind it, and Dr. Joe Jung, who convinced me that this opportunity was far too good to pass up. Dr. John Pott also deserves special recognition for his role, without his help and support none of this would have been possible.

I have interacted with some incredible people along the way. With great respect and thanks I'd like to acknowledge the following for hot chocolates, pints of ale, and stimulating conversation. In no particular order: Dr. Harish Narayanan, Krishna Siva Shankar Rudraraju, Kristian Ølgaard, and Devin O'Connor. I am particularly indebted to Dr. Bill Scherzinger and Dr. Arne Gullerud for keeping things in perspective for me.

Thank you to my parents, Nancy and Ted, who have somehow also been able to

trick me into believing that I am much more competent and intelligent than reality dictates. Also, thanks to Jean and Matt, for gracious hospitality and telling me what I needed to hear.

And by far the most important, I'd like to acknowledge that absolutely no one has agonized over the past three years more than my wife, Erin. I cannot imagine what adventurous path life will take us down after this, but I am glad that we will be travelling together.

TABLE OF CONTENTS

LIST OF FIGURES

Figure

LIST OF TABLES

Table

LIST OF ALGORITHMS

Algorithms

LIST OF APPENDICES

Appendix

CHAPTER 1

Introduction

The purpose of this dissertation is to present a numerical method for solving the partial differential equations that arise from a variationally-derived model of gradient plasticity. The main focus of the work is the employment of discontinuous Galerkin finite element principles to alleviate the strict continuity requirements that arise from the classical statement of the gradient plasticity problem in weak form. The model of gradient plasticity chosen for this work is physically motivated by considering the incompatibilities brought about by plastic deformation at the microscopic scale, and manipulated via Stokes' Theorem to obtain a continuum, tensorial treatment. Integration algorithms resembling those from the nonlinear classical theory of plasticity are used to solve a pair of partial differential equations that amount to the macroscopic and microscopic equations of equilibrium. Some numerical examples are used to demonstrate properties of the model and the method.

The novel contribution of this dissertation is the use of discontinuous Galerkin concepts in the formulation of the incompatibility based gradient plasticity theory. Algorithms for approximating the back-stress term in the yield condition are investigated, as well as integration algorithms for the mixed method.

This initial chapter provides some context for this work (Section 1.1) and an overview of the topics considered in the remainder of the dissertation (Section 1.2).

1.1 Background

The theory of *plasticity* covers the response of materials that have experienced loads exceeding their elastic limit, or outside of the realm in which the material can be expected to fully recover to its original configuration. The material retains a permanent distortion by some measure, and this distortion is governed by an irreversible, or dissipative, process. The physics underlying plastic deformation on a microscopic scale dictates the mechanical behavior of a material at the macroscopic scale, but is generally too complex to be modeled directly, and therefore phenomenological models are usually employed.

The history of the theory of plasticity began with attempts to describe the permanent deformation observed in metals that had experienced loads exceeding their elastic limit. Metals are generally polycrystalline materials, and at a microscopic scale plastic deformation results in changes at the scale of the crystal lattice. A number of useful texts have been written on the subject including Hill (1950), Kachanov (1971), and Lubliner (1990). Plastic deformation in metals is observed to be *isochoric*, or volume preserving. It follows that the deviatoric stress is responsible for driving plastic flow in metals, since it does not cause a volume change. Classical J_2 flow theory is named for its explicit relation to the second invariant of the deviatoric stress.

Computationally, the increased availability of computing resources and development of the finite element method for nonlinear problems allowed for the parallel development of the computational formulation of plasticity. Standard texts for the finite element method include Hughes (1987) and Zienkiewicz and Taylor (1989). Of utmost importance was the development of numerical integration schemes for clas-

sical plasticity, such as early work based on the radial return algorithm for perfect plasticity presented in Wilkins (1963). Extensions for hardening and finite strain for the radial return algorithm came in Krieg and Key (1976) and Key and Krieg (1982). Significant generalization of those ideas were presented in Ortiz and Simo (1986), Simo (1988a), Simo (1988b), and Simo (1992) where *return mapping* algorithms were introduced and analyzed in the context of hyperelasticity, multiplicative plasticity, and non-associative flow laws. Comprehensive references for the formulation and implementation of integration algorithms for inelastic constitutive equations can be found in Simo (1998) and Simo and Hughes (1998).

Gradient plasticity builds upon the classical theory of plasticity by introducing fields within the constitutive theory that are themselves, in some manner, gradients of strains. The motivation behind these additions are the inability of the classical theory to account for such phenomena as *size effects* and *softening* pathologies. Size effects are observed as a dependence of the plastic flow stress on a characteristic dimension of the specimen. Softening is an observed decrease in strength of a material for a given strain increment. Softening produces pathological mesh dependent behavior, which is a manifestation of the non-uniqueness of the solution when softening moduli are present, as the boundary value problem is ill-posed. Treatments for size effects and softening can come from adding a length scale to the continuum formulation, as in a gradient theory, or via numerical treatments, for example in a nonlocal damage theory.

In Coleman and Hodgdon (1985) the authors are motivated by the observations of adiabatic shear bands in metals and the softening of geological materials due to the accumulation of damage. In an analysis of shear bands, they propose including a term that accounts for the spatial derivative of the accumulated shear strain in

the evaluation of the stress field. In the generalization to three dimensions, the term becomes the Laplacian of the (scalar) accumulated distortion. It should be noted that the authors make a point of proclaiming the model is constructed to produce solutions similar to the observed behavior of some materials, and not motivated by first principles.

Aifantis undertakes a physically motivated exploration of dislocation phenomena, including the transition from micro-scale behaviors to the macro-scale, physically based finite deformation continuum theories, and applications of the theory to localization problems (Aifantis, 1987). The author introduces second gradients of the (scalar) equivalent plastic strain, similar to the work of Coleman and Hodgdon, that serve to regularize the solution of softening boundary value problems. In Muhlhaus and Aifantis (1991), a variational statement is presented that incorporates the Laplacian of the plastic consistency parameter. The weak form of the statement then requires the same interpolation functions for both the displacements and the plastic parameter, but introduces the need for boundary conditions related to the plastic fields.

The authors in Fleck and Hutchinson (1993) and Fleck et al. (1994) attempt a physical derivation of a gradient plasticity model with the intention of predicting size effects in materials. Motivated by a description of geometrically necessary dislocations in areas of a body with a gradient in strain, they incorporate the Cosserat couple stress theory to construct a constitutive model that depends both on the strain and the gradient of the strain. The model accounts for the accumulation of geometrically necessary dislocations in areas of intense strain gradients, and the authors use the model to explain observations of gradient dependent hardening in a series of torsion tests on wire with diameters ranging from 12 to 170 μm.

In Nix and Gao (1998), Gao et al. (1999), and Huang et al. (2000) the authors propose a theory of mechanism based strain gradient plasticity. The authors are motivated to resolve the observation in indentation experiments that the hardening response for a material increases as the size of the indenter decreases. The presumably occurs due to the strong gradient in the localization zone adjacent to the indenter. Again, the authors aim to account for the effective density of geometrically necessary dislocations that arise due to strong gradients. To accomplish this they introduce the concept of a dislocation density tensor, which is then used in the construction of the (continuum) theory.

In Cermelli and Gurtin (2001) the authors formally develop the notion of the Burger's tensor, including a thorough review of the many forms a dislocation based tensor has taken in the literature. Using that concept Gurtin (2004) and Gurtin (2005) employ a *micro force balance* to derive balance laws for plastically deforming materials that account for gradient effects via the dislocation tensor. It is upon these theories that the model presented in this dissertation will be built.

Other approaches for introducing length scales, motivated by localization phenomena in geological materials, are the *nonlocal* theories, where spatial dependence of the local quantities is achieved via sampling fields within a finite radius. Typically the nonlocal theories are concerned with the spatial dependence of damage, or the accumulated degradation of a material with strain, as in Bazant et al. (1984) and Bazant and Pijaudier-Cabot (1988). The length scale that is introduced is essentially the radius by which the damage field is integrated within, as the integration of damage dictates the width of shear bands in softening materials.

Experiments have been conducted with the expectation that at small enough scales, the micromechanics provided by dislocation theory will dominate the behav-

ior. Notably, in Fleck and Hutchinson (1993) microtorsion experiments are presented and compared with microtension experiments. The torsion experiments exhibit a marked dependence on the diameter of the copper wire, indicating a strong constitutive dependence on the gradient of the strain, while the tension experiments show an insignificant dependence on wire diameter. In Stölken and Evans (1998) the authors develop a microbending test to determine the gradient dependence of very thin foils of high purity nickel. The test method measures the deformed radius of curvature of an elastically unloaded foil. The results show that for a given surface strain, the applied bending moment increased noticeably as the thickness of the foil decreased, giving further credence to the notion of a size effect for plasticity at small scales. In Ma and Clarke (1995) the authors show that measured hardness for silver single crystals is also dependent on the size of the indentation. As the indenter sized decreased, especially below 10 μm, the measured hardness increased.

Each of the preceding gradient plasticity theories includes higher order terms associated with the newly introduced gradient dependence. For example, the theory from Fleck and Hutchinson includes a third-order stress term when the displacements are the only primal fields. Gurtin presents a model where an additional second-order stress term is included. With the introduction of higher order gradients within weak form of the plastic constitutive theory, usually in the form of partial differential equations, higher-order boundary conditions become necessary. Physically based notions of these boundary conditions have remained elusive, and in many cases are not discussed beyond the acknowledgement that they exist. More stringent continuity requirements also arise directly from the additional spatial derivatives found in gradient theories, specifically to address the additional boundary conditions. Additional requirements limit or eliminate the use of classical numerical techniques for these

higher-order theories.

The solution of higher-order theories by the finite element method involves employing some mechanism of achieving higher-order continuity of the basis functions in the weak form. In particular, for fourth order theories assuming a displacement based formulation, after repeated integration by parts, continuity requirements dictate that the solution basis functions be $\mathscr{C}^1$, which means that both the solution and its first derivative are continuous. Constructing $\mathscr{C}^1$ continuous basis functions in three dimensions is reported as anything from very complicated to intractable in the literature. An alternative approach is the introduction of another field, usually representative of the gradient of the original field, which allows the relaxation of the continuity requirements. Again, for a fourth-order theory each field would need $\mathscr{C}^0$ continuity. These *mixed methods*, unfortunately inherit additional stability requirements. As pointed out in Brezzi (1990), applicability of mixed methods is determined via mathematical analysis, which is generally a non-trivial task. Furthermore, stability will depend on the specific interpolations chosen for each field, with the unsettling result that some combinations of basis functions work, while others do not.

Discontinuous Galerkin (DG) methods are formulations in which the weak form is written to include integrals across inter-element interfaces. In the context of elliptic problems the fluxes that appear across the interfaces are approximated by so-called *numerical fluxes*. These numerical fluxes can be used to capture discontinuities in fields or manipulated in other ways to approximate derivatives in a distributional sense, in effect achieving an approximation of greater continuity. DG methods started appearing in the literature in the early 1970s. Reed and Hill (1973) developed a DG method to solve the hyperbolic neutron transport equations, but the methods were also being developed for elliptic problems. Nitsche (1971) proposed an early

symmetric and consistent method for elliptic problems that used an *interior penalty*, and more recently Bassi and Rebay (1997) applied DG methods to the Navier-Stokes equations by introducing a term later denoted as the *lifting operator*. Arnold et al. (2002) presented a unifying analysis of methods for elliptic problems.

Discontinuous Galerkin methods have become attractive in view of the difficulties associated with higher-order partial differential or differential-algebraic equations, including the need for $\mathscr{C}^1$-continuous elements. Discontinuous Galerkin based $\mathscr{C}^0$ finite element basis functions were developed for fourth-order elliptic problems related to thin beam and plate theory and gradient elasticity in Engel et al. (2002). The proposed methods used concepts from both the continuous and discontinuous Galerkin as well as stabilization techniques where low-order polynomials were used and continuity requirements were weakly enforced via stabilization of interior facet terms. Wells et al. (2004) and Molari et al. (2006) discuss strain gradient damage. The fourth-order Cahn-Hilliard equation for phase segregation gets a treatment in Wells et al. (2006). DG formulations for Kirchoff-Love plates and shells are presented in Wells and Dung (2007) and Noels and Radovitzky (2008). Djoko et al. (2007a), Djoko et al. (2007b) and McBride (2008) present a DG formulation for a gradient plasticity model similar to that of Aifantis.

1.2 An Overview

Chapter 2 serves the purpose of providing an introduction to the field of classical plasticity, which for the duration of this dissertation will be set in the small strain setting. To accomplish this relevant results from continuum mechanics and classical elasticity are presented. Topics include kinematics, stress, balance laws, and elastic constitutive equations. Plasticity is introduced, including a definition of the

yield surface along with hardening laws and a derivation and discussion of the J_2 theory of plasticity. Ideas and an algorithm for computational plasticity follow the classical theory. The main focus of the section being the introduction of the finite element method and its concepts, and integrating those concepts with the theoretical ideas to arrive at numerical solution strategies for classical plasticity. Topics include variational formulations, isochoric solution strategies, and numerical integration algorithms including a discussion of a radial return algorithm for J_2 plasticity with isotropic and kinematic hardening. A select few numerical results for classical plasticity are then presented. Perfect plasticity and hardening are illustrated for a torsional problem along with the differences between isotropic and kinematic hardening in a cyclic loading problem. In addition, the well known pathological mesh dependence of the classical methods is illustrated for a strain localization problem when the material is softening.

Chapter 3 has an introduction to dislocations and a discussion of the role dislocation motion plays in plastic deformation. Crystal structure and slip systems are introduced as precursors to the notion of a dislocation. Edge and screw dislocations are discussed, and an example of dislocation motion is presented. Hardening mechanisms related to the generation and interaction of dislocations are also presented. Then, leading up to a gradient plasticity constitutive theory, the discrete notion of incompatibility in a crystal lattice, or the Burger's vector, is manipulated to arrive at a continuum, tensorial quantity called the Burger's tensor.

Chapter 4 uses the continuum concepts of Burger's vector presented in Chapter 3 and constructs a constitutive model with a gradient dependence on the plastic part of the displacement gradient. A free energy is chosen to incorporate conjugate pairs for the elastic and plastic displacement gradients, as well as the curl of the plastic

part of the displacement gradient. A microforce balance is then used to derive a pair of partial differential equations that govern the macroscopic balance of momenta, or equilibrium, and the microscopic balance of forces that can be interpreted as the flow rule for the plasticity model.

Chapter 5 introduces discontinuous Galerkin methods by presenting a derivation of a method that can be used for linear elasticity, which uses a *discontinuous* basis for the displacement field. The structure of the variational formulation is noted, and compared with other methods modeling higher order physics. The applicability of the DG method for gradient plasticity is stated, followed by a derivation of the variational statement of the coupled set of partial differential equations derived in Chapter 4. DG methods are used to weakly enforce the necessary continuity requirements of the plastic fields. An algorithm describing the implementation of the variational form into a nonlinear finite element code is presented and discussed.

Chapter 6 provides numerical results using the implementation of the variational formulation of gradient plasticity presented in this paper. To illustrate features of the model, a cylinder undergoing a torsional deformation, which results in gradients in the strain field, is simulated to produce the well established size effect for a plastically deforming material at small scales. A comparison is made then to a uniform stress field where gradient terms are shown to have no effect. Finally, a localization problem is solved and the solution is shown to have mesh independent behavior when a length scale is introduced via gradient terms in the plasticity model.

Chapter 7 consists of conclusions and final comments. Model strengths and weaknesses are discussed, including a brief discussion on the need for additional experimental results, as well as possible future directions for both the gradient plasticity model and DG methods.

CHAPTER 2

Classical Plasticity

The objective of this chapter is to present the ideas of classical plasticity from a theoretical and computation perspective, and then provide some numerical examples, in order to provide background for the gradient plasticity theory and implementation discussed later in this dissertation. Results from continuum mechanics are used to develop the theory, and a classical solution algorithm is presented. The numerical examples illustrate specific hardening and softening behavior for a selection of boundary value problems.

2.1 Classical Theoretical Plasticity

The classical theory of plasticity can be viewed as an extension of the theory of elasticity to account for nonlinear material behavior including permanent deformation. For this reason the underpinnings of the theory of plasticity rely heavily on the standard statements of elasticity, which in turn are based on the results of continuum mechanics. For the purpose of this dissertation, subsequent discussion will be restricted to the infinitesimal deformation theory.

2.1.1 Selected Results from Continuum Mechanics

Continuum mechanics is a classical subject with many modern applications ranging from biology to electromagnetics, and of course, elasticity and plasticity. It is a subset of the larger field of continuum theories. A number of texts exist on the

subject of continuum mechanics, including Truesdell and Noll (1965) and Malvern (1969), and more recently Holzapfel (2000) and Gurtin (2003). For a brief introduction to the subject of nonlinear continuum mechanics relevant to the work at hand, please consult Appendix A. The remainder of this section selects specific results from the general theory as the foundation for all subsequent developments.

Kinematics

The relevant results from the kinematics of linearized solid continua are the definition of the displacement and the strain. In the small strain theory, the difference between the reference and current configurations is assumed small, so henceforth the domain of interest will be referred to as Ω.[1] In words, the displacement, $\boldsymbol{u}$, is the departure of a material point, at current position $\boldsymbol{x}$, from its original position $\boldsymbol{X}$.

$$\boldsymbol{u} = \boldsymbol{x} - \boldsymbol{X} \tag{2.1}$$

The strain is a measure of the deformation the body has undergone, where deformation is regarded as relative motion between neighboring material points. This is distinct from the displacement, which includes both rigid translation and rotation, neither of which contribute to the deformation (rigid actually implying no deformation) and hence should not impact the strain. For the purposes of this dissertation, the infinitesimal strain tensor, $\boldsymbol{\varepsilon}$, is used and is defined as the symmetric part of the displacement gradient. For more details see Section A.1.

$$\boldsymbol{\varepsilon} = \frac{1}{2}(\boldsymbol{\nabla u} + (\boldsymbol{\nabla u})^{\mathrm{T}}) \tag{2.2}$$

Stress

Determination of the stress in a body under a given load is the primary concern for both elasticity and plasticity. For a brief discussion of stress see Section A.2. In the

[1] As opposed to having two distinct configurations, the reference and the current.

linear elastic theory a *constitutive* assumption is made that the stress is proportional to the strain, $\boldsymbol{\varepsilon}$, via the fourth-order elasticity tensor, $\mathbb{C}$.

$$\sigma_{ij} = \mathbb{C}_{ijkl} : \varepsilon_{kl} \tag{2.3}$$

For small strains, the elasticity tensor can be defined as

$$\mathbb{C} = 2\mu\,\mathbb{I} + \lambda\,\mathbf{1} \otimes \mathbf{1}, \tag{2.4}$$

where λ and μ are the Lamé constants related to the Young's modulus, E, and Poisson's ratio, ν, through the following

$$\lambda = \frac{E\,\nu}{(1+\nu)(1-2\nu)}, \quad \mu = \frac{E}{2(1+\nu)}. \tag{2.5}$$

Also, $\mathbb{I}$ is the fourth-order symmetric identity tensor defined indicially as

$$(\mathbb{I})_{ijkl} = \frac{1}{2}(\delta_{ik}\delta_{jl} + \delta_{il}\delta_{jk}) \tag{2.6}$$

where δ_{ij} is the Kronecker delta, written in direct notation as the second-order identity tensor, $\mathbf{1}$. An alternative definition of the elasticity tensor, useful for use when the volumetric and deviatoric response is assumed uncoupled,

$$\mathbb{C} = \kappa\mathbf{1} \otimes \mathbf{1} - 2\mu\left(\mathbb{I} - \frac{1}{3}\mathbf{1} \otimes \mathbf{1}\right) \tag{2.7}$$

uses the bulk modulus $\kappa = \frac{E}{3(1-2\nu)}$. Note that (2.4) has both major symmetries, $\mathbb{C}_{ijkl} = \mathbb{C}_{klij}$, and minor symmetries, $\mathbb{C}_{ijkl} = \mathbb{C}_{jikl}$ and $\mathbb{C}_{ijkl} = \mathbb{C}_{ijlk}$. The elasticity tensor is positive definite,

$$\psi_{ij}\mathbb{C}_{ijkl}\psi_{kl} > 0 \quad \forall \boldsymbol{\psi} \neq \mathbf{0}, \tag{2.8}$$

which indicates pointwise stability and also convexity, which lead to favorable solution properties. It is also strongly elliptic,

$$n_i m_j \mathbb{C}_{ijkl} n_k m_l > 0 \quad \forall \boldsymbol{n},\ \boldsymbol{m} \neq \mathbf{0}, \tag{2.9}$$

which can be related to the Hadamard condition (see Marsden and Hughes (1994)) of the acoustic tensor indicating wave speeds in the material are real. Using (2.4) and the concept that stress depends linearly on the strain yields the familiar constitutive law for stress.

$$\boldsymbol{\sigma} = \mathbb{C} : \boldsymbol{\varepsilon} = 2\mu\, \boldsymbol{\varepsilon} + \lambda\, \mathrm{tr}(\boldsymbol{\varepsilon})\mathbf{1} \tag{2.10}$$

Balance Laws

Balance laws are fundamental physical principles that govern the behavior of materials. For a model of material behavior to have physical meaning, it must obey the laws presented below. A summary of relevant results from Section A.3 will follow.

Balance of mass becomes conservation of mass for a closed system in the material description of continuum mechanics, and for the purposes of this dissertation this view will suffice. The local statement of the conservation of mass is simply that material is neither created nor destroyed, and thus mass, m, remains constant.

$$m = \int_{\Omega} \rho \, \mathrm{dv} = \mathit{constant} \tag{2.11}$$

The relevant results from the balance of momenta are the equilibrium equation and the symmetry of the stress tensor, $\sigma_{ij} = \sigma_{ji}$. In the present work we will consider quasi-static scenarios, which renders the right hand side of the equilibrium equation null.

$$\mathrm{div}\boldsymbol{\sigma} + \boldsymbol{b} = \mathbf{0}, \quad \sigma_{ij,j} + b_i = 0 \tag{2.12}$$

2.1.2 Motivating Plasticity

The theory of plasticity is rooted in attempts to understand the behavior of metals that have experienced loading outside their elastic regime. The results of such loading is a permanent distortion, observed in metals as volume preserving. This *isochoric*

deformation has been built into phenomenological constitutive theories of deformable media, and this body of work comprises classical plasticity. The primary departures from elasticity are: 1) the additive decomposition of strain into elastic and plastic parts, 2) the construction of a *yield surface* which governs the admissible stress states the body can be in, 3) the accompanying *flow rule* which governs the notion of irreversibility of plastic flow, and 4) the stress response, including hardening. The mathematical formulation that follows holds for rate-independent plasticity.

Additive Decomposition

It is assumed at the outset that the strain tensor admits decomposition into elastic and plastic parts.

$$\boldsymbol{\varepsilon} = \boldsymbol{\varepsilon}^e + \boldsymbol{\varepsilon}^p \tag{2.13}$$

It should be noted that the plastic part of the strain tensor $\boldsymbol{\varepsilon}^p$ is defined below in Section 2.1.2, and that the total strain, $\boldsymbol{\varepsilon}$, can be thought of as an independent variable, since it is a function of the displacements, which are to be solved for. For this reason, the additive decomposition, (2.13) can be thought of as an expression for the elastic strain, $\boldsymbol{\varepsilon}^e = \boldsymbol{\varepsilon} - \boldsymbol{\varepsilon}^p$.

Stress Response

The stress response is driven by the elastic strain, which in lieu of (2.13) can be expressed as:

$$\boldsymbol{\sigma} = \mathbb{C} : (\boldsymbol{\varepsilon} - \boldsymbol{\varepsilon}^p). \tag{2.14}$$

Classical plasticity also introduces a strain-like variable, $\boldsymbol{\xi}$, which is called the equivalent plastic strain, conjugate to stress-like variables, $\boldsymbol{q}$, that govern material hardening, and thereby, the increased load necessary to continue deforming a material

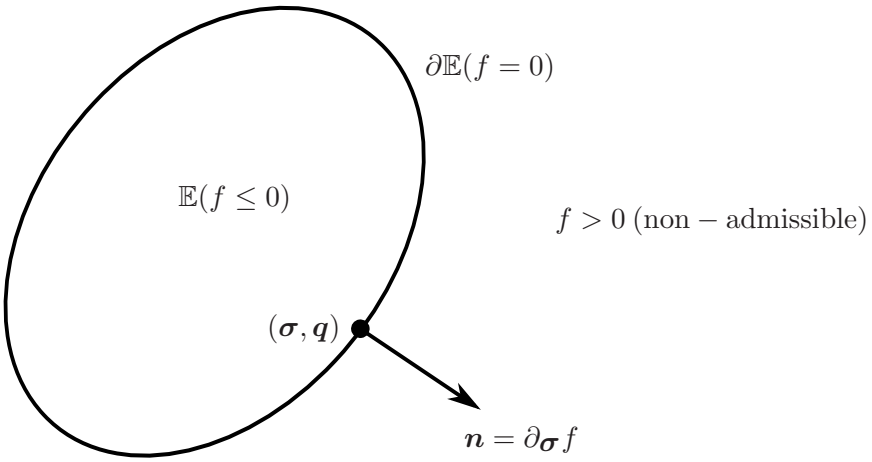

Figure 2.1: The elastic domain, in stress space

already having undergone plastic deformation. The stress state will be restricted to lie within the elastic domain, defined below, such that any stress state outside the elastic domain is considered *inadmissible*.

Yield Criteria

As an idealization of plastic deformation, a *yield surface* is constructed which defines the admissible states of stress of a material point. Define a function called the yield criterion, $f : \mathbb{S} \times \mathbb{R}^m \to \mathbb{R}$, where $\mathbb{S}$, is the space of symmetric second-order tensors and $\mathbb{R}^m$ is the space that the hardening fields live in. Then restrict the admissible stress state to

$$\mathbb{E} := \{(\boldsymbol{\sigma}, \boldsymbol{q}) \in \mathbb{S} \times \mathbb{R}^m : f(\boldsymbol{\sigma}, \boldsymbol{q}) \leq 0\}\,. \tag{2.15}$$

Figure 2.1 illustrates the restriction of the possible states of stress to either within or on the elastic domain. The yield surface, $\partial\mathbb{E}$, is introduced as the boundary of the elastic domain.

$$\partial\mathbb{E} := \{(\boldsymbol{\sigma}, \boldsymbol{q}) \in \mathbb{S} \times \mathbb{R}^m : f(\boldsymbol{\sigma}, \boldsymbol{q}) = 0\} \tag{2.16}$$

We will see that the restriction of the stress state, $(\boldsymbol{\sigma}, \boldsymbol{q})$, stated above is further exploited to require that plastic deformation can only occur when the stress state lies on the yield surface. Furthermore, the normal to the yield surface, $\boldsymbol{n} = \partial_{\boldsymbol{\sigma}} f$, plays an important role in the formulation of some models, see Section 2.1.3 below.

Flow Rule

Irreversibility of plastic flow is introduced by defining two functions, $\boldsymbol{r} : \mathbb{S} \times \mathbb{R}^m \to \mathbb{S}$ and $\boldsymbol{h} : \mathbb{S} \times \mathbb{R}^m \to \mathbb{R}^m$ that govern the direction of plastic flow and the type of hardening respectively. Then evolution equations are written for the plastic strain and the equivalent plastic strain.

$$\dot{\boldsymbol{\varepsilon}}^p = \gamma\, \boldsymbol{r}(\boldsymbol{\sigma}, \boldsymbol{q}), \quad \dot{\boldsymbol{\xi}} = \gamma\, \boldsymbol{h}(\boldsymbol{\sigma}, \boldsymbol{q}) \tag{2.17}$$

These equations are termed the flow rule and the hardening law, respectively. Consider a stress state inside the elastic domain; then the function $f < 0$ and correspondingly $\gamma = 0$, indicating no plastic deformation is occurring. Now consider the case where plastic deformation is occurring, $\gamma > 0$, then the stress state must lie on the yield surface to be admissible, $f = 0$. Together, the *consistency parameter*, γ, and the yield function, f, obey the *Kuhn-Tucker complementarity conditions*

$$\gamma \geq 0, \quad f(\boldsymbol{\sigma}, \boldsymbol{q}) \leq 0, \quad \textit{and} \quad \gamma f(\boldsymbol{\sigma}, \boldsymbol{q}) = 0. \tag{2.18}$$

Similarly, if the stress state lies on the yield surface, $f = 0$, then three possibilities exist. For the case where plastic loading is occurring, $\gamma > 0$, the time rate of change of the yield condition must be equal to zero, $\dot{f} = 0$. Also if $\dot{f} < 0$, then the consistency parameter must be equal to zero, $\gamma = 0$. The last option is for both $\dot{f}$ and γ to be zero. Combining these possibilities results in the *consistency requirement*

$$\gamma \dot{f}(\boldsymbol{\sigma}, \boldsymbol{q}) = 0. \tag{2.19}$$

Equations (2.18) and *consistency-requirement* play an important role in the numerical solution, where in practice, the yield condition is evaluated, and γ is activated only for those materials points whose *trial* stress state is deemed inadmissible.

2.1.3 J_2 Plasticity

The J_2 theory of metal plasticity has been widely studied and is a standard model used in simulating the response of metals undergoing plastic deformation. To consider the origin of the name, first consider the deviatoric part of the stress.

$$\boldsymbol{s} = \text{dev}(\boldsymbol{\sigma}) = \boldsymbol{\sigma} - \frac{1}{3}\text{tr}(\boldsymbol{\sigma})\mathbf{1} \tag{2.20}$$

Then the second principal invariant of $\boldsymbol{s}$ is denoted by J_2 and defined as

$$J_2 = \frac{1}{2}\boldsymbol{s} : \boldsymbol{s}. \tag{2.21}$$

Experiments on metal plasticity indicate that the trace of the stress has no influence on plastic deformation. For this reason the dependence of f upon σ is only through the deviatoric stress, and we can write $f(\boldsymbol{\sigma}, \boldsymbol{q}) = f(\boldsymbol{s}, \boldsymbol{q})$. Furthermore, for isotropic metals, it follows that $f(\boldsymbol{s}, \boldsymbol{q}) = f(J_1, J_2, J_3, \boldsymbol{q})$, where J_i is the corresponding principal invariant. Now, by definition of $\boldsymbol{s}$, we have $J_1 = \text{tr}\,(\boldsymbol{s}) = 0$. Experiments also show that J_3 has no influence on plastic deformation, leading to $f(\boldsymbol{\sigma}, \boldsymbol{q}) = f(J_2, \boldsymbol{q})$. In the case of perfect plasticity, i.e. no hardening, we have for the yield criterion

$$f := \sqrt{3J_2} - \sigma_y \leq 0. \tag{2.22}$$

The parameter σ_y is known as the yield strength of the material and represents the stress at which the material yields under uni-axial tension. The yield criterion is also often written in the alternate form

$$f := \|\boldsymbol{s}\| - \sqrt{\frac{2}{3}}\sigma_y \leq 0. \tag{2.23}$$

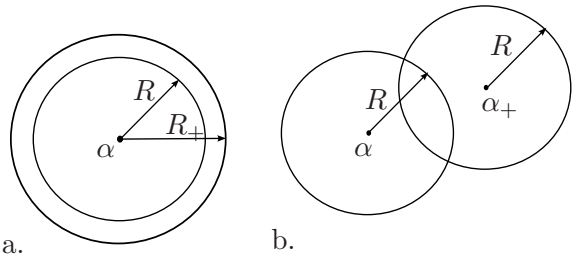

Figure 2.2: a. isotropic hardening and b. kinematic hardening

Hardening Laws

The classical theory includes two types of hardening, *isotropic* and *kinematic*. Isotropic hardening represents a uniform expansion of the yield surface, independent of the direction of plastic flow. Classical kinematic hardening represents a translation of the locus of the yield surface, in stress space, in the direction of plastic flow. An illustration of the differences between isotropic and kinematic hardening in stress space can be seen in Figure 2.2. In the figure, the αs are the locus of the yield surface, and the R's are the radii, and the $+$'s indicate an increment in hardening. The difference between isotropic and kinematic hardening is not evident until the loading path for the material is altered. For example, for cyclic loading from tension to compression, during the tension portion of the curve the stress-strain curve would appear identical. However, upon reverse loading into compression, the kinematic hardening material would yield at a smaller (in magnitude) loading level than the isotropic hardening material. A schematic of the stress-strain behavior for isotropic and kinematic hardening, with linear hardening modulus H, Young's modulus E, and yield strength σ_y, can be seen in Figure 2.3.

With the inclusion of hardening, it is necessary to recast the yield condition, (2.23), as

$$f := \|\boldsymbol{s} - \boldsymbol{q}\| - \sqrt{\frac{2}{3}}(\sigma_y + q) \leq 0, \tag{2.24}$$

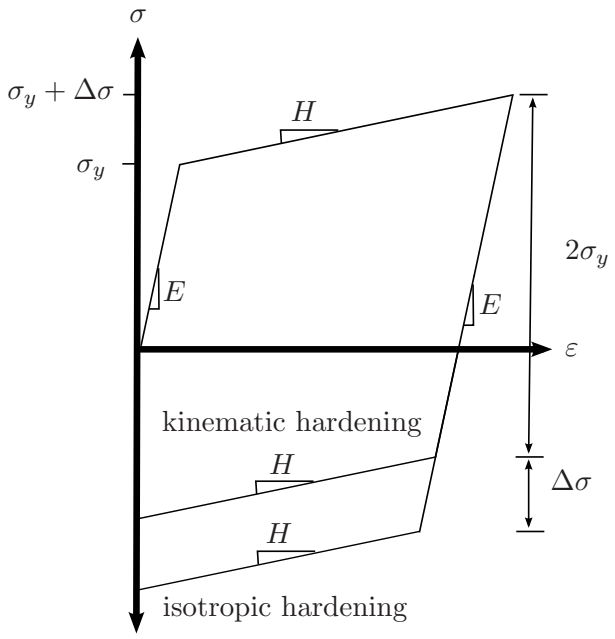

Figure 2.3: Stress-strain, uniaxial loading, isotropic vs. kinematic hardening

where $\boldsymbol{q}$ is known as the *back stress* and governs kinematic hardening, while q is the isotropic hardening parameter. Commonly used expressions for the hardening fields are

$$\dot{\boldsymbol{q}} = \frac{2}{3} H \dot{\boldsymbol{\varepsilon}}^p, \quad q = K(\xi), \quad \dot{\xi} = \sqrt{\frac{2}{3} \dot{\boldsymbol{\varepsilon}}^P : \dot{\boldsymbol{\varepsilon}}^p}, \tag{2.25}$$

where $\boldsymbol{\xi}$ is a strain like hardening variable, and ξ is a scalar hardening variable.

Associative Flow

An *associative* flow rule asserts that the direction of plastic flow occurs in a direction normal to the yield surface. Expressing the flow rule, (2.17), as associative allows for the expression of the plastic strain rate and hardening variables in terms of $\boldsymbol{n}$, the normal to the yield surface. Define a tensor $\boldsymbol{\beta} = \boldsymbol{s} - \boldsymbol{q}$.

$$\dot{\boldsymbol{\varepsilon}}^p = \gamma \partial_{\boldsymbol{\beta}} f = \gamma \boldsymbol{n}, \tag{2.26}$$

$$\dot{\boldsymbol{q}} = \frac{2}{3} H \gamma \partial_{\boldsymbol{\beta}} f = \frac{2}{3} H \gamma \boldsymbol{n}, \tag{2.27}$$

$$\dot{\xi} = \gamma \partial_q f = \gamma \sqrt{\frac{2}{3}} \tag{2.28}$$

The normal vector to the yield surface, $\boldsymbol{n}$ can be determined from (2.24) as

$$\boldsymbol{n} = \partial_{\boldsymbol{\beta}} f = \frac{\boldsymbol{\beta}}{\|\boldsymbol{\beta}\|}. \tag{2.29}$$

Tangent Moduli

To derive the tangent moduli for the J_2 plasticity model being considered we need to consider the rate form of the stress equation, (2.14). Then substitute the associative flow rule assumption for the plastic strain rate.

$$\dot{\boldsymbol{\sigma}} = \mathbb{C} : (\dot{\boldsymbol{\varepsilon}} - \gamma \boldsymbol{n}) \tag{2.30}$$

To complete the definition of the rate form of the stress, it would be beneficial to obtain an explicit representation of the consistency parameter, γ. Fortunately, we can exploit the consistency condition, (2.19). To begin, assume that the stress state lies on the yield surface and use the chain rule on the yield criterion, and then substitute in known quantities.

$$\begin{aligned}
\dot{f} &= \partial_{\boldsymbol{\beta}} f : \dot{\boldsymbol{\beta}} + \partial_q f \dot{q} && (2.31)\\
&= \partial_{\boldsymbol{\beta}} f : \dot{\boldsymbol{\sigma}} - \partial_{\boldsymbol{\beta}} f : \dot{\boldsymbol{q}} + \partial_q f \dot{q} && (2.32)\\
&= \partial_{\boldsymbol{\beta}} f : \mathbb{C} : (\dot{\boldsymbol{\varepsilon}} - \dot{\boldsymbol{\varepsilon}}^p) - \partial_{\boldsymbol{\beta}} f : \dot{\boldsymbol{q}} + \partial_q f \partial_\xi q \dot{\xi} && (2.33)\\
&= \boldsymbol{n} : \mathbb{C} : \dot{\boldsymbol{\varepsilon}} - \boldsymbol{n} : \mathbb{C} : \gamma \boldsymbol{n} - \boldsymbol{n} \frac{2}{3} \gamma H : \boldsymbol{n} - \frac{2}{3} \gamma K && (2.34)\\
&= \boldsymbol{n} : \mathbb{C} : \dot{\boldsymbol{\varepsilon}} - \gamma \left(\boldsymbol{n} : \mathbb{C} : \boldsymbol{n} + \frac{2}{3} H + \frac{2}{3} K \right) && (2.35)
\end{aligned}$$

We have used the fact that $\boldsymbol{n} : \boldsymbol{n} = 1$. Then, recognizing that $\dot{f} = 0$ by the consistency conditions, we can manipulate (2.35) to obtain the desired result.

$$\gamma = \frac{\langle \boldsymbol{n} : \dot{\boldsymbol{\varepsilon}} \rangle}{1 + \frac{H+K}{3\mu}} \tag{2.36}$$

Note that $\boldsymbol{n} : \mathbb{C} : \dot{\boldsymbol{\varepsilon}} = 2\mu\, \boldsymbol{n} : \dot{\boldsymbol{\varepsilon}}$ since $\boldsymbol{n}$ is a deviatoric tensor, which follows from the fact that $\operatorname{tr} \boldsymbol{\beta} = 0$ and (2.29). Then finally we can state the elastoplastic tangent

moduli, which is valid for the case of plastic loading, or $\gamma > 0$. Beginning with the rate form of the stress in (2.30), we can include the expression derived for γ and (2.7).

$$\mathbb{C}^{ep} = \kappa \mathbf{1} \otimes \mathbf{1} + 2\mu \left\{ \mathbb{I} - \frac{1}{3}\mathbf{1} \otimes \mathbf{1} - \frac{\boldsymbol{n} \otimes \boldsymbol{n}}{1 + \frac{H+K}{3\mu}} \right\} \tag{2.37}$$

The derivation of (2.37) is relevant for the case of linear isotropic and kinematic hardening laws, as discussed in this section.

2.2 Computational Plasticity

Computational plasticity involves the formulation and implementation of numerical algorithms to solve the global equilibrium equations and the local plasticity equations. Finite element methods are the numerical schemes of choice for solving boundary value problems in plasticity. Finite element methods are based on the variational, or weak, statement of the boundary value problem under consideration, along with the subsequent restriction to representation within a finite-dimensional basis, hence the name. The beginning of this section will give a summary of ideas related to the finite element method. Other topics of discussion are the numerical integration algorithms used in classical plasticity and treatment of the isochoric constraint encountered during plastic flow.

In order to set the stage for discussion of the algorithms used in classical numerical plasticity, the machinery of the finite element method will be presented in the context of the linear theory of elasticity. From there the extension to the nonlinear theory of plasticity is most natural. Developments in the next section will follow closely with Hughes (1987), Chapter 2.

2.2.1 Finite Elements

As a formal point of departure, consider the strong form of the boundary value problem from classical elasticity. Consider a domain Ω with boundary $\partial\Omega$ composed of disjoint subsets Γ_{g_i} and Γ_{h_i} such that $\partial\Omega = \overline{\Gamma_{g_i} \cup \Gamma_{h_i}}$.

Strong Form: Given $b_i : \Omega \to \mathbb{R}$, $g_i : \Gamma_{g_i} \to \mathbb{R}$, and $h_i : \Gamma_{h_i} \to \mathbb{R}$, find $u_i : \overline{\Omega} \to \mathbb{R}$ such that

$$\begin{aligned} \sigma_{ij,j} + b_i &= 0 \quad \text{in} \quad \Omega \\ u_i &= g_i \quad \text{on} \quad \Gamma_{g_i} \\ \sigma_{ij} n_j &= h_i \quad \text{on} \quad \Gamma_{h_i} \end{aligned} \tag{2.38}$$

where σ_{ij} is defined via (2.3), and g_i and h_i are the prescribed displacements and tractions respectively, for the i^{th} component. Figure 2.4 illustrates the independence of the boundary conditions in $\mathbb{R}^2$. The strong form of the boundary value problem should be familiar to those with a strength of materials background. For the quasi-static cases in question, the strong form of the problem specifies that static equilibrium is achieved given the prescribed external loads and displacement constraints.

To formulate the variational statement of the problem, we need to choose the space in which the trial solution and variational weighting function lie. Then the variation form can be obtained by multiplying terms by the weighting function and integrating over the domains. Usually, integration by parts is performed to transfer a derivative over to the weighting function in second order problems, facilitating the uses of $\mathscr{C}^0$ basis functions, discussed below. For the trial solution space we have

$$\mathscr{S}_i = \left\{ u_i | u_i \in H^1(\Omega), u_i = g_i \text{ on } \Gamma_{g_i} \right\}, \tag{2.39}$$

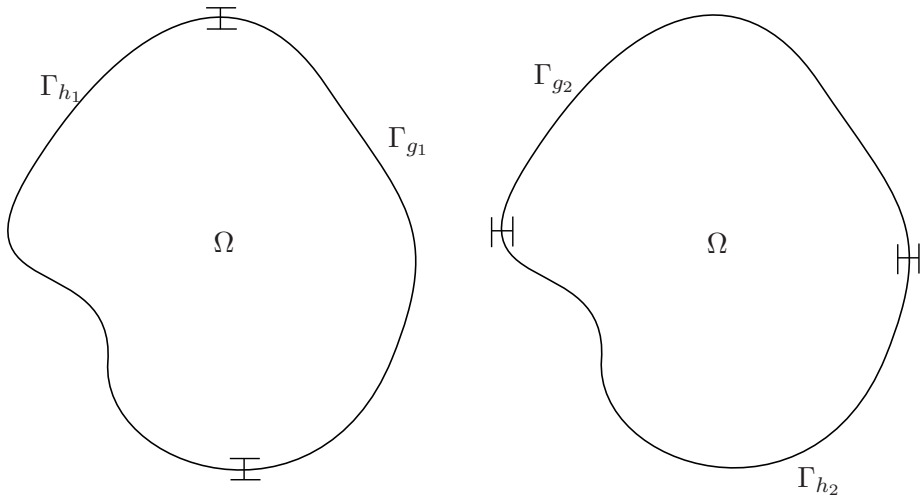

Figure 2.4: Independent specification of boundary conditions, including both traction and displacement, for each component

where the index i indicates that the space is valid for the i^{th} component of the function, and $H^1(\Omega)$ is a Sobolev space defined as

$$H^1(\Omega) = \{w | w \in L_2; w_{,x} \in L_2\}; \quad L_2(\Omega) = \left\{ w | \int_\Omega w^2 \mathrm{d}\Omega < \infty \right\}. \tag{2.40}$$

Then the weighting space is similarly defined as

$$\mathscr{V}_i = \left\{ w_i | w_i \in H^1(\Omega), w_i = 0 \text{ on } \Gamma_{g_i} \right\}. \tag{2.41}$$

Note that the preceding spaces, $\mathscr{S}_i$ and $\mathscr{V}_i$ have the displacement boundary conditions constructed from within, and in particular, the weighting functions vanish space on the known displacement boundary. These are known as the *essential* or *Dirichlet* boundary conditions. Now we have enough to make the variational, or weak, statement of the boundary value problem.

Weak Form: Given $b_i : \Omega \to \mathbb{R}$, $g_i : \Gamma_{g_i} \to \mathbb{R}$, and $h_i : \Gamma_{h_i} \to \mathbb{R}$, find $u_i \in \mathscr{S}_i$ such that for all $w_i \in \mathscr{V}_i$,

$$\int_\Omega w_{i,j} \sigma_{ij} \, \mathrm{d}\Omega = \int_\Omega w_i b_i \, \mathrm{d}\Omega + \sum_{i=1}^{n_{sd}} \left(\int_{\Gamma_{h_i}} w_i h_i \, \mathrm{d}\Gamma \right). \tag{2.42}$$

Standard exercises show the equivalence of the strong form and the weak form, for example see Hughes (1987), Chapter 1. Notice that a derivative from the div $\boldsymbol{\sigma}$ term has been transferred over to the weighting function, as mentioned above. The integration by parts gives rise to a boundary term in (2.42), called *natural* or *Neumann* boundary condition.

Having obtained the variational form of the boundary value problem, the next step is to construct approximations to the infinite-dimensional spaces that the trial solution and weighting functions reside in. For simplicity the finite-dimensional spaces $\mathscr{S}_i^h$ and $\mathscr{V}_i^h$ are introduced, each with its own basis functions, usually consisting of polynomials. Now we can represent approximations to the trial solution and weighting function as products of basis functions and degrees of freedom.

$$u_i^h = \sum_A^{n_{nodes}} N^A(\boldsymbol{x}) d_i^A \tag{2.43}$$

The global vector u_i^h in (2.43), being the size of the total number of nodes, A, is the representation of the displacement field in the chosen basis, and as such $N^A(\boldsymbol{x})$ are the basis functions and d_i^A are the coefficients, or displacement degrees of freedom. The argument, $\boldsymbol{x}$, of the basis function explicitly indicates the spatial dependence of the basis functions on the geometry of the domain. Similarly for the weighting function,

$$w_i^h = \sum_A^{n_{nodes}} N^A(\boldsymbol{x}) c_i^A, \tag{2.44}$$

where c_i^A are the variational degrees of freedom. Using the same basis functions for both the solution (displacements) and the weighting function makes the method a *Bubnov-Galerkin*, or simply *Galerkin*, approximation. Now we can state the Galerkin form of the boundary value problem.

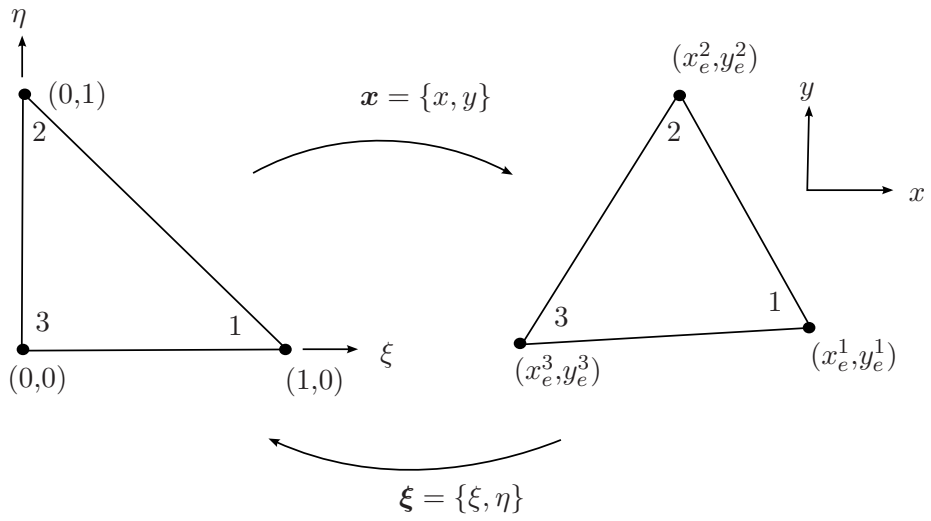

Figure 2.5: Isoparametric mapping for a linear triangle finite element

Galerkin Form: Given $b_i : \Omega \to \mathbb{R}$, $g_i : \Gamma_{g_i} \to \mathbb{R}$, and $h_i : \Gamma_{h_i} \to \mathbb{R}$, find $u_i^h \in \mathscr{S}_i^h$ such that for all $w_i^h \in \mathscr{V}_i^h$,

$$\int_\Omega w_{i,j}^h \sigma_{ij}^h \, \mathrm{d}\Omega = \int_\Omega w_i^h b_i \, \mathrm{d}\Omega + \sum_{i=1}^{n_{sd}} \left(\int_{\Gamma_{h_i}} w_i^h h_i \, \mathrm{d}\Gamma \right). \tag{2.45}$$

The concept of a *finite element* is the restriction of the finite-dimensional basis from the global discretized system to a local one, $N^A(\boldsymbol{x}) \to N_e^A(\boldsymbol{\xi})$, where $(\cdot)_e$ indicates a quantity of the element. The notion of an *isoparametric* finite element is introduced by expressing the geometric interpolation in the basis as well, such as

$$\boldsymbol{x}_e = \sum_A^{n_{en}} N_e^A(\boldsymbol{\xi}) \boldsymbol{x}_e^A, \tag{2.46}$$

where $\boldsymbol{x}_e^A$ are the global coordinates of the nodes that comprise the finite element, and n_{en} is the number of element nodes. See Figure 2.5 for an illustration of the local to global isoparametric mapping. We can then express the displacements and weighting functions in terms of this local basis.

$$\boldsymbol{u}_e^h = \sum_A^{n_{en}} N_e^A(\boldsymbol{\xi}) d_e^A, \quad \boldsymbol{w}_e^h = \sum_A^{n_{en}} N_e^A(\boldsymbol{\xi}) c_e^A \tag{2.47}$$

We can use (2.46) to take derivatives, with respect to the global coordinates, of the functions in (2.47) using the chain rule and the spatial independence of the

coefficients. For example the derivatives of the displacements can be written as follows.

$$(\boldsymbol{u}_e^h)_{,\boldsymbol{x}} = \sum_A (\boldsymbol{N}_e^A)_{,\boldsymbol{\xi}} \boldsymbol{\xi}_{,\boldsymbol{x}} (\boldsymbol{d}_e^A) \tag{2.48}$$

We do not have an explicit expression for the term $\boldsymbol{\xi}_{,\boldsymbol{x}}$, but because we have an expression for the coordinates that uses the same basis functions as the solution fields in terms of the local coordinates $\boldsymbol{\xi}$, we can compute the inverse relation $(\boldsymbol{x}_{,\boldsymbol{\xi}})^{-1}$ from (2.46). Using this we have an alternate expression for the local displacement gradient.

$$(\boldsymbol{u}_e^h)_{,\boldsymbol{x}} = \sum_A (\boldsymbol{N}_e^A)_{,\boldsymbol{\xi}} (\boldsymbol{x}_{,\boldsymbol{\xi}})^{-1} \boldsymbol{d}_e^A \tag{2.49}$$

Using a similar expression as in (2.49), the Galerkin Form can be restated by summing contributions from the total number of element, n_{el}.

Given $b_i : \Omega \to \mathbb{R}$, $g_i : \Gamma_{g_i} \to \mathbb{R}$, and $h_i : \Gamma_{h_i} \to \mathbb{R}$, find $u_i^h \in \mathscr{S}_i^h$ such that for all $w_i^h \in \mathscr{V}_i^h$,

$$\begin{aligned} &\sum_e^{n_{el}} \left(\int_{\Omega_e} (\boldsymbol{w}_e^h)_{,\boldsymbol{x}} : \mathbb{C} : (\boldsymbol{u}_e^h)_{,\boldsymbol{x}} \, \mathrm{d}\Omega \right) = \\ &\sum_e^{n_{el}} \left(\int_{\Omega_e} (\boldsymbol{w}_e^h) \cdot \boldsymbol{b} \, \mathrm{d}\Omega + \sum_{i=1}^{n_{sd}} \left(\int_{\Gamma_{h_i e}} (\boldsymbol{w}_e^h) \cdot \boldsymbol{h} \, \mathrm{d}\Gamma \right) \right) \end{aligned} \tag{2.50}$$

Matrix Form: The matrix form of the problem comes from assembling the global system of equations for all the degrees of freedom in the discretized domain. To do so we call upon the notion of the finite element and consider the contribution to the global system from the local element. Inserting the interpolation approximations into (2.50) we can derive the element stiffness matrix. Consider the left hand side of the equation, which can equivalently be expressed (after interpolation substitutions)

as

$$\sum_{e}^{n_{el}} \left(\boldsymbol{c}^{\mathrm{T}} \underbrace{\int_{\Omega_e} \boldsymbol{B}^{\mathrm{T}} \boldsymbol{C} \boldsymbol{B} \, \mathrm{d}V}_{\boldsymbol{k}_e} \boldsymbol{d} \right). \tag{2.51}$$

Here $\boldsymbol{C}$ is the matrix of elastic moduli derived from the fourth order tensor $\mathbb{C}$. Now consider the matrix $\boldsymbol{B}$, which serves as the discrete symmetric gradient operator. This is an operator used to act on vectors of coefficients to calculate the strain, or the variation in strain. Note that since the coefficients have no spatial dependence, the operator can be defined solely in terms of basis function derivatives. In two dimensions the nodal gradient operator, $\boldsymbol{B}_a$ for local node a is

$$\boldsymbol{B}_a = \begin{bmatrix} N_{a,1} & 0 \\ 0 & N_{a,2} \\ N_{a,2} & N_{a,1} \end{bmatrix}. \tag{2.52}$$

Note that for this two dimensional example, an assumption is made that the coefficients are ordered in (x,y) pairs as opposed to ordering all the x degrees of freedom first and then y degrees of freedom. In the latter case $\boldsymbol{B}_a$ would have a slightly different form. Also note that, as presented, there is a factor of two difference between the output of the symmetric gradient operator and the tensorial shear strain. This is typically accounted for in the constitutive matrix $\boldsymbol{C}$. Now, in the expression for the element stiffness matrix, (2.51), the total elemental symmetric gradient operator can be composed from each local node up to the total number of element nodes n_{en}.

$$\boldsymbol{B} = [\boldsymbol{B}_1, \boldsymbol{B}_2, ..., \boldsymbol{B}_{n_{en}}] \tag{2.53}$$

Using, (2.50), the local contributions are assembled into the global stiffness matrix, $\boldsymbol{K}$, and global force vector, $\boldsymbol{F}$, via the finite element assembly operator, $\mathbb{A}$. The

finite element assembly operator maps local degrees of freedom at the nodes to global degrees of freedom. For example for the stiffness matrix,

$$\boldsymbol{K} = \mathop{\mathbb{A}}_{e}^{n_{el}}(\boldsymbol{k}_e). \tag{2.54}$$

The global assembled system $\boldsymbol{K}\boldsymbol{d} = \boldsymbol{F}$ is solved for the displacement degrees of freedom, $\boldsymbol{d}$. With the solution vector $\boldsymbol{d}$, known, the element stress field can be recovered using the constitutive matrix and symmetric gradient operator as

$$\boldsymbol{\sigma} = \boldsymbol{C}\boldsymbol{B}_e\boldsymbol{d}_e, \tag{2.55}$$

where again, $\boldsymbol{d}_e$ would be the displacement coefficients restricted to the nodes comprising the element, and $\boldsymbol{B}_e$ would be the gradient operator for that element.

Incompressible Elasticity

The isochoric nature of plastic flow mimics the behavior of an elastic material in its incompressible limit, i.e. $\nu \to \frac{1}{2}$. For this reason finite element strategies for dealing with incompressible elasticity are relevant for the development of numerical methods for plasticity that do not exhibit locking. Locking is an observed phenomenon where the degrees of freedom for the system are overconstrained by boundary conditions and incompressibility, so that the only solution is trivially zero. It is a manifestation of non-uniqueness in the solution for the trace of the stress, and can be alleviated by projection techniques. One such approach that will be discussed here is the *mean dilatation* formulation, first introduced in Nagtegaal et al. (1974), generalized in Hughes (1980), and adapted to the finite-deformation regime in Simo et al. (1985).

A complete derivation of the method starts with the Hu-Washizu *3 field variational principle*, which considers both stress and strain as well as displacements as the primal field variables to be solved for. Consider the energy functional, Π, that

represents the total amount of energy available.

$$\Pi(\boldsymbol{u},\boldsymbol{\sigma},\boldsymbol{\varepsilon}) := \int_\Omega \frac{1}{2}\boldsymbol{\varepsilon} : \mathbb{C} : \boldsymbol{\varepsilon}\,\mathrm{dV} + \int_\Omega \boldsymbol{\sigma} : (\boldsymbol{\nabla}^s\boldsymbol{u} - \boldsymbol{\varepsilon})\,\mathrm{dV} - \int_\Omega \boldsymbol{u}\cdot\boldsymbol{b}\,\mathrm{dV} + \int_{\Gamma_h} \boldsymbol{u}\cdot\boldsymbol{h}\,\mathrm{dS} \tag{2.56}$$

Then we define the variations in displacements, stresses, and strains.

$$\boldsymbol{u}_\xi = \boldsymbol{u} + \xi\boldsymbol{w}, \quad \boldsymbol{\sigma}_\xi = \boldsymbol{\sigma} + \xi\boldsymbol{\tau}, \quad \boldsymbol{\varepsilon}_\xi = \boldsymbol{\varepsilon} + \xi\boldsymbol{\gamma}$$

In the usual way, we derive the variational equations by exploiting the stationarity condition

$$\frac{\mathrm{d}}{\mathrm{d}\xi}\Pi(\boldsymbol{u}_\xi,\boldsymbol{\sigma}_\xi,\boldsymbol{\varepsilon}_\xi)|_{\xi=0} = 0. \tag{2.57}$$

Bringing the scalar derivatives within the integrals of (2.56), evaluating the scalar parameter $\xi = 0$, and making standard arguments about the arbitrariness of the variational functions we arrive at three separate equations that define the stationarity condition. The first being defined with respect to the variations of the displacements.

$$\int_\Omega \boldsymbol{\sigma} : \boldsymbol{\nabla}^s\boldsymbol{w}\,\mathrm{dV} - \int_\Omega \boldsymbol{w}\cdot\,\mathrm{dV} - \int_{\boldsymbol{\Gamma_h}} \boldsymbol{w}\cdot\boldsymbol{h}\,\mathrm{dV} = \boldsymbol{0} \tag{2.58}$$

The second equation is with respect the variations in the stress,

$$\int_\Omega \boldsymbol{\tau} : (\boldsymbol{\nabla}^s\boldsymbol{u} - \boldsymbol{\varepsilon})\,\mathrm{dV} = 0, \tag{2.59}$$

and the third equation is with respect to the variations in the strain,

$$\int_\Omega \boldsymbol{\gamma} : (\mathbb{C} : \boldsymbol{\varepsilon} - \boldsymbol{\sigma})\,\mathrm{dV} = 0. \tag{2.60}$$

To recover the mean-dilatation formulation, we can choose the following functions of stress and strain as our additional variables, which are used to represent the pressure and dilatation.

$$p = \frac{1}{3}\mathrm{tr}\boldsymbol{\sigma}; \quad \theta = \mathrm{tr}(\boldsymbol{\varepsilon}) = \mathrm{div}(\boldsymbol{u}) \tag{2.61}$$

Then we can express the stress and the strain in terms of the pressure and dilatation fields.

$$\boldsymbol{\varepsilon} = \mathrm{dev}(\boldsymbol{\nabla}^s \boldsymbol{u}) + \frac{1}{3}\theta \mathbf{1}, \quad \boldsymbol{\sigma} = \mathrm{dev}(\mathbb{C} : \boldsymbol{\varepsilon}) + p\mathbf{1} \tag{2.62}$$

Inserting the expressions for stress and strain from (2.62) into the energy term $\boldsymbol{\sigma} : (\boldsymbol{\nabla}^s \boldsymbol{u} - \varepsilon)$ yields

$$\boldsymbol{\sigma} : (\boldsymbol{\nabla}^s \boldsymbol{u} - \boldsymbol{\varepsilon}) = p(\mathrm{div}\boldsymbol{u} - \theta). \tag{2.63}$$

Using (2.63), the total energy functional can be written in terms of displacement, pressure, and dilatation.

$$\begin{aligned} \Pi(\boldsymbol{u}, p, \theta) := &\int_\Omega \frac{1}{2}\boldsymbol{\varepsilon} : \mathbb{C} : \boldsymbol{\varepsilon} \,\mathrm{dV} + \int_\Omega p(\mathrm{div}\boldsymbol{u} - \theta) \,\mathrm{dV} \\ &- \int_\Omega \boldsymbol{u} \cdot \boldsymbol{b} \,\mathrm{dV} + \int_{\Gamma_h} \boldsymbol{u} \cdot \boldsymbol{h} \,\mathrm{dS} \end{aligned} \tag{2.64}$$

Next define the variations of primal fields, similar to above,

$$\boldsymbol{u}_\xi = \boldsymbol{u} + \xi \boldsymbol{w}, \quad p_\xi = p + \xi q, \quad \theta_\xi = \theta + \xi\gamma.$$

Revisiting the stationarity condition, (2.57), the variational equations can be expressed as

$$\begin{aligned} \int_\Omega \mathrm{dev}(\boldsymbol{\nabla}^s \boldsymbol{w}) : \mathbb{C} : \mathrm{dev}(\boldsymbol{\nabla}^s \boldsymbol{u}) \,\mathrm{dV} + &\int_\Omega \mathrm{div}(\boldsymbol{w}) p \,\mathrm{dV} \\ - \int_\Omega \boldsymbol{w} \cdot \boldsymbol{b} \,\mathrm{dV} - &\int_{\Gamma_h} \boldsymbol{w} \cdot \boldsymbol{h} \,\mathrm{dS} = 0 \end{aligned}$$

in terms of displacement variations,

$$\int_\Omega q(\mathrm{div}(\boldsymbol{u}) - \theta) \,\mathrm{dV} = 0 \tag{2.65}$$

in terms of pressure variations, and

$$\int_\Omega \gamma(\frac{1}{3}\mathrm{tr}(\mathbb{C} : \boldsymbol{\varepsilon}) - p) \,\mathrm{dV} = 0 \tag{2.66}$$

in terms of dilatation variations. From these three variational equations, we can make the Galerkin approximation and define finite dimensional spaces for the fields to reside in. For the displacements and their variations the usual spaces are used, $\boldsymbol{u}^h \in \mathscr{S}^h$, $\boldsymbol{w}^h \in \mathscr{V}^h$, as above in (2.39) and (2.41). Then the pressure, its variation, and the dilatation, and its variation are all assumed to be bounded, but discontinuous across elements, i.e. $p^h, q^h, \theta^h, \gamma^h \in \mathbb{L}^2(\Omega)$. The implications of placing the additional fields in $\mathbb{L}^2$ are the absence of a need for continuous derivatives, allowing for a local treatment. Definition of the interpolations of the primary fields and their variations follow below (the subscript e will be dropped for notational simplicity, even though the interpolations are still within the isoparametric structure).

$$\begin{aligned} \boldsymbol{u}^h &= \sum_{A=1}^{n_{en}} N^A \boldsymbol{d}^A, \quad \boldsymbol{w}^h = \sum_{A=1}^{n_{en}} N^A \boldsymbol{c}^A, \\ p^h &= \sum_{B=1}^{n_{pp}} \Gamma^B \alpha^B, \quad q^h = \sum_{B=1}^{n_{pp}} \Gamma^B \beta^B, \\ \theta^h &= \sum_{B=1}^{n_{pp}} \Gamma^B \delta^B, \quad \gamma^h = \sum_{B=1}^{n_{pp}} \Gamma^B \nu^B \end{aligned}$$

Here, Γ^B are the shape functions for the pressure and dilatation fields, and n_{pp} are the number of points used to represent the pressure and dilatation. Using these definitions we can revisit terms in the variational equations, starting with discrete form of (2.65), we solve locally for the degrees of freedom using the matrix form of the divergence operator, $\operatorname{div} \boldsymbol{u} = \sum_a \boldsymbol{b}^a \boldsymbol{d}^a$.

$$\int_{\Omega_e} q^h (\operatorname{div} \boldsymbol{u}^h - \theta^h) \, \mathrm{dV} = \beta^{\mathrm{T}} \int_{\Omega_e} \Gamma^{\mathrm{T}} (\boldsymbol{b}\boldsymbol{d} - \Gamma\delta) \, \mathrm{dV} = 0 \tag{2.67}$$

which can be re-arranged to and solve for δ using the following, $\boldsymbol{H} = \int_{\Omega_e} \Gamma^{\mathrm{T}}\Gamma \, \mathrm{dV}$.

$$\delta = \boldsymbol{H}^{-1} \left(\int_{\Omega_e} \Gamma^{\mathrm{T}} \boldsymbol{b} \, \mathrm{dV} \right) \boldsymbol{d} \tag{2.68}$$

Now we can define the modified discrete divergence operator from the definition

$\theta = \Gamma\delta$.

$$\bar{\boldsymbol{b}} = \Gamma \boldsymbol{H}^{-1} \left(\int_{\Omega_e} \Gamma^{\mathrm{T}} \boldsymbol{b} \, \mathrm{dV} \right) \boldsymbol{d} \tag{2.69}$$

This leads us to the equivalent expression of $\theta = \bar{\boldsymbol{b}}\boldsymbol{d}$, which is now written in terms of the displacement degrees of freedom. A similar procedure yields a simple expression for the pressure using the bulk modulus, where $\kappa = \lambda + \frac{2}{3}\mu$.

$$p = \Gamma^{\mathrm{T}} \boldsymbol{H}^{-1} \int_{\Omega e} \Gamma \kappa \theta \, \mathrm{dV} \tag{2.70}$$

Using the discrete divergence operator, (2.69), we can reformulate the equilibrium equation in terms of the modified discrete gradient operator, $\overline{\boldsymbol{B}}$, defined using the standard symmetric discrete gradient operator $\boldsymbol{B}$, and the identity matrix $\mathbf{1}$.

$$\overline{\boldsymbol{B}} = \boldsymbol{B} - \frac{1}{3}\mathbf{1}\boldsymbol{b} + \frac{1}{3}\mathbf{1}\bar{\boldsymbol{b}} \tag{2.71}$$

And the equilibrium equation in matrix form, minus forcing terms, reduces to

$$\int_{\Omega} \overline{\boldsymbol{B}}^{\mathrm{T}} \boldsymbol{C} \overline{\boldsymbol{B}} \, \mathrm{dV} = 0, \tag{2.72}$$

where $\boldsymbol{C}$ is the matrix of elastic moduli generated from the elasticity tensor, $\mathbb{C}$, as before.

2.2.2 Radial Return

The classical integration algorithm for computational plasticity is referred to as a closest point projection, which first appeared in the literature as the radial return algorithm of Wilkins (1963). The basic concept behind the algorithm is a backward Euler scheme used to integrate the equations of plasticity in time. In summary, to move in time from t_n to t_{n+1}, first the yield surface needs to be evaluated for every integration point in the domain assuming elastic constitutive behavior, which

is termed the trial state. If the yield condition is violated, indicating that the trail state is an inadmissible stress state at that point, a return mapping algorithm is used to bring the stress state back to the yield surface.

A brief discussion of the radial return algorithm for linear isotropic and kinematic hardening follows below. We will follow through with the presentation of section 2.1.3 to make matters concrete. To begin, we assume a complete characterization of the state of the material at time t_n, including the total strain, $\boldsymbol{\epsilon}_n$, plastic strain, $\boldsymbol{\epsilon}^p_n$, and any hardening data, $\boldsymbol{q}_n$. Then the elastic strain and stress can always be calculated using (2.13) and (2.14), which take the following discrete form.

$$\boldsymbol{\sigma}_n = \mathbb{C} : (\boldsymbol{\varepsilon}_n - \boldsymbol{\varepsilon}^p_n) \tag{2.73}$$

As a reminder, the scope of this presentation lies within the small strain theory.

With the complete state at t_n known, we calculate the increment in the strain tensor obtained from the incremental displacement field, $\Delta\boldsymbol{u}$, arising from evaluating the equilibrium equation. Then we calculate the trail state where$(\cdot)^{\text{tr}}$ indicates a trial state quantity.

$$(\boldsymbol{\varepsilon}^e_{n+1})^{\text{tr}} = \boldsymbol{\varepsilon}_n + \boldsymbol{\nabla}^s(\Delta\boldsymbol{u}) - \boldsymbol{\varepsilon}^p_n \tag{2.74}$$

$$\boldsymbol{\sigma}^{\text{tr}}_{n+1} = \mathbb{C} : (\boldsymbol{\varepsilon}^e_{n+1})^{\text{tr}} \tag{2.75}$$

$$\boldsymbol{q}^{\text{tr}}_{n+1} = \boldsymbol{q}_n \tag{2.76}$$

$$f^{\text{tr}}_{n+1} = f(\boldsymbol{\sigma}^{\text{tr}}_{n+1}, \boldsymbol{q}^{\text{tr}}_{n+1}) \tag{2.77}$$

Generally, the discrete gradient calculation can be carried out using the modified discrete symmetric gradient operator $\overline{\boldsymbol{B}}$ (2.71), derived in section 2.2.1, especially if volumetric locking is being observed in the global solution. For convenience, another stress termed the relative stress is defined as $\boldsymbol{\xi}^{\text{tr}}_{n+1} = \boldsymbol{\sigma}^{\text{tr}}_{n+1} - \boldsymbol{q}^{\text{tr}}_{n+1}$

In order to proceed, we need to be able to determine if a given stress state is inadmissible by defining the yield condition, $f(\boldsymbol{\sigma}, \boldsymbol{q})$. To accomplish this we need to revisit section 2.1.3 and use the discrete form of (2.24).

$$f_{n+1}^{\mathrm{tr}} := \|\mathrm{dev}\, \boldsymbol{\sigma}_{n+1}^{\mathrm{tr}} - \boldsymbol{q}_{n+1}^{\mathrm{tr}}\| - \sqrt{\frac{2}{3}}(\sigma_y + q_n) \tag{2.78}$$

Where we recall (2.25) in the definition of (2.78), and σ_y is typically the yield stress in tension. The equivalent plastic strain at time t_n is denoted as α_n, and for a linear isotropic hardening model $q_n = K\alpha_n$.

After completely defining the trial state and determining which integration points have violated the yield condition, i.e. $f_{n+1}^{\mathrm{tr}} > 0$, a return mapping algorithm is employed to locally return the local stress state to the yield surface. It is worth noting that in the classical associative methods, see section 2.1.3 the normal to the yield surface, $\boldsymbol{n}_{n+1}$ can be determined solely from the trial state.

$$\boldsymbol{n}_{n+1} = \frac{\mathrm{dev}\, \boldsymbol{\sigma}_{n+1}^{\mathrm{tr}} - \boldsymbol{q}_{n+1}^{\mathrm{tr}}}{\|\mathrm{dev}\, \boldsymbol{\sigma}_{n+1}^{\mathrm{tr}} - \boldsymbol{q}_{n+1}^{\mathrm{tr}}\|} = \frac{\boldsymbol{\xi}_{n+1}^{\mathrm{tr}}}{\|\boldsymbol{\xi}_{n+1}^{\mathrm{tr}}\|} \tag{2.79}$$

At this point, for notational simplicity, the quantity $\gamma\Delta t$ is usually written as $\Delta\gamma$, and it is this quantity which needs to be solved for. The classical methods exploit the fact that, from consistency imposed at t_{n+1}, $f(\boldsymbol{\sigma}_{n+1}, \boldsymbol{q}_{n+1}) = 0$, and solve the nonlinear equation for $\Delta\gamma$ in an iterative fashion using a Newton method. To illustrate the

system set up in Simo and Hughes (1998), Chapter 3, consider

$$\begin{aligned} g(\Delta\gamma^{(k)}) := & - \sqrt{\frac{2}{3}} K(\alpha_{n+1}^{(k)}) + \|\boldsymbol{\xi}_{n+1}^{\mathrm{tr}}\| \\ & - \left(2\mu\Delta\gamma^{(k)} + \sqrt{\frac{2}{3}}[H(\alpha_{n+1}^{(k)}) - H(\alpha_n)] \right) \\ Dg(\Delta\gamma^{(k)}) := & -2\mu \left(1 + \frac{H'(\alpha_{n+1}^{(k)}) + K'(\alpha_{n+1}^{(k)})}{3\mu} \right) \\ \Delta\gamma^{(k+1)} = & \Delta\gamma^{(k)} - \frac{g(\Delta\gamma^{(k)})}{Dg(\Delta\gamma^{(k)})} \\ \alpha_{n+1}^{(k+1)} = & \alpha_n + \sqrt{\frac{2}{3}}\Delta\gamma^{(k+1)} \end{aligned}$$

with initial conditions $\Delta\gamma^{(0)} = 0$ and $\alpha_{n+1}^{(0)} = \alpha_n$, and k^{th} iterate $(\cdot)^{(k)}$. The system is iteratively solved for $\Delta\gamma$ until $|g(\Delta\gamma^{(k)}|$ is small (i.e. less than some tolerance). Other methods could be employed that use direct evaluation of $f(\boldsymbol{\sigma}_{n+1}, \boldsymbol{q}_{n+1})$, which is then driven to zero. The choice between these and other equivalent methods is made on the basis of algorithmic convenience. An illustration of the example from Simo and Hughes can be seen in Algorithm 2.1.

Algorithm 2.1 Consistency condition for classical plasticity

Initialize
$\Delta\gamma^0 = 0$
$\alpha_{n+1}^0 = \alpha_n$
Iterate
while $|g(\Delta\gamma^{(k)})| > TOL$ **do**
$g(\Delta\gamma^{(k)}) := -\sqrt{\frac{2}{3}} K(\alpha_{n+1}^{(k)}) + \|\boldsymbol{\xi}_{n+1}^{\mathrm{tr}}\| - \left(2\mu\Delta\gamma^{(k)} + \sqrt{\frac{2}{3}}[H(\alpha_{n+1}^{(k)}) - H(\alpha_n)] \right)$
$Dg(\Delta\gamma^{(k)}) := -2\mu \left(1 + \frac{H'(\alpha_{n+1}^{(k)}) + K'(\alpha_{n+1}^{(k)})}{3\mu} \right)$
$\Delta\gamma^{(k+1)} = \Delta\gamma^{(k)} - \frac{g(\Delta\gamma^{(k)})}{Dg(\Delta\gamma^{(k)})}$
$\alpha_{n+1}^{(k+1)} = \alpha_n + \sqrt{\frac{2}{3}}\Delta\gamma^{(k+1)}$
end while

Once the quantity $\Delta\gamma$ is obtained, then the stress state is corrected, along the

direction (2.79) via the following update equations.

$$\boldsymbol{q}_{n+1} = \boldsymbol{q}_n + \sqrt{\frac{2}{3}}(H(\alpha_{n+1}) - H(\alpha_n))\boldsymbol{n}_{n+1} \tag{2.80}$$

$$\boldsymbol{\varepsilon}^p_{n+1} = \boldsymbol{\varepsilon}^p_n + \Delta\gamma \boldsymbol{n}_{n+1} \tag{2.81}$$

$$\boldsymbol{\sigma}_{n+1} = \boldsymbol{\sigma}^{\text{tr}}_{n+1} - 2\mu\Delta\gamma\boldsymbol{n}_{n+1} \tag{2.82}$$

In order to properly account for the tangent stiffness for a plastically deforming material point, we need to be able the compute the algorithmic consistent tangent. Again, for the model of J_2 plasticity being discussed here, we can follow Simo and Hughes (1998), Chapter 3, where the authors derive the consistent tangent. The derivation begins with a differentiation of the algorithmic expression for the stress, $\boldsymbol{\sigma}_{n+1} = \boldsymbol{C} : (\boldsymbol{\varepsilon}_{n+1} - \Delta\gamma\boldsymbol{n}_{n+1} - \boldsymbol{\varepsilon}^p_n)$, using the chain rule

$$\mathrm{d}\boldsymbol{\sigma}_{n+1} = \left[\mathbb{C} - 2\mu\boldsymbol{n}_{n+1} \otimes \frac{\partial\Delta\gamma}{\partial\boldsymbol{\varepsilon}_{n+1}} - 2\mu\Delta\gamma\frac{\partial\boldsymbol{n}_{n+1}}{\partial\boldsymbol{\varepsilon}_{n+1}}\right] : \mathrm{d}\boldsymbol{\varepsilon}_{n+1} \tag{2.83}$$

Then the two partial derivative quantities are given by

$$\frac{\partial\Delta\gamma}{\partial\boldsymbol{\varepsilon}_{n+1}} = \left[1 + \frac{K'(\alpha_{n+1}) + H'(\alpha_{n+1})}{3\mu}\right]^{-1}\boldsymbol{n}_{n+1} \tag{2.84}$$

$$\frac{\partial\boldsymbol{n}_{n+1}}{\partial\boldsymbol{\varepsilon}_{n+1}} = \frac{2\mu}{\|\boldsymbol{\xi}^{\text{tr}}_{n+1}\|}\left(\mathbb{I} - \frac{1}{3}\mathbf{1}\otimes\mathbf{1}\right)\left(\mathbb{I} - \boldsymbol{n}\otimes\boldsymbol{n}\right). \tag{2.85}$$

The portion of the tangent due to plasticity then follows as

$$\begin{aligned}\boldsymbol{C}^* = &-\frac{2\mu}{\|\boldsymbol{\xi}^{\text{tr}}_{n+1}\|}\left(\mathbb{I} - \frac{1}{3}\mathbf{1}\otimes\mathbf{1}\right)\\ &- 2\mu\left[\left[1 + \frac{K'(\alpha_{n+1}) + H'(\alpha_{n+1})}{3\mu}\right]^{-1} - \frac{2\mu\Delta\gamma}{\|\boldsymbol{\xi}^{\text{tr}}_{n+1}\|}\right]\boldsymbol{n}_{n+1}\otimes\boldsymbol{n}_{n+1}.\end{aligned} \tag{2.86}$$

Then the consistent elastoplastic tangent can be found by adding the plastic contribution to the elastic contribution.

$$\boldsymbol{C}^{ep} = \boldsymbol{C} + \boldsymbol{C}^* \tag{2.87}$$

This tangent is then used to evaluate the element stiffness matrix, (2.51), where $\boldsymbol{C}^{ep}$ is used instead of $\boldsymbol{C}$.

This completes the local radial return procedure, and the results are used in the global system of equilibrium equations. A sketch of the algorithm can be seen in Algorithm 2.2. The process repeats until the global residual is reduced to a sufficiently small number. Once convergence is reached for a given time step, the state is incremented and the solution process begins again, until the total simulation time is reached.

2.3 Numerical Examples

To illustrate the concepts presented in chapters 2 and 2.2 some example simulations are presented below. In particular, representative load-displacement curves for a hardening material are shown along with proper convergence for a material specimen in torsion. The differences between isotropic and kinematic hardening are demonstrated for a boundary value problem with a reversal in loading. Also, the pathological mesh dependence is observed when a material exhibits softening behavior. This failure of convergence is of particular importance in modeling localization and failure problems.

2.3.1 Hardening

For the purposes of demonstration, consider a cylinder placed in torsion. This boundary value problem (BVP) produces a gradient in the strain field, and will be used to show proper convergence for both perfect plasticity and isotropic hardening. A schematic of the problem can be seen in Figure 2.6, which shows that one end of the cylinder is fixed in all three degrees of freedom, while the other end of the cylinder is given a prescribed rotation in the θ direction.

Algorithm 2.2 Predictor-corrector algorithm for classical plasticity

Predictor stage
Compute trial state
for each element **do**
$\boldsymbol{\sigma}^{\mathrm{tr}}_{n+1,j} = \mathbb{C} : (\boldsymbol{\nabla}^s \boldsymbol{u}_{n+1} - \boldsymbol{\varepsilon}^p_n)$
$\boldsymbol{q}^{\mathrm{tr}}_{n+1,j} = \boldsymbol{q}_n$
$\boldsymbol{\xi}^{\mathrm{tr}}_{n+1} = \operatorname{dev} \boldsymbol{\sigma}^{\mathrm{tr}}_{n+1,j} - \boldsymbol{q}_n$
$f^{\mathrm{tr}} = f(\boldsymbol{\sigma}^{\mathrm{tr}}_{n+1,j}, \boldsymbol{q}^{\mathrm{tr}}_{n+1,j})$
if $f \geq 0$ **then**
Add current element to list of plastic elements
else
$\boldsymbol{\sigma}_{n+1,j} = \boldsymbol{\sigma}^{\mathrm{tr}}_{n+1,j}$
end if
end for
Corrector stage
for each element in set of plastic elements **do**
Compute plastic quantities
Find $\Delta\gamma$ from Algorithm 2.1
$\boldsymbol{n}_{n+1} = \dfrac{\boldsymbol{\xi}^{\mathrm{tr}}_{n+1}}{\|\boldsymbol{\xi}^{\mathrm{tr}}_{n+1}\|}$
$\alpha_{n+1} = \alpha_n + \sqrt{\frac{2}{3}}\Delta\gamma$
Update quantities
$\boldsymbol{\sigma}_{n+1} = \boldsymbol{\sigma}^{\mathrm{tr}}_{n+1,j} - 2\mu\Delta\gamma\boldsymbol{n}_{n+1}$
$\boldsymbol{\varepsilon}^p_{n+1} = \boldsymbol{\varepsilon}^p_n + \Delta\gamma\boldsymbol{n}_{n+1}$
$\boldsymbol{q}_{n+1} = \boldsymbol{q}_n + \sqrt{\frac{2}{3}}\left(H(\alpha_{n+1} - \alpha_n)\right)\boldsymbol{n}_{n+1}$
Compute consistent tangent from (2.86) and (2.87)
end for
Assemble global stiffness and residual
Solve for $\boldsymbol{u}_{n+1,j+1}$
Check for global convergence
if $\|\boldsymbol{R}_{n+1,j}\| < \mathrm{TOL}$ **then**
Advance state $(\cdot)_{n+1} \rightarrow (\cdot)_n$
else
Increment equilibrium iteration, $j \rightarrow j+1$, return to predictor
end if

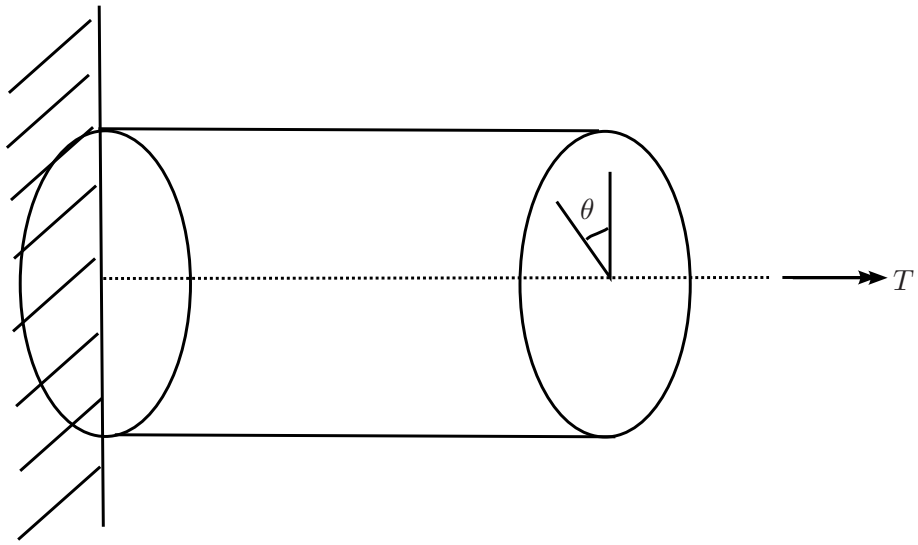

Figure 2.6: Schematic of the torsion BVP

First consider the case of perfect plasticity, which coincides with a hardening parameter of zero. This means that the deviatoric stress in the body cannot exceed a certain value, no matter how much the body is deformed. This is a useful test since we can obtain, in the asymptotic limit, an analytical solution for the torque when the cylinder has entered the fully plastic regime. From elasticity we know that the torque on a circular cross section is equal to the integral over the area of the shear stress multiplied by the radius. In this case the shear stress is limited by perfect plasticity to be $\tau_y = \sigma_y/\sqrt{3}$, where τ_y is the yield stress in shear and σ_y in the uni-axial yield strength. An expression for the torque follows.

$$T = \int_A (\tau_y r) r \, \mathrm{d}r \, \mathrm{d}\theta \tag{2.88}$$

$$T = \frac{\sigma_y \, 2\pi \, R^3}{3\sqrt{3}} \tag{2.89}$$

For the particular problem in question, with material constants from Table 2.1, the analytical solution for the applied torque is $T = 147.371$ [N-mm]. In Figure 2.7, torque versus radians of twist are plotted for increasingly fine mesh densities. Each curve is labeled by a mesh number. The number of tetrahedral elements for each

Parameter	Value [units]
Young's modulus, E	200.0E3 [MPa]
Poisson's ratio, ν	0.3
Yield strength, σ_y	975.0 [MPa]
Cylinder radius, R	0.5 [mm]

Table 2.1: Parameters used in the simulation of the torsion BVP

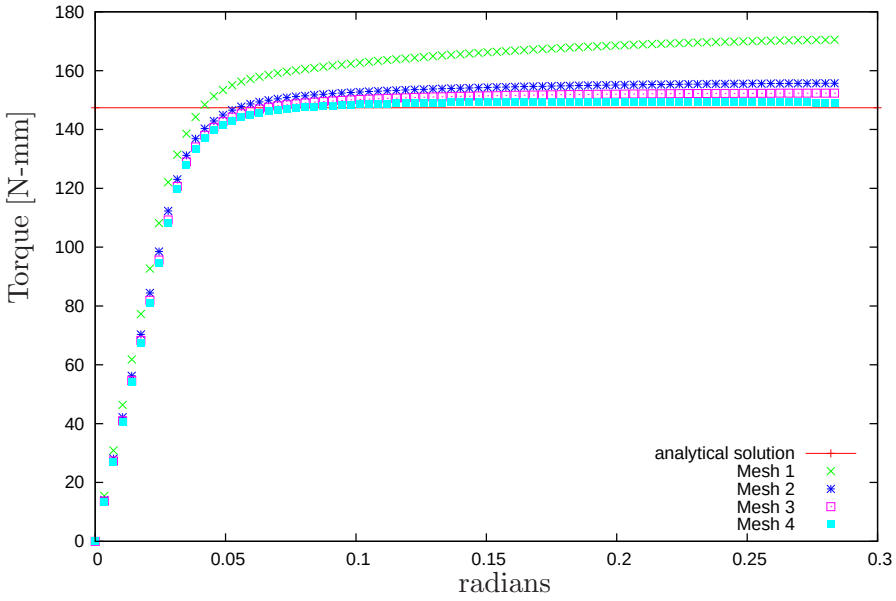

Figure 2.7: Perfect plasticity for the torsion BVP

mesh can be found in Table 2.2. The curves approach the analytical solution with mesh refinement, which shows that the computed solution is converging to the correct answer.

Next, we set the hardening parameter to be non-zero. As an example, we will choose it to be $22 * 10^3$ [MPa] (simply for convenience). Then, the same torsion BVP is solved for each of the meshes used in the perfect plasticity study, and the results

Mesh	Number of tets
Mesh 1	1031
Mesh 2	3882
Mesh 3	12159
Mesh 4	21517

Table 2.2: Number of elements per mesh for the torsion BVP

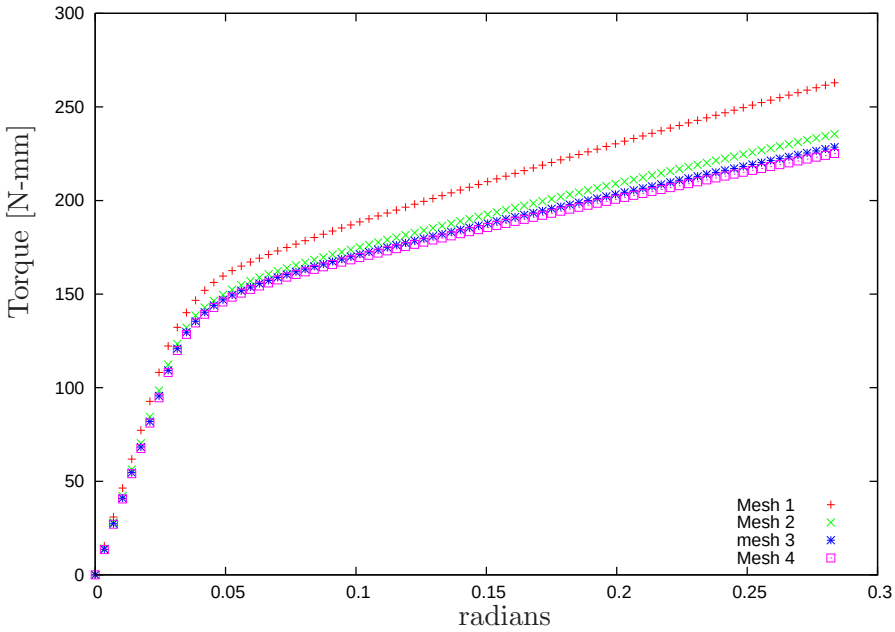

Figure 2.8: Isotropic hardening for the torsion BVP

can be seen in Figure 2.8. Again, note that as the mesh is refined, the curves begin to converge to one solution. It should be intuitive from Figures 2.7 and 2.8, even without the mathematical machinery of a solution convergence analysis, that classical plasticity with hardening and perfect plasticity are well-posed and well behaved. This is true even rigorously, but is not the case where the hardening modulus becomes negative, which is the subject of Section 2.3.2.

Another important example, reverse loading, differentiates isotropic hardening from kinematic hardening. Recall from Section 2.1.3 that isotropic hardening expands the yield surface isotropically, whereas kinematic hardening is a translation of the yield locus in stress space. Kinematic hardening is used to model the *Bauschinger effect*, which is observed as a decrease in yield strength of a material when the direction of loading is changed. In the isotropic case, upon reverse loading after experiencing plastic deformation in the first direction, the radius of the yield surface will have expanded, which leads to a compressive yield stress larger in magnitude

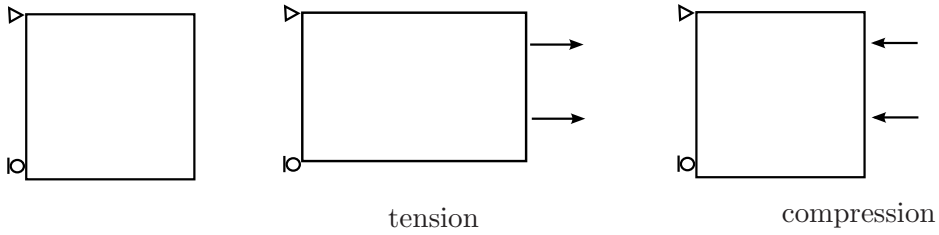

Figure 2.9: Cyclic loading: tension followed by compression

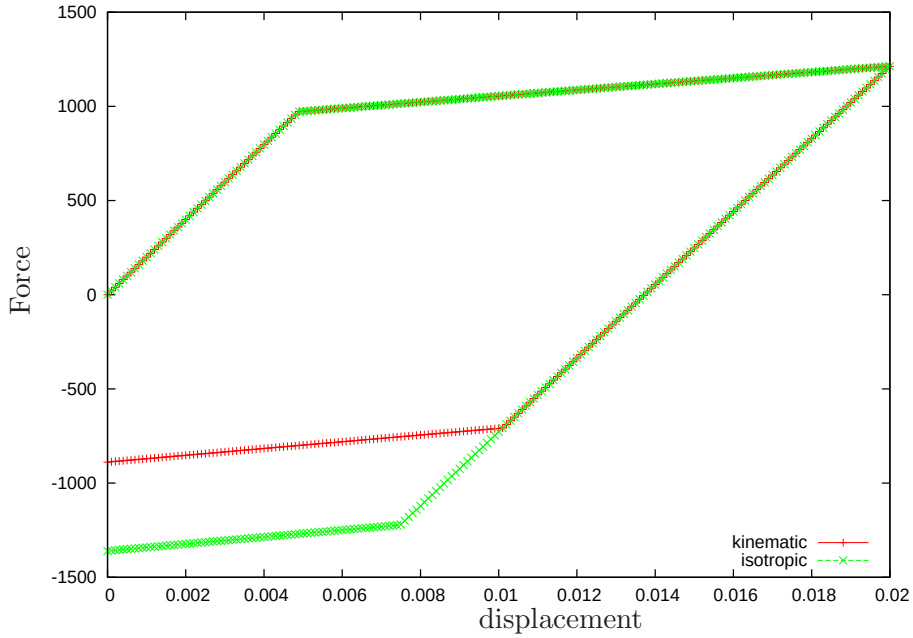

Figure 2.10: Illustration of the Bauschinger effect

than the initial yield stress. For kinematic hardening, the radius of the yield surface does not change, so that upon unloading the magnitude of the compressive yield point turns out to be smaller than the initial yield stress by an amount equal to the hardening experienced in the first stage. For a schematic of the loading, see Figure 2.9 and for a plot of both isotropic and kinematic hardening models, see Figure 2.10.

2.3.2 Softening

To illustrate the pathological mesh dependence induced by material softening, we now consider a plane strain BVP of a plate in compression. The intent is to reproduce a localization in the body such as a shear band, see Lewandowski and

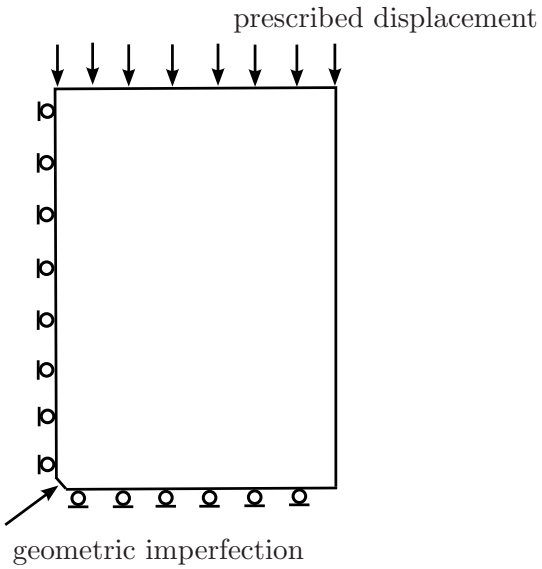

Figure 2.11: Schematic of the plane strain compression BVP

Greer (2005) and Meyers et al. (2003). For a schematic of the simulation, refer to Figure 2.11. The plate is modeled with a geometric imperfection to force consistent localization in a band oriented at 45°. The same elastic properties were used as in the torsion BVP above, but now the hardening modulus is prescribed as an exponentially decreasing function of the equivalent plastic strain, α. The form of the hardening modulus indicates material softening, and can be seen in (2.90).

$$K(\alpha) = 975.0 \exp(-3\alpha) \tag{2.90}$$

Figure 2.12 shows a negative slope on the load-displacement curve after the yield point, and also that as the mesh is refined, the solution no longer begins to converge to a unique solution as the slope tends to get more negative. Table 2.3 provides the number of elements used in each of the four meshes, in ascending order. This is one view of the mesh dependence associated with softening.

Another, somewhat more direct view of the mesh dependence of softening can come from examination of the shear band produced for each mesh resolution, see Figure 2.13. The equivalent plastic strain, α, was plotted on each deformed mesh,

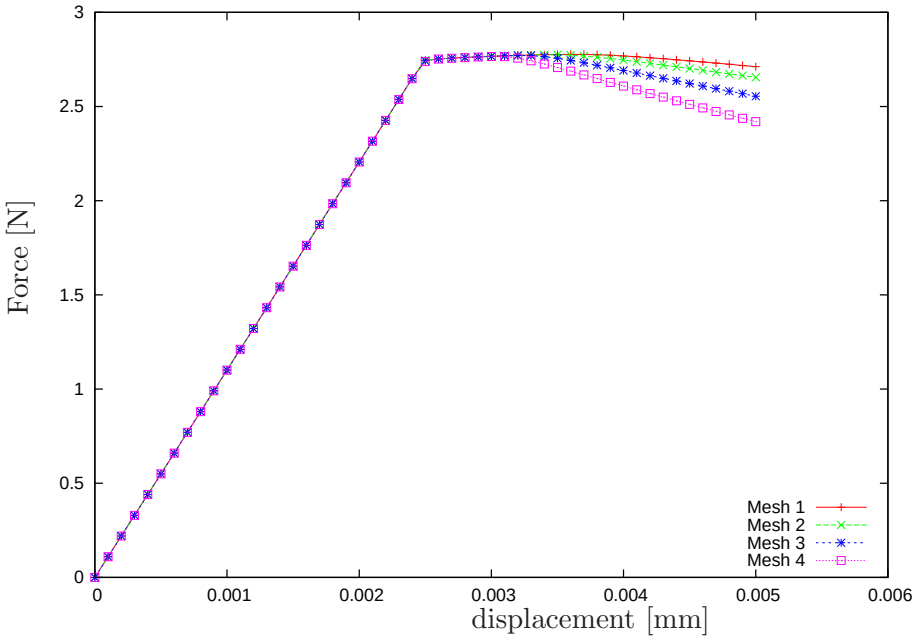

Figure 2.12: Softening in the plane strain compression BVP

Mesh	Number of tets
Mesh 1	3420
Mesh 2	7998
Mesh 3	37226
Mesh 4	111916

Table 2.3: Number of elements per mesh for the plane strain compression BVP

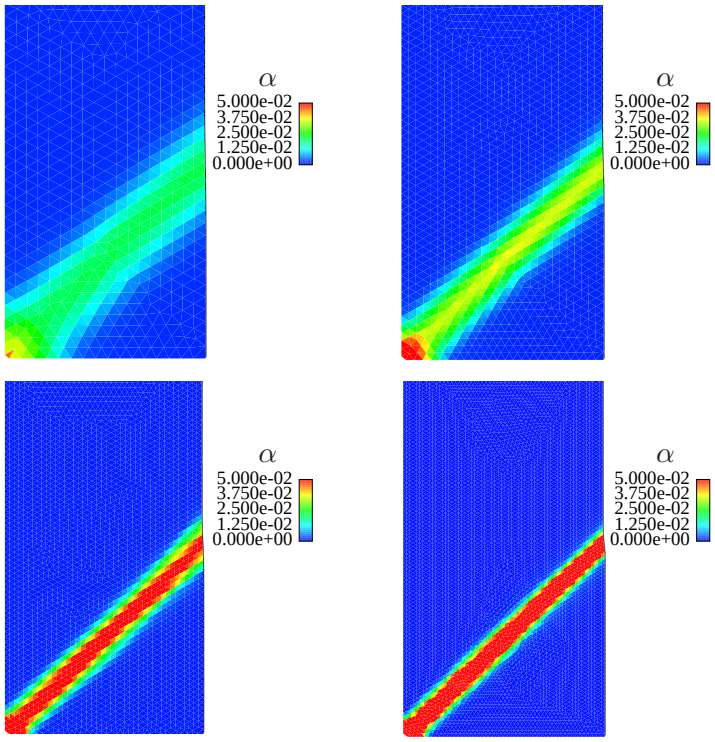

Figure 2.13: Equivalent plastic strain for each mesh

and set to the same scale for comparison. Note that there is no convergence of the shear band as the mesh is refined, indicating an underlying ill-posedness of the classical theory. Mesh dependence in strain localization problems is a direct consequence of the fact that the solution is not unique. The elements along the shear bands seen in Figure 2.13 introduce a length scale to the problem by which the energy associated with plastic deformation gets dissipated. Since there is no naturally occurring length scale in the continuum formulation of the problem to govern the dissipation of energy, every mesh with a different characteristic length scale will produce a different result, the very definition of mesh dependence. One interpretation of this phenomenon is an ill-posedness of strain softening problems, as the tangent modulus tensor loses *strong ellipticity*. Various methods to introduce a length scale and regularize solutions have been presented. Variational multiscale approaches are introduced in Garikipati and

Hughes (1998) and Garikipati and Hughes (2000), where a fine scale is introduced to model the microstructure. Nonlocal approaches were introduced in Bazant et al. (1984), which introduce a length scale by integrating a volume with a given radius, usually encompassing multiple element diameters. For gradient models, the introduction of another gradient, say of the plastic strain, needs some sort of length scale to remain dimensionally consistent. For example, the model in Aifantis (1987) that includes the Laplacian of the equivalent plastic strain introduces such a length scale. That model is applicable to problems of localization and shear as shown here. In Fleck and Hutchinson (2001) multiple length scales are introduced in an effort to model different micromechanical deformation mechanisms. These length scales can then be utilized as mechanisms for energy dissipation, rendering the solution mesh independent.

CHAPTER 3

Dislocation Based Plasticity

This chapter is devoted to an elementary discussion of dislocation theory in the context of describing plastic deformation, and the extension of these ideas into a continuum treatment. Dislocation theory provides some insight into the micro-mechanical behavior of single and polycrystalline materials. In particular, the origins of dislocation theory are concerned with metals, which are indeed polycrystalline. Dislocation theory, however, does not provide a definitive model of plastic behavior at the macro scale, the reason being that interactions between dislocations and their surrounding environments, which may include obstacles such as grain boundaries or even other dislocations, are far too numerous and complex to be efficiently modeled. All encompassing theory lacking, some aspects of plastic deformation can be described quite well by dislocation theory and for that reason, and the fact that the generally accepted mechanism for plastic flow is dislocation motion, it is worth taking the time to understand.

3.1 Plasticity in Crystals

A crystal is a solid formed by a three-dimensional pattern of repeating atoms which form a lattice. For metals, there are three particular patterns which occur most often, hexagonal close packed (HCP), face centered cubic (FCC), and body centered cubic (BCC). Figure 3.1 shows examples of each of these crystal structures,

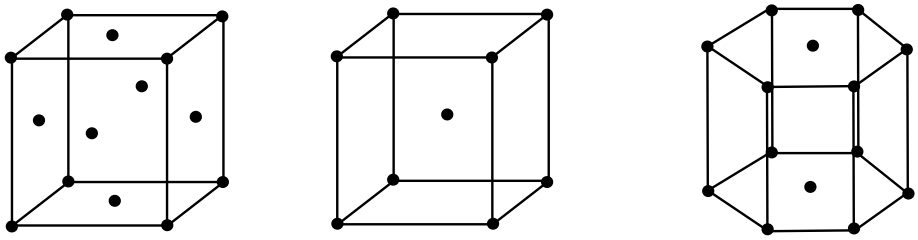

a) b) c)

Figure 3.1: Common metal crystals: a) FCC, b) BCC, c) HCP

Crystal Structure	Metal
FCC	Aluminum, Copper, Gold
BCC	α-Iron, Tungsten
HCP	Zinc, Magnesium

Table 3.1: Examples of FCC, BCC, and HCP metals

and Table 3.1 gives examples for each crystal structure. The notion of *slip* embodies the idea of the relative motion between atoms. The lattice structure, or pattern, gives rise to two crystallographic quantities, slip planes and slip directions. Slip planes are planes which are parallel to the planes of atoms which have the closest packing distance. The closest packing distance is the direction in which the distance between atoms is the smallest. Within a slip plane, directions parallel to the closest packing distance are called slip directions. Together for a given crystal, slip planes and slip directions are known as *slip systems*. It is observed experimentally that plastic deformation is the result of the slip, or relative atomic motion, along slip planes under a given shear stress.

One method for determining the shear stress necessary to achieve slip along the favorable crystallographic directions is know as Schmid's law. Consider a single crystal tensile specimen under a stress σ along its axis, which forms an angle ϕ with the normal of a slip plane, and another angle λ with the slip direction. The shear stress resolved along the slip plane that produces plastic deformation, known as the critically resolved shear stress, can be seen in (3.1). For a schematic depiction of the

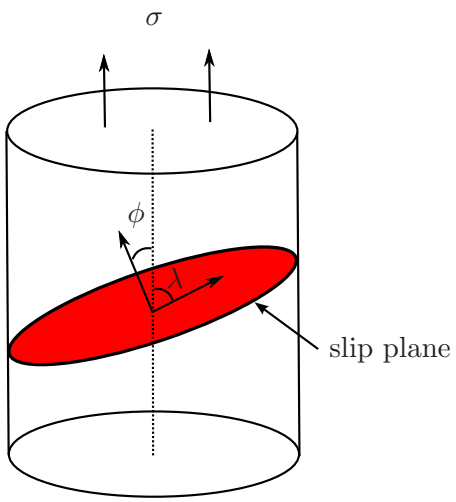

Figure 3.2: Slip plane in a body under uniaxial tension

process, see Figure 3.2.

$$\tau_c = \cos\phi \cos\lambda \, \sigma \tag{3.1}$$

If we consider that slip is the primary mechanism for plastic deformation, then it is plausible to determine the shear stress necessary to displace one plane of atoms over another. The result is the theoretical shear strength of a material. To calculate a simple approximation, assume the stress necessary to move the top plane of atoms in Figure 3.3 is periodic. This assumption is justified by noting that if the lattice is initially in equilibrium, then a displacement of $x = b$ will return it to equilibrium, and a displacement of $x = b/2$ would place it in an unstable equilibrium.

$$\tau = \tau_{max} \sin \frac{2\pi x}{b} \tag{3.2}$$

Now to first-order, $\tau = 2\pi\tau_{max}x/b$, and for a small displacement, x, we know from elasticity that $\tau = G\gamma$, where the shear strain $\gamma = x/a$. It follows that

$$\tau_{max} = \frac{Gb}{2\pi a}. \tag{3.3}$$

Observe that in (3.3), the theoretical shear strength of a material is within an order of magnitude of the shear modulus G if b is close to a. The startling observation that

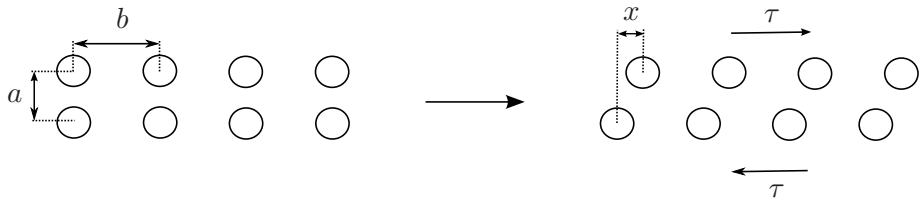

Figure 3.3: Relative displacement of a whole plane of atoms

prompted development of the theory of dislocations was that actual measurements of the shear strength of single crystals are *three to five orders of magnitude less* than the shear modulus. Obviously, the mechanism for plastic deformation was not whole planes of atoms in relative motion.

To resolve the discrepancy between the theoretical shear strength and measured values the concept of dislocations as specific defects in the lattice was proposed by both G.I. Taylor and E. Orowan circa 1934, for reference see the work by Taylor Taylor (1938). The basic idea proposes dislocations as line defects in a lattice, or a line of vacancies, which then permit the relative motion of only a few atoms to achieve slip. This theory sufficiently accounts for observed shear strengths, as will be seen below. Two basic types of dislocations exist: edge and screw. Edge dislocations can be thought of as arising from inserting an extra plane of atoms into an existing crystal. At the termination of the extra plane the lattice becomes distorted. The imperfection in the distorted lattice can be characterized by the lack of closure of a loop, or *Burger's circuit*, through the unperturbed lattice around the imperfection. This characterization is referred to as the Burger's vector, and can be thought of as a measure of the *incompatibility* of the lattice. For an illustration of the Burger's vector, $\boldsymbol{b}$,[1] for an edge dislocation, see Figure 3.4. Note that the dislocation line, recalling that dislocations are line defects, would continue in and out of the page from the point of imperfection, and that the dislocation line is perpendicular to the

[1]Not to be confused with a body force, which should subsequently be clear from the context.

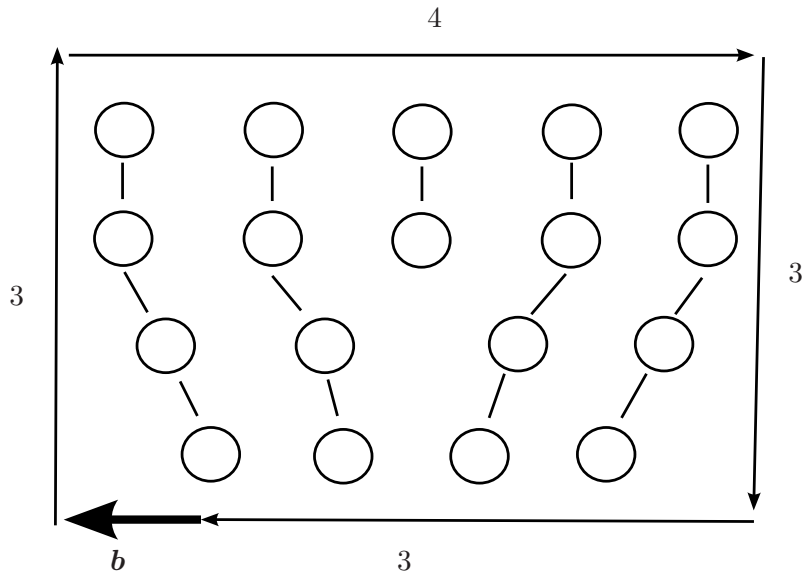

Figure 3.4: An edge dislocation with Burger's vector, $\boldsymbol{b}$

Burger's vector for an edge dislocation. A screw dislocation, as can be seen in the three dimensional schematic in Figure 3.5, can be thought of as making a partial cut through a lattice, and then displacing the cut portions in a shear direction until the lattice lines up again. A significant distinction between edge and screw dislocations is the fact that while edge dislocations have $\boldsymbol{b}$ perpendicular to the dislocation line, screw dislocations have $\boldsymbol{b}$ parallel to the dislocation line. In reality, dislocations may be of mixed character, meaning that a portion of the dislocation has edge character, and a portion has screw character. However, the Burger's vector is conserved.

To make concrete the connection between plasticity and dislocations, consider a lattice with a dislocation present under an applied shear stress. When the stress reaches a critical value, it becomes energetically favorable for bonds between atoms to switch, effectively transporting the dislocation through the lattice. This *dislocation motion* is the primary mechanism for plastic deformation in crystalline materials. It is worth pointing out that while the presence of a dislocation within a crystal lattice induces a local elastic stress field, plastic deformation is not realized until a

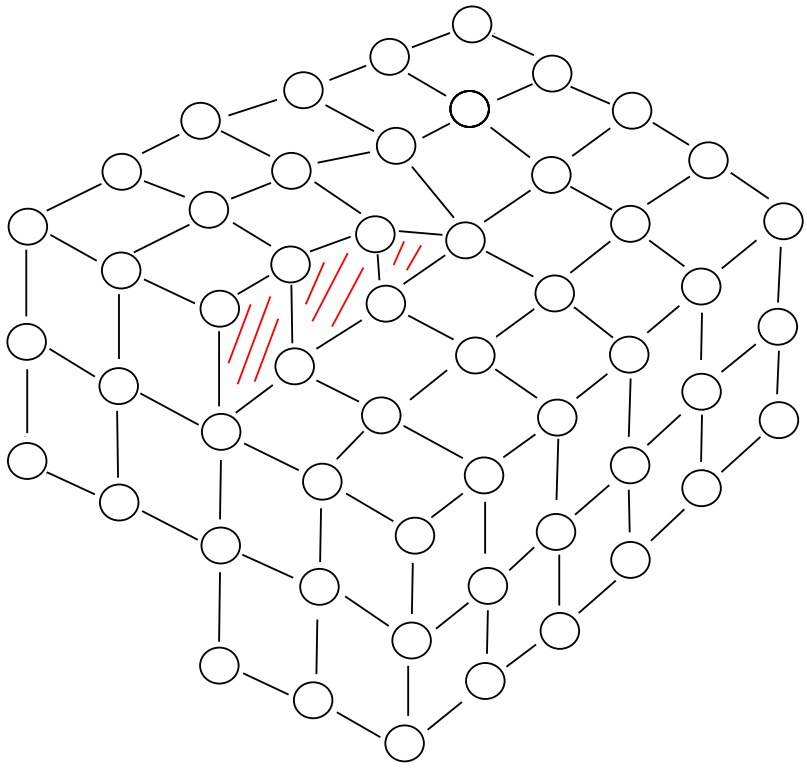

Figure 3.5: A screw dislocation

sufficient applied stress causes that dislocation to move. A simple schematic of an edge dislocation progressing through a lattice under an applied shear stress, τ, can be seen in Figure 3.6.

A better approximation for the applied stress necessary to produce dislocation

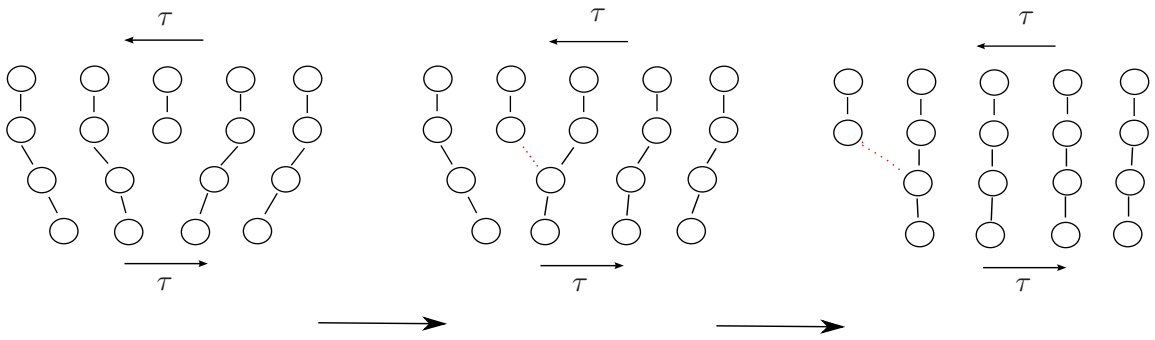

Figure 3.6: Edge dislocation moving through a lattice

motion than the theoretical shear strength (3.3) is given by the Peirls-Nabarro stress.

$$\tau_{PN} = \frac{2G}{1-\nu} \exp\left(\frac{-2\pi h}{d(1-\nu)}\right) \tag{3.4}$$

In (3.4), h denotes the distance between adjacent planes of atoms, d denotes the distance between atoms in each plane, G is the shear modulus, and ν is Poisson's ratio. The first notable observation from (3.4) is that the predicted critical shear stress is on the order of experimental observations for single crystals. Second, as the ratio h/d increases, τ_{PN} decreases, which corresponds to more densely packed planes and/or larger separation between close packed planes, which is consistent with the notion of slip systems playing an important role in a material's plastic behavior.

Dislocation theory can also be applied to explain how a material work hardens under an applied load. The notion of hardening at the micro-structural level can be expressed as the increased load necessary to continue to move a dislocation through a lattice when it has encountered an obstacle. This increased load manifests as hardening in a macroscopic load displacement curve. Consider a polycrystalline aggregate, such as a metal, comprised of multiple grains at different orientations. Then the crystal structure is generally not continuous across grain boundaries. Consider also that within each grain the crystal structure is likely imperfect and contains dislocations of various character. Now consider an applied load sufficient in magnitude to produce dislocation motion. Taking an elementary view yields two observations. First, as dislocations move within a crystal grain, they will encounter other dislocations that will serve as obstacles, increasing the stress necessary to propagate them further. Second, grain boundaries will also act to impede the motion of dislocations, again increasing the applied load necessary to produce dislocation motion. These are two of the simplest examples of hardening in a polycrystalline material.

An explanation for the Bauschinger effect, discussed in Sections 2.1.3 and 2.3.1,

comes from the idea that dislocations tend to pile-up at grain boundaries. To further this notion, the idea of *dislocation annihilation* needs to be introduced. Imagine another edge dislocation, similar to Figure 3.4, except that the extra plane of atoms is inserted from the bottom of the lattice instead of from the top. These two dislocations would have opposite *sign*. It follows that when two dislocations of opposite sign interact, the net result is dislocation annihilation, leaving the lattice unperturbed. Another point to make is that dislocations of the same sign have stress fields that tend to repulse one another. With these two concepts stated, the Bauschinger effect can be explained as follows in two parts. First, upon loading dislocations of like sign pile up at grain boundaries, creating a back stress due to the same sign repulsion. Upon unloading, the repulsion aids in dislocation motion in the reverse direction, effectively reducing the yield strength. The second part to the explanation assumes that dislocations of the opposite sign are produced when the loading is reversed, and the interaction of the new dislocations with those already existing causes annihilation, reducing the total number of potential obstacles and the yield strength in the process.

It is left to describe how dislocations are produced within a crystal in order to explain both the second explanation of the Bauschinger effect, and the fact that some materials can achieve extremely high levels of plastic deformation. For the latter, if the dislocation number was fixed from the initial state, a material would be limited in the amount of plastic deformation it could experience by the number of dislocations it has, which is not the case. One such explanation for dislocation generation is known as a Frank-Read source. To begin, consider a dislocation line, fixed at the nodes A and B, subject to an applied load. The obstacles preventing the motion of the dislocations at A and B are not important for this description, but could be point defects or other obstacles that render the dislocation immobile

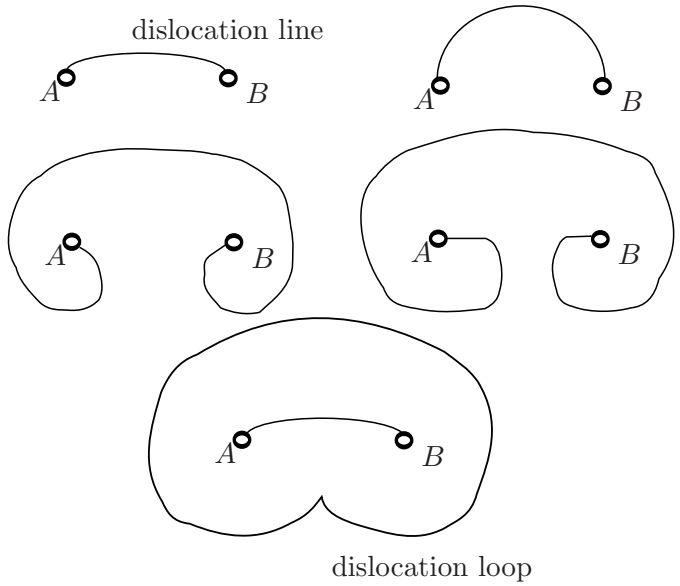

Figure 3.7: A Frank-Read source for dislocation generation

at those points. Under the applied load, the dislocation line will bulge out in the direction of the stress, and will eventually reach a critical point where it will spiral around the pinning points. When the dislocation loop meets with itself, it annihilates creating a complete dislocation loop and a new dislocation line between the pinning points, A and B. For a visual depiction of the Frank-Read source, refer to Figure 3.7. Other dislocation generation mechanisms exist as well, such as multiple cross slip, which will not be discussed here.

The ideas presented above represent just an elementary view of the science of dislocations. Concepts such as temperature dependence, dislocation glide and climb, velocity and density have been omitted from this discussion. It should be clear that dislocation motion is capable of describing plasticity and hardening mechanisms in single crystals and polycrystalline aggregates. Lacking is an efficient and general bridge between the micro-mechanical behaviors and the macro-scale continuum theories of plasticity. Subsequent developments in this document will attempt to address this issue, presenting an incompatibility based hardening mechanism within the con-

text of a continuum theory.

3.2 Extending Burger's Vector to the Continuum

The objective of this section is to use the concept of the Burger's vector, $\boldsymbol{b}$, introduced above and develop a continuum measure of incompatibility. The continuum quantity that can be related to a measure of the incompatibility in a lattice is termed the *Burger's tensor*, and is denoted by $\boldsymbol{G}$. The concept of the Burger's tensor has been extensively studied, for background see Cermelli and Gurtin (2001) and references within. Modern treatments begin in the general setting with the multiplicative decomposition of the deformation gradient into elastic and plastic parts, as in (3.5), due largely to Lee (1969) and Kroner and Teodosiu (1972).

$$\boldsymbol{F} = \boldsymbol{F}^e \boldsymbol{F}^p \tag{3.5}$$

Note that in the context of finite deformation the additive decomposition, (2.13), no longer holds in general, but can be recovered from the general theory under certain small strain assumptions. The physical significance of (3.5) in the context of crystal plasticity can be found in Asaro (1983), where the plastic part of the deformation gradient, $\boldsymbol{F}^p$, is due solely to the plastic slip along the slip planes of the lattice in question.

Using the multiplicative decomposition, various definitions of $\boldsymbol{G}$ are compared and contrasted in Cermelli and Gurtin (2001). The main objective of the remainder of this section will be to derive a $\boldsymbol{G}$ suitable for formulating a small strain continuum constitutive theory, and for this reason the following material will follow closely with the work in Gurtin (2004). We can restrict the theory to the small strain context pertinent to this dissertation by recalling a particular definition of the deformation gradient seen in (A.9). Then the small strain version of the multiplicative

decomposition of the deformation gradient becomes the additive decomposition of the displacement gradient as in (3.6).

$$\boldsymbol{\nabla u} = \boldsymbol{H}^e + \boldsymbol{H}^p \tag{3.6}$$

Here, $\boldsymbol{H}^e$ is now the elastic part of the displacement gradient, and $\boldsymbol{H}^p$ is the plastic part of the displacement gradient. As plastic deformation is observed to be isochoric, an additional restriction is placed on the plastic part of the displacement gradient, or plastic distortion, namely $\operatorname{tr} \boldsymbol{H}^p = 0$. The insistence that $\boldsymbol{H}^p$ be deviatoric is similar to the construction of $\boldsymbol{\varepsilon}^p$ as deviatoric in the classical theory. A pertinent feature of the theory is that there is no assumption, *a priori*, that the plastic spin, $\boldsymbol{\omega}^p = \operatorname{skew} \boldsymbol{H}^p$,[2] provides no contribution to the free energy of the plastically deformed body as in the classical theory. In fact, assuming zero plastic spin is the simplest possible assumption to recover the additive decomposition of strain in the classical theory, because the classical theory only deals with strains, which are the symmetric part of the displacement gradients. The inclusion of the plastic spin occurs as a natural consequence of the characterization of the Burger's tensor in a continuum body. A measure of the incompatibility in the plastic distortion, $\boldsymbol{H}^p$, can be related to the Burger's vector via Stokes' theorem, which integrates an infinitesimal loop, similar to the Burger's circuit mentioned above. In the small strain setting where configuration mapping terms can be neglected, for a smooth oriented surface, S with boundary ∂S

$$\oint_{\partial S} \boldsymbol{H}^p \, \mathrm{d}\boldsymbol{X} = \int_S (\operatorname{curl} \boldsymbol{H}^p)^{\mathsf{T}} \boldsymbol{n} \, \mathrm{d}A, \tag{3.7}$$

where $\boldsymbol{n}$ is the unit normal to the surface S. Then the definition of the Burger's

[2]Recall the Euclidean decomposition of a second rank tensor, $\boldsymbol{T}$, into its symmetric and skew symmetric parts, $T_{ij} = S_{ij} + W_{ij}$, where $S_{ij} = S_{ji}$ and $W_{ij} = -W_{ji}$. Then we say the $\boldsymbol{H}^p$ can be decomposed into the plastic strain and plastic spin as $\boldsymbol{H}^p = \boldsymbol{\varepsilon}^p + \boldsymbol{\omega}^p$.

tensor follows as

$$\boldsymbol{G} = \operatorname{curl} \boldsymbol{H}^p. \tag{3.8}$$

The quantity $\boldsymbol{G}^{\mathrm{T}}\boldsymbol{n}$ gives a measure of the Burger's vector, per unit area, for a plane with unit normal, $\boldsymbol{n}$. It is worth noting that for a theory to properly capture the effects of the Burger's tensor, the evolution of the plastic spin must be accounted for, since $\boldsymbol{H}^p = \boldsymbol{\varepsilon}^p + \boldsymbol{\omega}^p$, and $\boldsymbol{G} = \operatorname{curl} \boldsymbol{H}^p$. It follows that classical methods, which do not have any notion of plastic spin, are not equipped to deal with the notion of the Burger's vector correctly.

The Burger's vector, per unit area, $\boldsymbol{G}^{\mathrm{T}}\boldsymbol{n}$, can be thought of as evolving according to a balance. Consider the time rate of change,

$$\dot{\overline{\boldsymbol{G}^{\mathrm{T}}\boldsymbol{n}}} = (\operatorname{curl} \dot{\boldsymbol{H}}^p)^{\mathrm{T}}\boldsymbol{n} = -\operatorname{div}\,(-\dot{\boldsymbol{H}}^p(\boldsymbol{n}\times)), \tag{3.9}$$

where $(\boldsymbol{n}\times)$ is the skew tensor $(\boldsymbol{n}\times)_{ij} = \varepsilon_{irj}n_r$, and $\dot{\boldsymbol{H}}^p(\boldsymbol{n}\times)$ represents a tensorial Burger's vector flux through planes with normal $\boldsymbol{n}$. As a result of this balance, we have the following result,

$$\dot{\boldsymbol{H}}^p(\boldsymbol{n}\times) = 0, \tag{3.10}$$

which holds at a particular point if and only if there is no Burger's vector flow across the plane with unit normal $\boldsymbol{n}$.

CHAPTER 4

Gradient Plasticity

The objectives of this chapter are the development of a gradient dependent plasticity constitutive model using the concepts introduced in Chapter 3. The constitutive model is based on the work of Gurtin (Gurtin, 2004) and uses the concept of the Burger's tensor, $\boldsymbol{G}$, introduced in Section 3.2.

4.1 Constitutive Model

To begin the development of the gradient dependent constitutive model, recall the additive decomposition of the displacement gradient into elastic and plastic parts from Section 3.2.

$$\boldsymbol{\nabla u} = \boldsymbol{H}^e + \boldsymbol{H}^p$$

Also recall that $\operatorname{tr} \boldsymbol{H}^p = 0$, indicating the deviatoric nature of the plastic distortion. A priority in development of the theory is a mechanism by which to account for the Burger's vector and Burger's vector flux, and so the theory will depend on the definition of the Burger's tensor,

$$\boldsymbol{G} = \operatorname{curl} \boldsymbol{H}^p.$$

The principal of virtual power will be employed to derive the macroscopic balance of momenta, and what Gurtin terms the microforce balance, by which we will determine the flow rule. In order to achieve a theory that accounts for incompatibilities,

two stresses are introduced, $\boldsymbol{T}^p$ and $\mathbb{S}$, conjugate to $\boldsymbol{H}^p$ and $\boldsymbol{G}$ respectively. Then we can define the internal power as

$$\mathscr{W}_{int} = \int_\Omega \boldsymbol{\sigma} : \dot{\boldsymbol{H}}^e + \boldsymbol{T}^p : \dot{\boldsymbol{H}}^p + \mathbb{S} : \dot{\boldsymbol{G}} \, \mathrm{d}V \tag{4.1}$$

where $\boldsymbol{\sigma}$ is the Cauchy stress, $\boldsymbol{T}^p$ is termed the microstress which has deviatoric nature like $\boldsymbol{H}^p$ ($\operatorname{tr} \boldsymbol{T}^p = 0$), and $\mathbb{S}$ is termed the defect stress. Next, the external power can be defined as

$$\mathscr{W}_{ext} = \int_\Omega \boldsymbol{b} \cdot \dot{\boldsymbol{u}} \, \mathrm{d}V + \int_{\partial\Omega} \boldsymbol{S}(\boldsymbol{n}) : \dot{\boldsymbol{H}}^p + \boldsymbol{t}(\boldsymbol{n}) \cdot \dot{\boldsymbol{u}} \, \mathrm{d}S, \tag{4.2}$$

where $\boldsymbol{b}$ is now the body force (not to be confused with the Burger's vector which henceforth will not be explicitly mentioned), $\boldsymbol{t}(\boldsymbol{n})$ is a macroscopic traction, and $\boldsymbol{S}(\boldsymbol{n})$ is a microtraction related to the flow of dislocations across surfaces. All stress and stress-like quantities are assumed to be invariant under superposed rigid rotations. For a brief introduction to material frame invariance, or objectivity, see Section A.4 in the Appendix.

Using the expressions in (4.1) and (4.2), we denote a set of virtual velocities, $\mathscr{V} = (\boldsymbol{w}, \boldsymbol{v}, \boldsymbol{V})$ corresponding to $\dot{\boldsymbol{u}}$, $\dot{\boldsymbol{H}}^e$, and $\dot{\boldsymbol{H}}^p$. The following requirements are placed on the virtual velocities, consistent with their non-virtual counterparts.

$$\nabla \boldsymbol{w} = \boldsymbol{v} + \boldsymbol{V} \tag{4.3}$$

$$\operatorname{tr}(\boldsymbol{V}) = 0 \tag{4.4}$$

It is assumed that the virtual velocities transform under superposed rigid rotations in a similar manner as the quantities from which they are derived, which gives $\boldsymbol{v} \to \boldsymbol{v} + \boldsymbol{W}$ for a rigid rotation, $\boldsymbol{W}$, while $\boldsymbol{V}$ and $\operatorname{curl} \boldsymbol{V}$ are invariant. We arrive at the virtual internal and external power by inserting the relevant virtual terms into (4.1)

and (4.2).

$$\mathscr{W}_{int}(\mathscr{V}) = \int_\Omega \boldsymbol{\sigma} : \boldsymbol{v} + \boldsymbol{T}^p : \boldsymbol{V} + \mathbb{S} : \operatorname{curl} \boldsymbol{V} \, \mathrm{d}V \tag{4.5}$$

$$\mathscr{W}_{ext}(\mathscr{V}) = \int_\Omega \boldsymbol{b} \cdot \boldsymbol{w} \, \mathrm{d}V + \int_{\partial\Omega} \boldsymbol{S}(\boldsymbol{n}) : \boldsymbol{V} + \boldsymbol{t}(\boldsymbol{n}) \cdot \boldsymbol{w} \, \mathrm{d}S \tag{4.6}$$

The principal of virtual power can then be stated as a balance between virtual internal and external power, and frame indifference of the internal virtual power.

$$\mathscr{W}_{int}(\mathscr{V}) = \mathscr{W}_{ext}(\mathscr{V}) \tag{4.7}$$

Next, the macroscopic momentum balances will be derived. As a validation exercise, we attempt to obtain the classical balance of momenta by considering a rigid rotation, $\boldsymbol{Q}$. The only term in the virtual power that is not invariant by construction is $\boldsymbol{v}$ (the virtual velocity of $\dot{\boldsymbol{H}}^e$), which transforms as $\boldsymbol{v} + \boldsymbol{Q}$. As in the classical theory, for invariance to hold, $\boldsymbol{\sigma} : \boldsymbol{Q} = 0$, which implies that the Cauchy stress must be symmetric, precisely the same result obtained from the balance of angular momentum.[1] Now, considering a generalized virtual velocity $\boldsymbol{V} = 0$, such that $\nabla \boldsymbol{w} = \boldsymbol{v}$, we can, in the standard way, use the divergence theorem to obtain the classical statement of equilibrium and the traction condition. Starting with (4.7) and using (4.5) and (4.6) with $\boldsymbol{V} = 0$ we obtain

$$\int_{\partial\Omega} \boldsymbol{t}(\boldsymbol{n}) \cdot \boldsymbol{w} \, \mathrm{d}S + \int_\Omega \boldsymbol{b} \cdot \boldsymbol{w} \, \mathrm{d}V = \int_\Omega \boldsymbol{\sigma} : \boldsymbol{v} \, \mathrm{d}V = \int_\Omega \boldsymbol{\sigma} : \nabla \boldsymbol{w} \, \mathrm{d}V, \tag{4.8}$$

where the second equality holds since $\boldsymbol{v} = \boldsymbol{\nabla} \boldsymbol{w}$. We can use the divergence theorem to obtain

$$\int_{\partial\Omega} (\boldsymbol{t}(\boldsymbol{n}) - \boldsymbol{\sigma}\boldsymbol{n}) \cdot \boldsymbol{w} \, \mathrm{d}S + \int_\Omega (\operatorname{div} \boldsymbol{\sigma} + \boldsymbol{b}) \cdot \boldsymbol{w} \, \mathrm{d}V = 0, \tag{4.9}$$

[1] In Gurtin's work he does not assume at the outset, as we have here, that the stress, which he denotes as $\boldsymbol{T}$, is symmetric, and uses this exercise to show that the classical stress measure is recovered. Here we are simply verifying what we already know from the balance of angular momentum, namely that $\boldsymbol{\sigma}$ must be symmetric.

from which, using the arbitrariness of $\boldsymbol{w}$, we arrive at the desired result.

$$\operatorname{div} \boldsymbol{\sigma} + \boldsymbol{b} = \boldsymbol{0} \tag{4.10}$$

$$\boldsymbol{t}(\boldsymbol{n}) = \boldsymbol{\sigma}\boldsymbol{n} \tag{4.11}$$

The flow rule for this theory comes from a microforce balance. The microforce balance can be thought of as the microscopic counterpart of the macroscopic balances. To that end we introduce an identity that is essentially the integration by parts of one of the terms in the virtual internal power. For tensor fields $\boldsymbol{A}$ and $\boldsymbol{B}$,

$$-\int_{\partial\Omega} (\boldsymbol{n} \times \boldsymbol{A}) : \boldsymbol{B}^{\mathrm{T}} \, \mathrm{d}S = \int_{\Omega} \left(\boldsymbol{A} : \operatorname{curl} \boldsymbol{B} - \boldsymbol{B}^{\mathrm{T}} : \operatorname{curl} \left(\boldsymbol{A}^{\mathrm{T}} \right) \right) \, \mathrm{d}V. \tag{4.12}$$

For a proof of (4.12), please see Appendix B, Section B.2. The tensor $\boldsymbol{n}\times$ is the skew object created from defining the axial vector $\boldsymbol{n}$. This becomes a useful way to restate the first term in (4.12). Moving on, we choose a virtual velocity $\boldsymbol{w} = 0$, so that $\boldsymbol{v} = -\boldsymbol{V}$, and we then write the associated virtual power relation from (4.7), again using (4.5) and (4.6).

$$\int_{\partial\Omega} \boldsymbol{S}(\boldsymbol{n}) : \boldsymbol{V} \, \mathrm{d}S = \int_{\Omega} \left((\boldsymbol{T}^{p} - \boldsymbol{\sigma}) : \boldsymbol{V} + \mathbb{S} : \operatorname{curl} \boldsymbol{V} \right) \, \mathrm{d}V \tag{4.13}$$

Now we use (4.12) to obtain

$$\int_{\partial\Omega} \left(\boldsymbol{S}(\boldsymbol{n}) + ((\boldsymbol{n}\times)\mathbb{S})^{\mathrm{T}} \right) : \boldsymbol{V} \, \mathrm{d}S = \int_{\Omega} \left((\boldsymbol{T}^{P} - \boldsymbol{\sigma} + (\operatorname{curl} (\mathbb{S}^{\mathrm{T}}))^{\mathrm{T}} \right) : \boldsymbol{V} \, dV. \tag{4.14}$$

From this we deduce the microforce balance using the fact that $\boldsymbol{V}$ is deviatoric and $\boldsymbol{\sigma}$ is symmetric.

$$\boldsymbol{s} = \boldsymbol{T}^{p} + (\operatorname{dev} \operatorname{curl} (\mathbb{S}^{\mathrm{T}}))^{\mathrm{T}} \tag{4.15}$$

Where bs[2] is the deviatoric part of the Cauchy stress. Similarly, we arrive at the

[2]Care must be taken to distinguish between the deviatoric part of the Cauchy stress, $\boldsymbol{s}$, the defect stress, $\mathbb{S}$, and the microtraction, $\boldsymbol{S}(\boldsymbol{n})$.

microtraction condition using the fact that for the skew tensor $(\boldsymbol{n}\times)^{\mathrm{T}} = -(\boldsymbol{n}\times)$.

$$\boldsymbol{S}(\boldsymbol{n}) = \operatorname{dev}\left(\mathbb{S}^{\mathrm{T}}(\boldsymbol{n}\times)\right) \tag{4.16}$$

To complete the model we need to develop constitutive expressions for the various stresses. In formulating the constitutive theory, a free energy is chosen of the form $\Psi(\boldsymbol{\varepsilon}^e, \boldsymbol{G})$, and the macro and micro stresses are defined to be thermodynamically conjugate to the kinematic tensors $\boldsymbol{\varepsilon}^e$ and $\boldsymbol{G}$, respectively. The elastic free energy is defined in the standard way as $\Psi^e(\boldsymbol{\varepsilon}^e) = \frac{1}{2}\boldsymbol{\varepsilon}^e : \mathbb{C} : \boldsymbol{\varepsilon}^e$, such that the usual definition of stress results, $\boldsymbol{\sigma} = \mathbb{C} : \boldsymbol{\varepsilon}^e$.

$$\Psi(\boldsymbol{\varepsilon}^e, \boldsymbol{G}) = \Psi^e(\boldsymbol{\varepsilon}^e) + \frac{1}{2}k|\boldsymbol{G}|^2 \tag{4.17}$$

$$\boldsymbol{\sigma} = \frac{\partial \Psi}{\partial \boldsymbol{\varepsilon}^e} = \mathbb{C} : \boldsymbol{\varepsilon}^e \tag{4.18}$$

$$\mathbb{S} = \frac{\partial \Psi}{\partial \boldsymbol{G}} = k\,\boldsymbol{G} = k\,\operatorname{curl}\boldsymbol{H}^p \tag{4.19}$$

Taking the symmetric part of the additive decomposition of the displacement gradient, (3.6), we get an expression for the total strain, $\boldsymbol{\varepsilon} = \boldsymbol{\varepsilon}^e + \boldsymbol{\varepsilon}^p$. From this we can deduce an expression for the elastic strain, and thus recover the classical definition of the Cauchy stress, restated here for convenience.

$$\boldsymbol{\sigma} = \mathbb{C} : (\boldsymbol{\varepsilon} - \boldsymbol{\varepsilon}^p) \tag{4.20}$$

Next, a constitutive relation is assumed for the micro-stress,

$$\boldsymbol{T}^p = Y(d^p)\dot{\boldsymbol{H}}^p, \tag{4.21}$$

where d^p is an effective distortion rate.

$$d^p = \|\dot{\boldsymbol{H}}^p\| = \sqrt{\dot{\boldsymbol{H}}^p : \dot{\boldsymbol{H}}^p} \tag{4.22}$$

With (4.18), (4.19), and (4.21) in hand, we can revisit the microforce balance, (4.15), and state the flow rule.

$$\boldsymbol{s} - \Big(\operatorname{dev}\operatorname{curl}\left(k\operatorname{curl}\boldsymbol{H}^p\right)^{\mathrm{T}}\Big)^{\mathrm{T}} = Y(d^p)\dot{\boldsymbol{H}}^p \tag{4.23}$$

Attention is drawn to the form of (4.23), which is that of a flow rule with kinematic hardening for $k > 0$ (recall (2.24)). In this interpretation, $\operatorname{dev}\operatorname{curl}\left(k\operatorname{curl}\boldsymbol{H}^p\right)^{\mathrm{T}}$ plays the role of a deviatoric back stress. Rate independent behavior is obtained when the function $Y(d^p)$ is specified to be σ_y/d^p, where σ_y is the uniaxial yield strength, and this is the form that will be used henceforth.

For the partial differential equation describing the microforce balance, additional boundary conditionals are necessary. For simplicity, we will concentrate on boundary conditions that provide no expenditure of power on the boundary. To begin, we start with the microtraction condition, (4.16). Then we introduce a projection operator, $\mathbb{P}(\boldsymbol{e}) = \mathbf{1} - \boldsymbol{e}\otimes\boldsymbol{e}$, which provides the projection onto the plane perpendicular to $\boldsymbol{e}$. Note that for the skew matrix associated with $\boldsymbol{n}$, $(\boldsymbol{n}\times)\mathbb{P}(\boldsymbol{n}) = (\boldsymbol{n}\times)$, which is true because $(\boldsymbol{n}\times)(\boldsymbol{n}\otimes\boldsymbol{n}) = (\boldsymbol{n}\times\boldsymbol{n})\otimes\boldsymbol{n}$ and $\boldsymbol{n}\times\boldsymbol{n} = \mathbf{0}$. Using the projection, we have

$$\operatorname{dev}\left(\mathbb{S}^{\mathrm{T}}(\boldsymbol{n}\times)\right) : \dot{\boldsymbol{H}}^p = \left(\mathbb{S}^{\mathrm{T}}(\boldsymbol{n}\times)\right) : \dot{\boldsymbol{H}}^p \tag{4.24}$$

$$= \left(\mathbb{S}^{\mathrm{T}}(\boldsymbol{n}\times)\mathbb{P}(\boldsymbol{n})\right) : \dot{\boldsymbol{H}}^p \tag{4.25}$$

$$= \left(\mathbb{S}^{\mathrm{T}}(\boldsymbol{n}\times)\right) : \dot{\boldsymbol{H}}^p\mathbb{P}(\boldsymbol{n}). \tag{4.26}$$

Thus we can arrive at two separate conditions providing a null expenditure of external power, either

$$\operatorname{dev}\left(\mathbb{S}^{\mathrm{T}}(\boldsymbol{n}\times)\right) = 0, \tag{4.27}$$

or

$$\dot{\boldsymbol{H}}^p(\boldsymbol{n}\times) = 0, \tag{4.28}$$

where we have utilized the fact that for a tensor $\boldsymbol{A}$, $\boldsymbol{A}\mathbb{P}(\boldsymbol{n}) = \boldsymbol{0} \iff \boldsymbol{A}(\boldsymbol{n}\times) = \boldsymbol{0}$.

Consider the latter, the homogeneous essential boundary condition denoted the *microhard* boundary condition. The microhard condition corresponds to a vanishing flux of the Burgers vector, $\boldsymbol{G}^{\mathrm{T}}\boldsymbol{e}$, for all planes with normal $\boldsymbol{e}$ intersecting Γ_H, where Γ_H is regarded as the microhard boundary, see Section 3.2. The complementary natural boundary condition corresponds to a micro-stress free boundary, Γ_S, and is referred to as the *microfree* boundary condition.

CHAPTER 5

Discontinuous Galerkin Methods

Discontinuous Galerkin (DG) methods were first introduced in 1973 in Reed and Hill (1973) which addresses the neutron transport equation. Essentially they developed a method that allows for a flux term to be discontinuous across element boundaries. They demonstrate the new method's superiority, in terms of accuracy and robustness, over methods where the same flux is continuous. Further application to problems from fluid mechanics came in Cockburn and Shu (1989) and Bassi and Rebay (1997) and the references within. Efforts towards elliptic problems are summarized and analyzed in Arnold et al. (2002). The main idea for the so called *interior penalty (IP)* methods is the approximation of continuity in the unknown discontinuous variable by penalizing jump terms across element boundaries. Another variant introduces a *lifting operator* which sums element boundary contributions.

5.1 Preliminaries

In order to present the ideas of DG methods in a familiar setting, below in Section 5.2, we will derive the DG variational statement for linear elasticity. In preparation for that exercise certain concepts need to first be defined. Consider a domain, Ω, discretized into a collection of disjoint subdomains or elements, Ω_e. Then the collection of interior domains, $\widetilde{\Omega}$, is given as the union of all elements as in (5.1), and the collection of interior domain boundaries, $\widetilde{\Gamma}$, is given as the union of the intersection

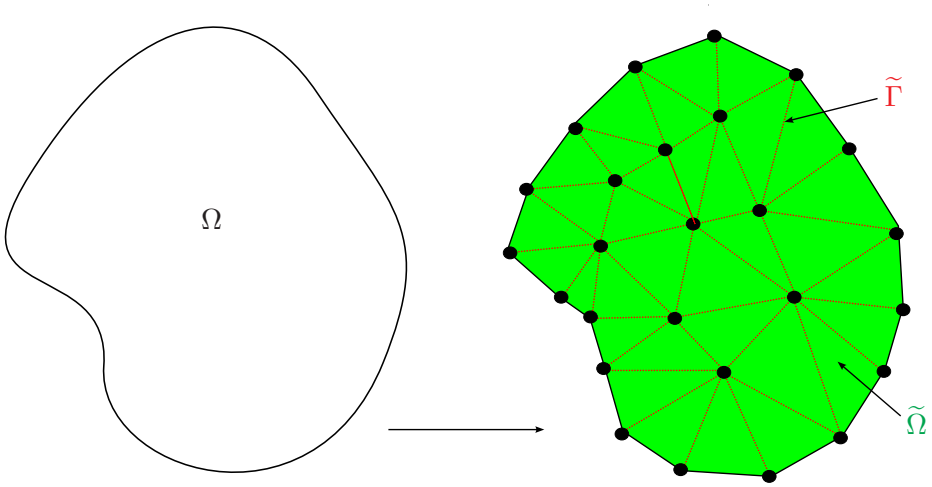

Figure 5.1: Interior domains and interior domain boundaries

of element boundaries as in (5.2).

$$\widetilde{\Omega} = \bigcup_{e=1}^{n_{el}} \mathrm{int}(\Omega_e) \tag{5.1}$$

$$\widetilde{\Gamma} = \bigcup_{e_1,e_2=1}^{n_{el}} \left(\partial\Omega_{e_1} \bigcap \partial\Omega_{e_2} \right) \tag{5.2}$$

For an illustration of these concepts, refer to Figure 5.1.

Next, we define a discontinuous field, (5.3), the jump operator, (5.4), the average operator, (5.5), and the element diameter, (5.6). The jump operator and average operator are defined by elements on either side of the interior boundary in question, denoted by the superscript $+$ and $-$, as seen in the definition of the discontinuous field, refer to Figure 5.2.

$$\text{Discontinuous field} \quad : \quad f^{\pm}\Big|_{\widetilde{\Gamma}} = \lim_{\varepsilon \to 0} f(\boldsymbol{x} \mp \varepsilon \boldsymbol{n}) \tag{5.3}$$

$$\text{Jump operator} \quad : \quad [\![f]\!] = f^{+} - f^{-} \tag{5.4}$$

$$\text{Average operator} \quad : \quad \langle f \rangle = \frac{1}{2}\left(f^{+} + f^{-}\right) \tag{5.5}$$

$$\text{Element diameter} \quad : \quad h = \mathrm{diam}(\Omega_e) \tag{5.6}$$

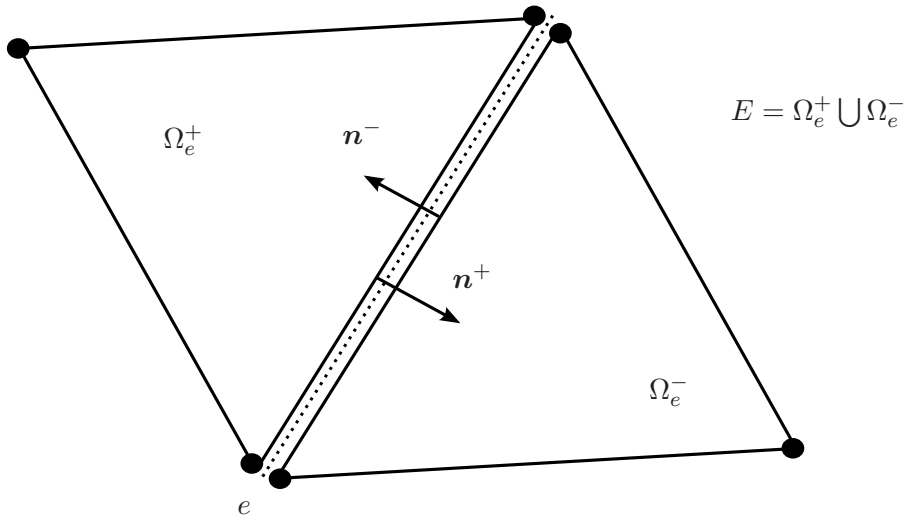

Figure 5.2: Schematic of a shared interior facet, e

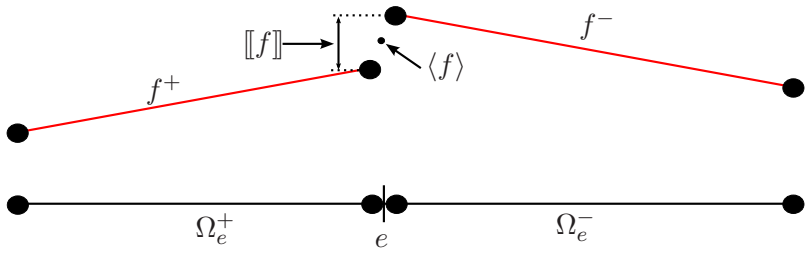

Figure 5.3: Jump and average of a scalar field, f

For tensorial fields, $\boldsymbol{f}$, an alternate definition of the jump operator can be used that utilizes the normals, with respect to the attached elements, of the interior boundary, $\boldsymbol{n}^+$ and $\boldsymbol{n}^-$.

$$\text{Jump operator}: [\![\boldsymbol{f}]\!] = \boldsymbol{f}^+\boldsymbol{n}^+ + \boldsymbol{f}^-\boldsymbol{n}^- \tag{5.7}$$

Using the fact that $\boldsymbol{n}^+ = -\boldsymbol{n}^-$, (5.7) can also be written as $[\![\boldsymbol{f}]\!] = (\boldsymbol{f}^+ - \boldsymbol{f}^-)\boldsymbol{n}^+$, which will be useful for subsequent developments. For an illustration of the jump and average for a scalar field, refer to Figure 5.3.

5.2 DG Variational Statement for Linear Elasticity

Matters proceed with an exploration of the concepts of DG methods within the familiar context of linear elasticity. To begin with, recall the strong form of the

statement presented in Chapter 2.2 in (2.38), and for simplicity, assume an absence of body forces and applied tractions. For the description of the DG variational form, we now assume that the trial solution and weighting spaces can be discontinuous across element boundaries. Now the accompanying trial and solution spaces are simply in L_2, which incidentally consists of a larger set of functions.

$$\mathscr{S}_i = \{u_i | u_i \in L_2(\Omega), u_i = g_i \text{ on } \Gamma_{g_i}\} \tag{5.8}$$

$$\mathscr{V}_i = \{w_i | w_i \in L_2(\Omega), w_i = 0 \text{ on } \Gamma_{g_i}\}\,. \tag{5.9}$$

As before, we multiply through by a weighting function and perform integration by parts. Now consider that the domain of interest is discretized into a collection of disjoint subdomains, such as triangles in two dimensions or tetrahedra in three dimensions. As a consequence of the discontinuity of the displacements, interior domain boundary terms that resemble tractions arise after the integration by parts, see (5.10).

$$\int_\Omega w_{i,j}\mathbb{C}_{ijkl}u_{(k,l)}\,\mathrm{d}\Omega - \int_{\widetilde{\Gamma}}[\![w_i\left(\mathbb{C}_{ijkl}u_{(k,l)}n_j\right)]\!]\,\mathrm{d}\Gamma = 0 \tag{5.10}$$

From here, we say that for equilibrium to hold in the same sense as for the continuous problem, the traction terms on the interior boundaries must be continuous, which implies that the jumps in those terms must evaluate to zero in a weak sense.

At this point, the *symmetric DG interior penalty method* for linear elasticity is stated, and the following discussion will show consistency of the method by deriving the Euler-Lagrange equations. Recalling the assumption of no body forces or applied tractions, and appropriate definitions of the function spaces we have:

$$\begin{aligned}&\int_\Omega w_{i,j}\mathbb{C}_{ijkl}u_{(k,l)}\,\mathrm{d}\Omega - \int_{\widetilde{\Gamma}}[\![w_i]\!]\langle\left(\mathbb{C}_{ijkl}u_{(k,l)}n_j\right)\rangle\,\mathrm{d}\Gamma \\ &- \int_{\widetilde{\Gamma}}[\![u_i]\!]\langle\left(\mathbb{C}_{ijkl}w_{(k,l)}n_j\right)\rangle\,\mathrm{d}\Gamma + \underbrace{\frac{\alpha}{h}\int_{\widetilde{\Gamma}}[\![w_i]\!][\![u_i]\!]\,\mathrm{d}\Gamma}_{\text{penalty term}} = 0.\end{aligned} \tag{5.11}$$

Derivation of the Euler-Lagrange equations will make use of the following identity.

$$[\![f_i g_i]\!] = \langle f_i \rangle [\![g_i]\!] + [\![f_i]\!] \langle g_i \rangle \tag{5.12}$$

For a proof of (5.12), please see Appendix B, Section B.1. Beginning with (5.11), motivated by the desire to obtain an expression similar to (5.10), we add and subtract the following, noting the net result is simply zero.

$$+ \int_{\widetilde{\Gamma}} \langle w_i \rangle [\![(\mathbb{C}_{ijkl} u_{k,l}) n_j]\!] \, \mathrm{d}\,\Gamma - \int_{\widetilde{\Gamma}} \langle w_i \rangle [\![(\mathbb{C}_{ijkl} u_{k,l}) n_j]\!] \, \mathrm{d}\,\Gamma \tag{5.13}$$

Incorporating (5.13) with (5.11), we make use of the identity in (5.12).

$$\int_{\widetilde{\Gamma}} [\![w_i (\mathbb{C}_{ijkl} u_{k,l}) n_j]\!] \, \mathrm{d}\Gamma = \int_{\widetilde{\Gamma}} [\![w_i]\!] \langle (\mathbb{C}_{ijkl} u_{k,l}) n_j \rangle \, \mathrm{d}\Gamma + \int_{\widetilde{\Gamma}} \langle w_i \rangle [\![(\mathbb{C}_{ijkl} u_{k,l}) n_j]\!] \, \mathrm{d}\Gamma \tag{5.14}$$

After the preceding manipulations, we have a set of terms as follows.

$$\begin{aligned} &\int_{\Omega} w_{i,j} \mathbb{C}_{ijkl} u_{(k,l)} \, \mathrm{d}\Omega - \int_{\widetilde{\Gamma}} [\![w_i (\mathbb{C}_{ijkl} u_{k,l}) n_j]\!] \, \mathrm{d}\Gamma \\ &- \int_{\widetilde{\Gamma}} [\![u_i]\!] \langle (\mathbb{C}_{ijkl} w_{(k,l)}) n_j \rangle \, \mathrm{d}\Gamma + \int_{\widetilde{\Gamma}} \langle w_i \rangle [\![(\mathbb{C}_{ijkl} u_{k,l}) n_j]\!] \, \mathrm{d}\,\Gamma \\ &+ \frac{\alpha}{h} \int_{\widetilde{\Gamma}} [\![w_i]\!] [\![u_i]\!] \, \mathrm{d}\Gamma = 0. \end{aligned} \tag{5.15}$$

Integration by parts on $(5.15)_{1,2}$ yields the classical domain term from linear elasticity,

$$\int_{\Omega} w_i (\mathbb{C}_{ijkl} u_{k,l})_{,j} \, \mathrm{d}\Omega = \int_{\Omega} w_{i,j} \mathbb{C}_{ijkl} u_{k,l} \, \mathrm{d}\Omega - \int_{\widetilde{\Gamma}} [\![w_i (\mathbb{C}_{ijkl} u_{k,l}) n_j]\!] \, \mathrm{d}\Gamma, \tag{5.16}$$

such that, with standard arguments about the variations, the Euler-Lagrange equations are stated below.

$$\int_{\Omega} w_i (\mathbb{C}_{ijkl} u_{k,l})_{,j} \, \mathrm{d}\Omega = 0 \tag{5.17}$$

$$\int_{\widetilde{\Gamma}} [\![u_i]\!] \langle \left(\mathbb{C}_{ijkl} w_{(k,l)} \right) n_j \rangle \, \mathrm{d}\Gamma = 0 \tag{5.18}$$

$$\int_{\widetilde{\Gamma}} \langle w_i \rangle [\![(\mathbb{C}_{ijkl} u_{k,l}) n_j]\!] \, \mathrm{d}\,\Gamma = 0 \tag{5.19}$$

Interpretation of (5.17) reveals the standard equilibrium condition, written in strong form as div $\boldsymbol{\sigma} = \mathbf{0}$. The other equations, (5.18) and (5.19), are weak impositions of the continuity of displacement and traction, respectively. The equations, (5.17)–(5.19) show consistency between the symmetric DG IP method and the classical continuous method.

Note that the penalty term adds a positive definite contribution, stabilizing the formulation. The choice of the penalty parameter, α, is usually obtained via trial and error, as values that are too small fail to stabilize the solution, whereas values that are too large ill-condition the system, impacting accuracy. For the linear elasticity problem, good behavior is observed for penalty values on the order of 100 to 10000 times an elastic modulus such as E or λ. Figure 5.4 compares the solutions of the continuous and discontinuous Galerkin linear elastic methods. The contours in Figure 5.4 are the magnitude of the displacement. In particular, two different values of α are shown, illustrating poor stability for the choice of small penalty parameter. The continuous and stable DG solutions are identical, however the size of the system being solved varies drastically. The cubic mesh shown has 64 nodes and 162 elements. For the continuous solution in three dimensions, there are 64×3=192 degrees of freedom. For the DG system, each element has 12 degrees of freedom corresponding to the 4 nodes of each tetrahedron and 3 dimensions. So the total number of degrees of freedom come to 12×162=1944, an order of magnitude greater than for the continuous problem. The computational cost of DG is certainly not justified for linear elasticity.

Another formulation can be derived by following the presentation in Brezzi et al. (2000), which itself is a modified version of the method discussed in Bassi and Rebay (1997). The formulation is based on the construction of a lifting operator defined on

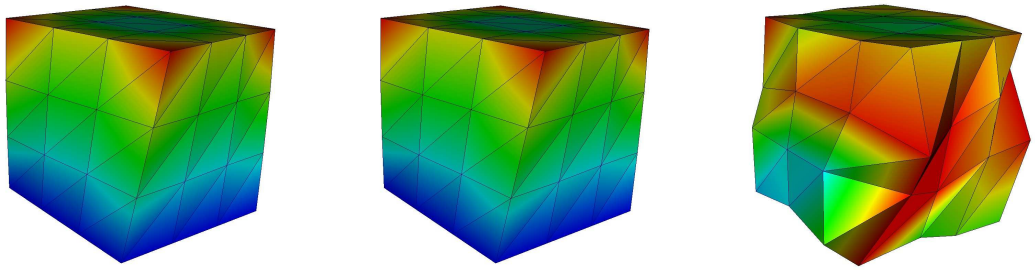

Figure 5.4: Continuous solution, DG solution, α=1E4 λ, DG solution, α=1E-4 λ

the element interior boundaries. First, consider the union of adjacent elements, E, and the shared edge as e, as in Figure 5.2, then for the linear elasticity problem, the lifting operator can be defined as follows.

$$\int_E \boldsymbol{v} : \boldsymbol{r}^e(\boldsymbol{u}) \, \mathrm{d}\Omega = -\int_e \langle \boldsymbol{v} \rangle [\![\boldsymbol{u} \otimes \boldsymbol{n}]\!] \, \mathrm{d}\Gamma \tag{5.20}$$

Then an additional function is defined as the sum of the edge contributions from the lifting operator.

$$\boldsymbol{R}(\boldsymbol{u}) = \sum_{e \in \widetilde{\Gamma}} \boldsymbol{r}^e(\boldsymbol{u}) \tag{5.21}$$

Then the variational statement for the lifting variation of the DG formulation for linear elasticity can be written.

$$\begin{aligned} &\int_\Omega (w_{i,j} + R_{ij}(\boldsymbol{w})) \mathbb{C}_{ijkl} (u_{(k,l)} + R_{kl}(\boldsymbol{u})) \, \mathrm{d}\Omega + \\ &\sum_{e \in \widetilde{\Gamma}} \eta \int_\Omega r^e_{ij}(\boldsymbol{w}) \mathbb{C}_{ijkl} r^e_{kl}(\boldsymbol{u}) \, \mathrm{d}\Omega = 0 \end{aligned} \tag{5.22}$$

Now a new stabilization parameter, η is introduced. The lifting formulation carries advantages over the IP formulation, namely that the method is stable for $\eta > 0$, see Brezzi et al. (2000). However the lifting formulation is also more expensive to compute during the finite element assembly.

5.3 DG Methods for Higher Order Theories

For linear elasticity, either the DG IP method or the lifting method are considerably more complicated than the physics require. For that reason, it would not be effective nor efficient to solve linear elastic problems with those methods. However, the ability to approximate inter-element continuity positions DG methods to handle higher order theories nicely. One of the most prominent challenges with higher order theories are the continuity requirements of the solution fields. For a fourth-order problem, after successive integration by parts to move derivatives over to the weighting function, $\mathscr{C}^1$ continuity is required of the basis for second gradient terms to make sense. The additional degrees of freedom necessary in a $\mathscr{C}^1$ formulation (versus the standard $\mathscr{C}^0$ formulation) impose difficulties in implementation, particularly for three dimensional problems, as well as permitting undesirable oscillatory behavior on the interior of the element not seen in the standard case. Mixed methods, which to some extent address the two issues raised above, have their own drawbacks, including stability requirements that aren't easily discernible. However, DG methods allow for the formulation and solution of fourth-order theories without the need to impose $\mathscr{C}^1$ continuity or introduce additional solution fields.

To illustrate the practical application, a few examples where DG methods are applied to fourth-order problems are presented. First, consider the Cahn-Hilliard equation, which is a fourth-order nonlinear parabolic partial differential equation with origins in governing phase segregation in binary alloys, but which has also been used to model multiphase fluid flow, image processing, and planet formation, see Wells et al. (2006) and references therein. The DG formulation studied is a variant of the symmetric DG IP method derived above for linear elasticity, and performs

comparably to a mixed formulation, possibly admitting lower-order polynomial interpolation and having no reliance on the stability condition inherent in the mixed formulation.

Another example can be found in Wells et al. (2004), which discusses a gradient-dependent damage model. Gradient damage models can be used to model strain localization in the presence of softening, an example of which is seen in Section 2.3.2, as well as size effects in materials. Again, the authors use a variant of the symmetric DG IP formulation for the damage variable, and the results from the rather simple model compare well with the chosen benchmark solution.

In Engel et al. (2002) the authors discuss the application of DG methods to thick beams and plates. Currently, the most prominent formulations for structural elements add a rotational solution field to ensure proper continuity at the element boundaries, driven again by the $\mathscr{C}^1$ continuity requirement emanating from the fourth-order theory. For example, the DG formulation of Poisson-Kirchoff plate theory presented uses a symmetric IP method and employs no derived variables such as rotations, simplifying matters. Furthermore, in Wells and Dung (2007) the authors use a lifting formulation and show improved stability properties over the IP method. Further research into this area is warranted as high fidelity plate and shell simulations are in high demand.

Lastly, the adaptation of DG methods into strain gradient plasticity theories are the most relevant for this dissertation. Some of the earliest and most successful attempts at adding gradient terms into plasticity models came from Aifantis (1987), where the author added a Laplacian of the equivalent plastic strain into the flow rule in an effort to regularize strain localization problems. However, the formulation involved the use of $\mathscr{C}^1$ basis functions. A more recent approach utilizing DG method-

ologies is given in McBride (2008), where the author uses, again, the symmetric DG IP method to evaluate the Laplacian of the equivalent plastic strain. The methodology and algorithms that form the core of the work in this dissertation, which begin in earnest in the next section, are modeled somewhat after those in McBride (2008).

5.4 Variational Formulation for Gradient Plasticity

From the previous section we arrived at two partial differential equations, the first describing the macroscopic equilibrium condition, or balance of linear momentum, and the second governing the flow rule for the gradient plasticity model.

$$\operatorname{div} \boldsymbol{\sigma} + \boldsymbol{b} = \mathbf{0} \tag{5.23}$$

$$\underbrace{\boldsymbol{T}^p - \boldsymbol{s}}_{\text{standard term}} + \underbrace{\left(\operatorname{dev} \operatorname{curl} \left(k \operatorname{curl} \boldsymbol{H}^p\right)^{\mathrm{T}}\right)^{\mathrm{T}}}_{\text{gradient term}} = \mathbf{0} \tag{5.24}$$

We will derive a formulation from (5.23) and (5.24), first by noting explicitly how the two equations are coupled. To accomplish this they will be restated solely in terms of $\boldsymbol{u}$ and $\boldsymbol{H}^p$.[1]

$$\operatorname{div} \mathbb{C} : (\boldsymbol{\nabla}^s \boldsymbol{u} - \boldsymbol{\varepsilon}^p) + \boldsymbol{b} = \mathbf{0} \tag{5.25}$$

$$\frac{Y}{d^p} \dot{\boldsymbol{H}}^p - \mathbb{C} : (\operatorname{dev} \boldsymbol{\nabla}^s \boldsymbol{u} - \boldsymbol{\varepsilon}^p) + \left(\operatorname{dev} \operatorname{curl} \left(k \operatorname{curl} \boldsymbol{H}^p\right)^{\mathrm{T}}\right)^{\mathrm{T}} = \mathbf{0} \tag{5.26}$$

It follows that the coupling of the equations comes from the Cauchy stress terms in both equations, specifically the displacement gradient and the symmetric part of $\boldsymbol{H}^p$.

For the equilibrium equation, we proceed in a similar fashion as in Chapter 2.2 to arrive at a weak statement of (5.23), namely integration by parts after multiplying through by a weighting function, $\boldsymbol{w}$, and integrating over the domain. In abstract

[1] Recall that $\boldsymbol{\varepsilon}^p = \operatorname{sym} \boldsymbol{H}^p$.

notation,

$$(\boldsymbol{\nabla w}, \mathbb{C} : (\boldsymbol{\nabla}^s \boldsymbol{u} - \boldsymbol{\varepsilon}^p))_\Omega = (\boldsymbol{w}, \boldsymbol{b})_\Omega + (\boldsymbol{w}, \boldsymbol{t}(\boldsymbol{n}))_{\Gamma_t}. \tag{5.27}$$

Where Γ_t is the part of the boundary with prescribed tractions. In a similar fashion, we arrive at a weak statement of (5.24), where now we are using integration by parts to transport a curl over to the weighting function, $\boldsymbol{V}$. First we note that $\boldsymbol{A} : \boldsymbol{B}^{\mathrm{T}} = \boldsymbol{A}^{\mathrm{T}} : \boldsymbol{B}$, and then we use the result of (4.12) on the gradient term of the flow rule and the fact that $\boldsymbol{V}$ is constructed to be deviatoric.

$$\left(\boldsymbol{V}^{\mathrm{T}}, \operatorname{curl}\left(k \operatorname{curl} \boldsymbol{H}^p\right)^{\mathrm{T}}\right)_\Omega = (\operatorname{curl} \boldsymbol{V}, k \operatorname{curl} \boldsymbol{H}^p)_\Omega - (\boldsymbol{V}, \mathbb{S}^{\mathrm{T}}(\boldsymbol{n}\times))_\Gamma \tag{5.28}$$

Then noting the microtraction condition, (4.16), applicable for the microtraction boundary, Γ_S, the statement of the classical Galerkin weak form of the problem is the following: Find $\{\boldsymbol{u}, \boldsymbol{H}^p\} \in \mathscr{S} \times \mathscr{P} \subset H^1(\Omega) \times \operatorname{dev} H^1(\Omega)$ s.t. $\forall \{\boldsymbol{w}, \boldsymbol{V}\} \in \mathscr{V} \times \mathscr{Q} \subset H^1(\Omega) \times \operatorname{dev} H^1(\Omega)$

$$(\nabla \boldsymbol{w}, \boldsymbol{\sigma})_\Omega = (\boldsymbol{w}, \boldsymbol{b})_\Omega + (\boldsymbol{w}, \boldsymbol{t}(\boldsymbol{n}))_{\Gamma_t} \tag{5.29}$$

$$(\boldsymbol{V}, \boldsymbol{T}^p - \boldsymbol{s})_\Omega + (\operatorname{curl} \boldsymbol{V}, k \operatorname{curl} \boldsymbol{H}^p)_\Omega = (\boldsymbol{V}, \boldsymbol{S}(\boldsymbol{n}))_{\Gamma_S} \tag{5.30}$$

With two primal fields, the displacements, $\boldsymbol{u}$, and the plastic distortion, $\boldsymbol{H}^p$, the resulting formulation necessarily involves a mixed method. The solution of the displacement field will come in the standard way, using a piecewise continuous basis. The treatment of the flow rule is the main topic for the rest of this section. The classical statement of the gradient plasticity model could be implemented using continuous interpolations for both $\boldsymbol{u}$ and $\boldsymbol{H}^p$. However, the solution spaces, $\mathscr{P}, \mathscr{Q} \subset \operatorname{dev} H^1(\Omega)$ imply a minimum of 32 degrees of freedom for $\boldsymbol{H}^{ph} \in \mathscr{P}^1(\Omega_e)$. If the regularity assumptions can be relaxed, i.e. if we can choose $\mathscr{P}, \mathscr{Q} \subset \operatorname{dev} L^2(\Omega)$, then the minimum number of degrees of freedom can be reduced to 8, and, furthermore, larger

functional spaces become available. Continuity would still be required, but could be enforced in a weak sense, which motivates use of DG methodology in constructing an alternate variational formulation.

Revisiting Section 5.2 for motivation in manipulating the equations, we consider discontinuous $\boldsymbol{H}^p$ and arrive at the following equation in terms of interior domains, $\widetilde{\Omega}$ and interior facets, $\widetilde{\Gamma}$.

$$\begin{aligned}(\boldsymbol{V}, \boldsymbol{T}^p - \boldsymbol{s})_\Omega + (\operatorname{curl} \boldsymbol{V}, k \operatorname{curl} \boldsymbol{H}^p)_{\widetilde{\Omega}} \\ + (\llbracket \boldsymbol{V}, \mathbb{S}^{\mathrm{T}}(\boldsymbol{n}\times)^{\mathrm{T}} \rrbracket)_{\widetilde{\Gamma}} = (\boldsymbol{V}, \boldsymbol{S}(\boldsymbol{n}))_{\Gamma_S}\end{aligned} \tag{5.31}$$

We then apply the following identity to (5.31).

$$\llbracket \boldsymbol{A}(\boldsymbol{n}\times) : \boldsymbol{B} \rrbracket = \llbracket \boldsymbol{A}(\boldsymbol{n}\times) \rrbracket : \langle \boldsymbol{B} \rangle + \langle \boldsymbol{A} \rangle : \llbracket \boldsymbol{B}(\boldsymbol{n}\times)^{\mathrm{T}} \rrbracket \tag{5.32}$$

The proof of (5.32) can be found in Appendix B, in Section B.3. It is a variant of the identity in Section B.1, and its motivation becomes apparent below. Now employing (5.32) on the relevant term in (5.31) yields the following.

$$\begin{aligned}(\boldsymbol{V}, \boldsymbol{T}^p - \boldsymbol{s})_\Omega + (\operatorname{curl} \boldsymbol{V}, k \operatorname{curl} \boldsymbol{H}^p)_{\widetilde{\Omega}} \\ + (\llbracket \boldsymbol{V}(\boldsymbol{n}\times) \rrbracket, \langle \mathbb{S}^{\mathrm{T}} \rangle)_{\widetilde{\Gamma}} + (\langle \boldsymbol{V} \rangle, \llbracket \mathbb{S}^{\mathrm{T}}(\boldsymbol{n}\times)^{\mathrm{T}} \rrbracket)_{\widetilde{\Gamma}} = (\boldsymbol{V}, \boldsymbol{S}(\boldsymbol{n}))_{\Gamma_S}\end{aligned} \tag{5.33}$$

An IP method requires two more pieces, a consistent term for the weak continuity of $\boldsymbol{H}^p(\boldsymbol{n}\times)$, and a penalty term. The first such term is motivated again by the desire for symmetry with the term that arises naturally through integration by parts.

$$(\langle (k \operatorname{curl} \boldsymbol{V})^{\mathrm{T}} \rangle, \llbracket \boldsymbol{H}^p(\boldsymbol{n}\times) \rrbracket)_{\widetilde{\Gamma}} \tag{5.34}$$

Recall that $\mathbb{S} = k \operatorname{curl} \boldsymbol{H}^p$ from (4.19). The penalty term appears as

$$\frac{\alpha\, k}{h} (\llbracket \boldsymbol{V}(\boldsymbol{n}\times) \rrbracket, \llbracket \boldsymbol{H}^p(\boldsymbol{n}\times) \rrbracket)_{\widetilde{\Gamma}}. \tag{5.35}$$

Note that the penalty parameter, α, gets multiplied by the gradient modulus, k, in (5.35). Lastly, the term with $\llbracket \mathbb{S}^{\mathrm{T}}(\boldsymbol{n}\times)^{\mathrm{T}} \rrbracket$ is omitted, as it will return below when the

Euler-Lagrange equations are derived to serve the purpose of enforcing continuity of the microtraction.

All the components are in place to state the symmetric DG IP variational formulation for the model of gradient plasticity discussed above. Find $\{\boldsymbol{u}^h, \boldsymbol{H}^{ph}\} \in \mathscr{S}^h \times \mathscr{P}^h \subset H^1(\Omega) \times \operatorname{dev} L^2(\Omega)$ s.t. $\forall \{\boldsymbol{w}^h, \boldsymbol{V}^h\} \in \mathscr{V}^h \times \mathscr{Q}^h \subset H^1(\Omega) \times \operatorname{dev} L^2(\Omega)$ macroscopic equilibrium is satisfied,

$$(\nabla \boldsymbol{w}^h, \boldsymbol{\sigma}^h)_\Omega = (\boldsymbol{w}^h, \boldsymbol{b})_\Omega + (\boldsymbol{w}^h, \boldsymbol{t})_{\Gamma_t}, \tag{5.36}$$

and the flow rule is also satisfied,

(5.37)

$$\begin{aligned}(\boldsymbol{V}^h, \boldsymbol{T}^{ph} - \boldsymbol{\sigma}^h)_\Omega + (\operatorname{curl} \boldsymbol{V}^h, k \operatorname{curl} \boldsymbol{H}^{ph})_{\widetilde{\Omega}} \\ +([\![\boldsymbol{V}^h(\boldsymbol{n}\times)]\!], \langle (k \operatorname{curl} \boldsymbol{H}^{ph})^{\mathrm{T}} \rangle)_{\widetilde{\Gamma}} + (\langle (k \operatorname{curl} \boldsymbol{V}^h)^{\mathrm{T}} \rangle, [\![\boldsymbol{H}^{ph}(\boldsymbol{n}\times)]\!])_{\widetilde{\Gamma}} \\ + \frac{\alpha\, k}{h} ([\![\boldsymbol{V}^h(\boldsymbol{n}\times)]\!], [\![\boldsymbol{H}^{ph}(\boldsymbol{n}\times)]\!])_{\widetilde{\Gamma}} = (\boldsymbol{V}^h, \boldsymbol{S}(\boldsymbol{n}))_{\Gamma_S}.\end{aligned}$$

Variational consistency of the formulation is demonstrated by applying integration by parts to arrive at (5.42)–(5.46). Note that to recover the curl-curl domain term in the flow rule we need to reverse the steps of the derivation using (5.32) after adding and subtracting the term with $[\![{\mathbb{S}^h}^{\mathrm{T}}(\boldsymbol{n}\times)^{\mathrm{T}}]\!]$. Modelling the steps from the linear elastic case and focusing on the flow rule, we add the following to the method:

$$+ (\langle \boldsymbol{V}^h \rangle, [\![{\mathbb{S}^h}^{\mathrm{T}}(\boldsymbol{n}\times)^{\mathrm{T}}]\!])_{\widetilde{\Gamma}} - (\langle \boldsymbol{V}^h \rangle, [\![{\mathbb{S}^h}^{\mathrm{T}}(\boldsymbol{n}\times)^{\mathrm{T}}]\!])_{\widetilde{\Gamma}}, \tag{5.38}$$

and now we can use (5.32), giving,

$$([\![\boldsymbol{V}^h, {\mathbb{S}^h}^{\mathrm{T}}(\boldsymbol{n}\times)^{\mathrm{T}}]\!])_{\widetilde{\Gamma}} = +(\langle \boldsymbol{V}^h \rangle, [\![{\mathbb{S}^h}^{\mathrm{T}}(\boldsymbol{n}\times)^{\mathrm{T}}]\!])_{\widetilde{\Gamma}} + ([\![\boldsymbol{V}^h(\boldsymbol{n}\times)]\!], \langle {\mathbb{S}^h}^{\mathrm{T}} \rangle)_{\widetilde{\Gamma}}. \tag{5.39}$$

After these manipulations, the terms remaining in the flow rule can be seen below.

(5.40)

$$(\boldsymbol{V}^h, \boldsymbol{T}^{ph} - \boldsymbol{\sigma}^h)_\Omega + (\operatorname{curl} \boldsymbol{V}^h, k \operatorname{curl} \boldsymbol{H}^{ph})_{\widetilde{\Omega}}$$
$$+([\![\boldsymbol{V}^h, \mathbb{S}^{h^{\mathrm{T}}}(\boldsymbol{n}\times)^{\mathrm{T}}]\!])_{\widetilde{\Gamma}} + (\langle (k \operatorname{curl} \boldsymbol{V}^h)^{\mathrm{T}} \rangle, [\![\boldsymbol{H}^{ph} (\boldsymbol{n}\times)]\!])_{\widetilde{\Gamma}}$$
$$- \left(\langle \boldsymbol{V}^h \rangle, [\![(k \operatorname{curl} \boldsymbol{H}^{ph})^{\mathrm{T}} (\boldsymbol{n}\times)]\!]\right)_{\widetilde{\Gamma}} + \frac{\alpha\, k}{h}([\![\boldsymbol{V}^h(\boldsymbol{n}\times)]\!], [\![\boldsymbol{H}^{ph}(\boldsymbol{n}\times)]\!])_{\widetilde{\Gamma}} = (\boldsymbol{V}^h, \boldsymbol{S}(\boldsymbol{n}))_{\Gamma_S}.$$

Integration by parts can be used on $(5.40)_{2,3}$ to recover the curl-curl domain term.

$$(\boldsymbol{V}^{h^{\mathrm{T}}}, \operatorname{curl}(k \operatorname{curl} \boldsymbol{H}^{ph})^{\mathrm{T}})_\Omega = (\operatorname{curl} \boldsymbol{V}^h, k \operatorname{curl} \boldsymbol{H}^{ph})_{\widetilde{\Omega}} + ([\![\boldsymbol{V}^h, \mathbb{S}^{h^{\mathrm{T}}}(\boldsymbol{n}\times)^{\mathrm{T}}]\!])_{\widetilde{\Gamma}} \tag{5.41}$$

Similar integration by parts occurs for the macroscopic equilibrium equation in the standard way. The resulting Euler-Lagrange equations are stated below.

$$\left(\boldsymbol{w}^h, \operatorname{div} \boldsymbol{\sigma}^h + \boldsymbol{b}\right)_\Omega = 0 \tag{5.42}$$

$$\left(\boldsymbol{V}^h, \boldsymbol{T}^{ph} - \boldsymbol{\sigma}^h + (\operatorname{curl}(k \operatorname{curl} \boldsymbol{H}^{ph})^{\mathrm{T}})^{\mathrm{T}}\right)_{\widetilde{\Omega}} = 0 \tag{5.43}$$

$$(\langle (k \operatorname{curl} \boldsymbol{V}^h)^{\mathrm{T}} \rangle, [\![\boldsymbol{H}^{ph} (\boldsymbol{n}\times)]\!])_{\widetilde{\Gamma}} = 0 \tag{5.44}$$

$$\left(\langle \boldsymbol{V}^h \rangle, [\![(k \operatorname{curl} \boldsymbol{H}^{ph})^{\mathrm{T}} (\boldsymbol{n}\times)]\!]\right)_{\widetilde{\Gamma}} = 0 \tag{5.45}$$

$$\left(\boldsymbol{V}^h, (\mathbb{S}^{\mathrm{T}} (\boldsymbol{n}\times) - \boldsymbol{S}(\boldsymbol{n}))\right)_{\Gamma_S} = 0 \tag{5.46}$$

From these Euler-Lagrange equations it is clear that the exact solution also satisfies the interior penalty discontinuous Galerkin weak from (5.36) and (5.37), which is the classical requirement for consistency of a finite element formulation. Note that (5.45) is equivalently expressed as $\left(\langle \boldsymbol{V}^h \rangle, [\![\mathbb{S}^{h^{\mathrm{T}}} (\boldsymbol{n}\times)]\!]\right)_{\widetilde{\Gamma}} = 0$, implying continuity of the microtraction in a weak sense. Now note that, using standard arguments about the arbitrariness of the weighting function, $\boldsymbol{V}$, we have enforced the flow rule, and weak continuity of the primal field and the microtraction, verifying consistency. As mentioned above, for $\mathscr{C}^0$-continuous $\boldsymbol{H}^{ph}$, i.e. $\boldsymbol{H}^{ph} \in \mathscr{P}^1(\Omega_e)$, at least 32 degrees of freedom are needed. However for $\mathscr{C}^{-1}$-continuous $\boldsymbol{H}^{ph}$, i.e. $\boldsymbol{H}^{ph} \in \mathscr{P}^0(\Omega_e)$, only

8 degrees of freedom are needed. The reduction in degrees of freedom is attractive, but the cost is that for $\boldsymbol{H}^{ph} \in \mathscr{P}^0(\Omega_e)$, the gradient/backstress component of the model lies entirely within the interior penalty term, which depends on the penalty parameter α.

5.5 Implementation

Implementation of the model is carried out in a nonlinear finite element code using a Newton-Raphson iterative procedure. The `FEniCS` project was chosen to be the framework for the implementation. Please refer to Appendix C for an overview of the `FEniCS` project. The displacement field is chosen to be $\mathscr{C}^0$ continuous, or piecewise continuous, in the standard way, while the plastic displacement gradient field in chosen to be $\mathscr{C}^{-1}$ continuous, or piecewise constant. This choice of space for $\boldsymbol{H}^p$ significantly reduces the number of degrees of freedom necessary for representation, as mentioned above, and also simplifies the notion of boundary conditions for the flow rule PDE. The microhard and microfree boundary conditions apply only to the boundary of the plastic domain, and thus for linear or higher-order fields, it would be possible for the elastic-plastic boundary to exist within elements and special consideration would be necessary to properly define the normal vector and hence apply boundary conditions. For piecewise constant plastic fields, the most natural decision is to use the element faces which are already available, and no additional surfaces need to be created to apply boundary conditions.

Using piecewise constants for $\boldsymbol{H}^p$ simplifies the variational formulation since all the curl terms evaluate to zero. The benefit of this is simplicity and efficiency, while the drawback is the aforementioned issue with the gradient term being inseparable from the penalty term. Also, we will be considering only Dirichlet boundary con-

ditions and no body forces, which further simplifies the formulation. Lastly, the solution procedure will be solving for increments in displacement and plastic distortion, and so interpolations will be written for incremental quantities. For completeness, the simplified variational form is stated as: find $\{\delta \boldsymbol{u}^h, \delta \boldsymbol{H}^{ph}\} \in \mathscr{S}^h \times \mathscr{P}^h \subset H^1(\Omega) \times \operatorname{dev} L^2(\Omega)$ s.t. $\forall \{\boldsymbol{w}^h, \boldsymbol{V}^h\} \in \mathscr{V}^h \times \mathscr{Q}^h \subset H^1(\Omega) \times \operatorname{dev} L^2(\Omega)$ macroscopic equilibrium is satisfied,

$$(\nabla \boldsymbol{w}^h, \boldsymbol{\sigma}^h)_\Omega = 0, \tag{5.47}$$

and the flow rule is also satisfied,

$$(\boldsymbol{V}^h, \boldsymbol{T}^{ph} - \boldsymbol{\sigma}^h)_\Omega + \frac{\alpha\, k}{h}([\![\boldsymbol{V}^h(\boldsymbol{n}\times)]\!], [\![\boldsymbol{H}^{ph}(\boldsymbol{n}\times)]\!])_{\widetilde{\Gamma}} = 0. \tag{5.48}$$

The interpolations for the solution and variational fields are defined as

$$\delta \boldsymbol{u}^h = \sum_a^{n_{nodes}} \boldsymbol{N}^a \boldsymbol{d}^a \qquad \delta \boldsymbol{w}^h = \sum_a^{n_{nodes}} \boldsymbol{N}^a \boldsymbol{c}^a, \tag{5.49}$$

$$\delta \boldsymbol{H}^{ph} = \sum_b^{n_p} \boldsymbol{\phi}^b \boldsymbol{\eta}^b \qquad \delta \boldsymbol{V}^h = \sum_b^{n_p} \boldsymbol{\phi}^b \boldsymbol{\theta}^b, \tag{5.50}$$

where the index a cycles through the number of nodes in the element, and the index b cycles through the number of integration points used to represent the $\boldsymbol{H}^p$ degrees of freedom. Since we will be using piecewise constants to interpolate $\boldsymbol{H}^p$, we will only have one integration point per element. Also the basis functions in (5.50) will simply be identity matrices. Henceforth, for notational simplicity, the superscript h denoting finite dimensional approximations, will be dropped. The resulting system differs from the plasticity model discussed in Chapters 2 and 2.2 in a number of ways. First, due to the gradient term, the plastic fields are governed by a PDE, with implications of a larger system of equations to solve. Second, the system of equations now includes a term defined on the interior facets, $\widetilde{\Gamma}$, stemming from the

DG formulation. Third, the plastic field $\boldsymbol{H}^p$ is not necessarily a symmetric tensor, and in fact, its deviation from symmetry will solely come from the gradient term.

As in the standard case, a yield surface needs to be defined. Recall that the gradient term has the appearance of a backstress, call it $\boldsymbol{\beta}$, in the flow rule. Then using the concepts discussed in Chapter 2, we formulate the yield surface.

$$f(\boldsymbol{\sigma}, \boldsymbol{\beta}) := \|\boldsymbol{s} - \boldsymbol{\beta}\| - \sqrt{\frac{2}{3}}\sigma_y \tag{5.51}$$

And the restriction holds that $f \leq 0$.

The temporal solution is achieved via a backward Euler time integration scheme, therefore the solution procedure is implicit. To do this, a given time step is concerned with advancing the solution from the time t_n to the time t_{n+1}, where the time step Δt is then defined as $t_{n+1} - t_n$. Since the data at t_n is known (as it is potentially a converged solution), the algorithm is constructed using plastic quantities defined at t_n. To begin, we will define some algorithmic quantities below. Consider the Cauchy stress at time t_{n+1}.

$$\boldsymbol{\sigma}_{n+1} = \mathbb{C} : (\boldsymbol{\varepsilon}_{n+1} - \boldsymbol{\varepsilon}^p_{n+1}) \tag{5.52}$$

Where $\boldsymbol{\varepsilon}_{n+1} = \boldsymbol{\nabla}^s \boldsymbol{u}_{n+1}$ and $\boldsymbol{\varepsilon}^p_{n+1} = \operatorname{sym} \boldsymbol{H}^p_{n+1}$. For the microstress $\boldsymbol{T}^P$ we need to approximate the quantity $\dot{\boldsymbol{H}}^p$.

$$\boldsymbol{T}^p_{n+1} = \frac{\sigma_y}{d^p}\dot{\boldsymbol{H}}^p \approx \frac{\sigma_y}{d^p}\left(\frac{\boldsymbol{H}^p_{n+1} - \boldsymbol{H}^p_n}{\Delta t}\right) \tag{5.53}$$

Recall the equation for d^p, (4.22) which can be approximated as

$$d^p_{n+1} \approx \left\|\frac{\boldsymbol{H}^p_{n+1} - \boldsymbol{H}^p_n}{\Delta t}\right\| = \frac{\|\boldsymbol{H}^p_{n+1} - \boldsymbol{H}^p_n\|}{\Delta t}. \tag{5.54}$$

Combining (5.53) and (5.54) the time step factors cancel by construction, which necessitates rate independent stress. A simplified representation of the microstress,

without the time step factors, can be seen in (5.55), which has the form of a magnitude times a direction. Note that for this formulation, the magnitude of $\boldsymbol{T}^p$ is fixed to be σ_y.

$$\boldsymbol{T}^p_{n+1} = \sigma_y \left(\frac{\boldsymbol{H}^p_{n+1} - \boldsymbol{H}^p_n}{\|\boldsymbol{H}^p_{n+1} - \boldsymbol{H}^p_n\|} \right) \tag{5.55}$$

A predictor-corrector solution strategy is used. A discussion of the strategy follows below, and the algorithm can be seen in Algorithm 5.1. A trial state is evaluated and the yield condition is checked during the predictor stage, and solution of the flow rule is computed for the set of elements that have violated the yield condition in the corrector stage. This solution strategy is analogous to that of classical plasticity, the main difference being the global solution of the flow rule PDE in the gradient plasticity case, versus the local solution in the classical case.

For the predictor stage, we first apply the Dirichlet boundary conditions assuming elastic constitutive behavior and solve to get an initial guess for the displacement field at t_{n+1}. Then we define the trial state with respect to the displacements at time t_{n+1}, but the plastic fields at time t_n, as mentioned above. Again, $(\cdot)^{\text{tr}}$ denotes a quantity in its trial state.

$$\boldsymbol{\sigma}^{\text{tr}}_{n+1} = \mathbb{C} : (\boldsymbol{\nabla}^s \boldsymbol{u}_{n+1} - \boldsymbol{\varepsilon}^p_n) \tag{5.56}$$

$$\boldsymbol{\beta}^{\text{tr}}_{n+1} = \boldsymbol{\beta}_n \tag{5.57}$$

$$f^{\text{tr}}_{n+1} = f(\boldsymbol{\sigma}^{\text{tr}}_{n+1}, \boldsymbol{\beta}^{\text{tr}}_{n+1}) \tag{5.58}$$

Now the yield condition is evaluated using (5.51), and any element that violates the requirement that $f \leq 0$ is determined to be in the set of plastic elements.

In the corrector stage, the flow rule PDE is assembled and solved in an iterative fashion using a Newton-Raphson method. We assume that the displacement field,

Algorithm 5.1 Predictor-corrector algorithm for gradient plasticity, global equilibrium iteration j, and time step $n+1$

Predictor stage
if $j == 0$ **then**
  Use elastic tangent
else
  Compute trial state
  for each element **do**
    $\boldsymbol{\sigma}^{\text{tr}}_{n+1,j} = \mathbb{C} : (\boldsymbol{\nabla}^s \boldsymbol{u}_{n+1} - \boldsymbol{\varepsilon}^p_n)$
    $\boldsymbol{\beta}^{\text{tr}}_{n+1,j} = \boldsymbol{\beta}_n$
    $f^{\text{tr}} = f(\boldsymbol{\sigma}^{\text{tr}}_{n+1,j}, \boldsymbol{\beta}^{\text{tr}}_{n+1,j})$
    if $f \geq 0$ **then**
      Add current element to list of plastic elements
    else
      $\boldsymbol{\sigma}_{n+1,j} = \boldsymbol{\sigma}^{\text{tr}}_{n+1,j}$
    end if
  end for
end if
Corrector stage
while flow rule residual, $\|\boldsymbol{R}^p_{n+1,k}\| > \text{TOL}$ **do**
  for each element in set of plastic elements **do**
    Compute plastic quantities
    $\Delta \boldsymbol{H}^p_{n+1,k} = \boldsymbol{H}^p_{n+1,k} - \boldsymbol{H}^p_n$
    $\widetilde{d^p}_{n+1,k} = \|\Delta \boldsymbol{H}^p_{n+1,k}\|$
    $\boldsymbol{T}^p_{n+1,k} = \frac{\sigma_y}{\widetilde{d^p}_{n+1,k}} \Delta \boldsymbol{H}^p_{n+1,k}$
    $\boldsymbol{\sigma}_{n+1} = \mathbb{C} : (\boldsymbol{\nabla}^s \boldsymbol{u}_{n+1} - \boldsymbol{\varepsilon}^p_{n+1,k})$
  end for
  Assemble $\boldsymbol{K}^p_{n+1,k}$, $\boldsymbol{R}^p_{n+1,k}$
  Solve (5.67) and update $\boldsymbol{H}^p_{n+1,k+1} = \boldsymbol{H}^p_{n+1,k} + \delta \boldsymbol{H}^p$
  Increment flow rule iteration, $k \rightarrow k+1$
end while
Assemble global equilibrium (5.79) solve for $\boldsymbol{u}_{n+1,j+1}$
Check for global convergence
if $\|\boldsymbol{R}^{eq}_{n+1,j}\| < \text{TOL}$ **then**
  Advance state $(\cdot)_{n+1} \rightarrow (\cdot)_n$
else
  Increment equilibrium iteration, $j \rightarrow j+1$, return to predictor
end if

and thus the strain, is constant during the iterative solve of the flow rule. In this sense the method proposed is a staggered approach at solving a coupled pair of PDEs. In order to assemble the system, certain quantities need to be computed. The first of these is the incremental quantity $\Delta \boldsymbol{H}^p_{n+1,k}$, where k is the current iterate in the flow rule iterative solve.

$$\Delta \boldsymbol{H}^p_{n+1,k} = \boldsymbol{H}^p_{n+1,k} - \boldsymbol{H}^p_n \tag{5.59}$$

Then a rate independent approximation for d^p is made as

$$\widetilde{d^p}_{n+1,k} = \|\Delta \boldsymbol{H}^p_{n+1,k}\|, \tag{5.60}$$

from which $\boldsymbol{T}^p_{n+1,k}$ is computed as

$$\boldsymbol{T}^p_{n+1,k} = \frac{\sigma_y}{\widetilde{d^p}_{n+1,k}} \Delta \boldsymbol{H}^p_{n+1,k}. \tag{5.61}$$

To evaluate the Cauchy stress, the plastic strain is computed and the stress is calculated via (5.52). Equations (5.61) and (5.52) define the microstress and the Cauchy stress, which are regarded as element quantities in the set of plastic elements that make up the plastic domain. The other term from (5.48) considers quantities defined on the interior facets of the plastic domain, and uses the current iterate of $\boldsymbol{H}^p_{n+1,k}$ and the normal vector for the facet being integrated, meaning that no fields need to be computed to assemble that term. The residual for the method then comes from assembling the variational form with the current iterate.

$$\mathscr{R}^p_{n+1,k} = (\boldsymbol{V}, \boldsymbol{T}^p_{n+1,k} - \boldsymbol{\sigma}_{n+1})_\Omega + \frac{\alpha\, k}{h} (\llbracket \boldsymbol{V}(\boldsymbol{n}\times) \rrbracket, \llbracket \boldsymbol{H}^p_{n+1,k}(\boldsymbol{n}\times) \rrbracket)_{\widetilde{\Gamma}} \tag{5.62}$$

When assembled into matrix form, (5.62) can be expressed as

$$\boldsymbol{\theta}^{\mathrm{T}} \left\{ \boldsymbol{R}^p_{n+1,k} \right\}, \tag{5.63}$$

where the vector $\boldsymbol{\theta}$ are the degrees of freedom associated with $\boldsymbol{V}$, as seen in (5.50). Lastly, the flow rule needs to be linearized with respect to an increment in $\boldsymbol{H}^p$. The approach taken is a first-order Taylor expansion of the residual.

$$\mathscr{R}_{n+1,k+1} = \mathscr{R}_{n+1,k} + \frac{\partial \mathscr{R}_{n+1,k}}{\partial \boldsymbol{H}^p} : \delta \boldsymbol{H}^p = 0 \tag{5.64}$$

The linearization of the flow rule, to obtain the derivative term in (5.64), can be seen in the Appendix in Section B.4, and the result is shown below.

$$\begin{aligned} &\frac{\partial \mathscr{R}_{n+1,k}}{\partial \boldsymbol{H}^p} : \delta \boldsymbol{H}^p = \\ &\left(\boldsymbol{V}, \left[\frac{\sigma_y}{\widetilde{d^p}_{n+1,k}} \mathbf{1} \otimes \mathbf{1} - \frac{\sigma_y}{\widetilde{d^p}^3_{n+1,k}} \Delta \boldsymbol{H}^p_{n+1,k} \otimes \Delta \boldsymbol{H}^p_{n+1,k} + \mathbb{C} \right] : \delta \boldsymbol{H}^p \right)_\Omega \\ &+ \frac{\alpha k}{h} (\llbracket \boldsymbol{V}(\boldsymbol{n}\times) \rrbracket, \llbracket \delta \boldsymbol{H}^p (\boldsymbol{n}\times) \rrbracket)_{\widetilde{\Gamma}} \end{aligned} \tag{5.65}$$

From (5.65), the consistent tangent can be assembled into the stiffness matrix for the flow rule, $\boldsymbol{K}^p_{n+1,k}$, and iteratively solved for $\delta \boldsymbol{H}^p_k$, the increment in the plastic distortion. In matrix form the system for the flow rule, (5.64), looks as

$$\boldsymbol{\theta}^{\mathrm{T}} \left\{ \boldsymbol{R}^p_{n+1,k} \right\} + \boldsymbol{\theta}^{\mathrm{T}} \left[\boldsymbol{K}^p_{n+1,k} \right] \boldsymbol{\eta} = 0, \tag{5.66}$$

where $\boldsymbol{\eta}$ is the vector of degrees of freedom associated with $\delta \boldsymbol{H}^p$. Due to the arbitrariness of the variational degrees of freedom $\boldsymbol{\theta}$, we arrive at the following system, for $\boldsymbol{\eta}$.

$$\left[\boldsymbol{K}^p_{n+1,k} \right] \boldsymbol{\eta} = -\boldsymbol{R}^p_{n+1,k} \tag{5.67}$$

Then the iteration proceeds with the update of the field using (5.67) and the interpolations for $\delta \boldsymbol{H}^p$ in (5.50)

$$\boldsymbol{H}^p_{n+1,k+1} = \boldsymbol{H}^p_{n+1,k} + \delta \boldsymbol{H}^p_k, \tag{5.68}$$

and $k \longrightarrow k+1$.

The backstress, $\boldsymbol{\beta}_{n+1}$, comes directly from the flow rule, (5.24), and as such is defined as

$$\boldsymbol{\beta}_{n+1} = \left(\text{dev curl } \left(k \text{ curl } \boldsymbol{H}^p_{n+1}\right)^{\mathrm{T}}\right)^{\mathrm{T}}. \tag{5.69}$$

However, the choice of a constant basis for $\boldsymbol{H}^p$ renders (5.69) insufficient to determine the backstress, since the curl terms evaluate to zero. In order to construct a consistent backstress the variational form of the flow rule, and specifically the fact that it is driven to zero, is exploited. Given a converged solution of the flow rule where we are substituting (5.69) in for the gradient term,

$$\boldsymbol{T}^p_{n+1} - \text{dev } \boldsymbol{\sigma}_{n+1} + \boldsymbol{\beta}_{n+1} = \boldsymbol{0}, \tag{5.70}$$

we can approximate the back stress as,

$$\boldsymbol{\beta}_{n+1} \approx \boldsymbol{T}^p_{n+1} - \text{dev } \boldsymbol{\sigma}_{n+1}. \tag{5.71}$$

Inspection of the method shows that for a hardening modulus of zero, $k = 0$, $\boldsymbol{T}^p_{n+1} = \text{dev } \boldsymbol{\sigma}_{n+1}$ and no backstress is accumulated. Intuitively, the backstress term comes directly from the interior facet gradient term. In practice, once the flow rule solution procedure has converged, $\boldsymbol{\beta}_{n+1}$ is calculated, and the solution of macroscopic equilibrium follows.

The solution of the equilibrium equation follows a successful solution of the flow rule. In a similar fashion the $\boldsymbol{H}^p$ degrees of freedom are held constant during this solve, and further, the fact that the flow rule has been satisfied is exploited, which essentially allows the whole mixed system to be assembled and solved. The global equilibrium residual, for iterate j, is constructed as

$$\mathscr{R}^{eq}_{n+1,j} = \left\{ \begin{array}{c} (\boldsymbol{\nabla} \boldsymbol{w}, \boldsymbol{\sigma}_{n+1,j})_\Omega \\ \\ \boldsymbol{0} \end{array} \right\}, \tag{5.72}$$

which in matrix form appears as,

$$\left\{ \begin{array}{c} \boldsymbol{c} \\ \boldsymbol{\theta} \end{array} \right\}^{\mathrm{T}} \left\{ \begin{array}{c} \boldsymbol{R}^{eq}_{n+1,j} \\ \boldsymbol{0} \end{array} \right\}, \tag{5.73}$$

where the $\boldsymbol{0}$ is indicative that the flow rule has already been satisfied, leaving a zero residual for the $\boldsymbol{H}^p$ degrees of freedom. After relatively simple linearization, the equilibrium tangent can be split into partitions defined as

$$(\boldsymbol{\nabla w}, \mathbb{C} : \boldsymbol{\nabla}^s \delta \boldsymbol{u}) \tag{5.74}$$

$$+ \quad (\boldsymbol{\nabla w}, -\mathbb{C} : (\mathrm{sym}\, \delta \boldsymbol{H}^p))_\Omega \tag{5.75}$$

$$+ \quad (\boldsymbol{V}, -\mathbb{C} : \boldsymbol{\nabla}^s \delta \boldsymbol{u})_\Omega \tag{5.76}$$

$$+ \quad \left(\boldsymbol{V}, \left[\frac{\sigma_y}{\widetilde{d^p}_{n+1,k}} \mathbf{1} \otimes \mathbf{1} - \frac{\sigma_y}{\widetilde{d^p}^3_{n+1,k}} \Delta \boldsymbol{H}^p_{n+1,k} \otimes \Delta \boldsymbol{H}^p_{n+1,k} + \mathbb{C} \right] : \delta \boldsymbol{H}^p \right)_\Omega \tag{5.77}$$

$$+ \frac{\alpha k}{h} (\llbracket \boldsymbol{V}(\boldsymbol{n}\times) \rrbracket, \llbracket \delta \boldsymbol{H}^p (\boldsymbol{n}\times) \rrbracket)_{\widetilde{\Gamma}},$$

which lead to the matrix equations for the linearized global equilibrium system.

$$\left\{ \begin{array}{c} \boldsymbol{c} \\ \boldsymbol{\theta} \end{array} \right\}^{\mathrm{T}} \left(\left\{ \begin{array}{c} \boldsymbol{R}^{eq}_{n+1,j} \\ \boldsymbol{0} \end{array} \right\} + \left[\begin{array}{cc} \boldsymbol{K}^{uu}_{n+1,j} & \boldsymbol{K}^{uh}_{n+1,j} \\ \boldsymbol{K}^{hu}_{n+1,j} & \boldsymbol{K}^{hh}_{n+1,j} \end{array} \right] \left\{ \begin{array}{c} \boldsymbol{d} \\ \boldsymbol{\eta} \end{array} \right\} \right) = 0 \tag{5.78}$$

The result of (5.78), when considering the arbitrariness of the variations, is the system of equations seen below.

$$\left[\begin{array}{cc} \boldsymbol{K}^{uu}_{n+1,j} & \boldsymbol{K}^{up}_{n+1,j} \\ \boldsymbol{K}^{pu}_{n+1,j} & \boldsymbol{K}^{pp}_{n+1,j} \end{array} \right] \left\{ \begin{array}{c} \boldsymbol{d} \\ \boldsymbol{\eta} \end{array} \right\} = - \left\{ \begin{array}{c} \boldsymbol{R}^{eq}_{n+1,j} \\ \boldsymbol{0} \end{array} \right\} \tag{5.79}$$

Note that the matrix $\boldsymbol{K}^{pp}_{n+1,j}$ is precisely the same matrix from the converged solution of the flow rule, $\boldsymbol{K}^{p}_{n+1,k}$, and thus can be reused during assembly of the global equilibrium system. At this time, the global system is assembled and solved. However, further manipulation of the system is possible, and could impact the efficiency

of the algorithm. Consider the global system in (5.79), which can be written into two equations.

$$\boldsymbol{K}^{uu}_{n+1,j}\boldsymbol{d} + \boldsymbol{K}^{up}_{n+1,j}\boldsymbol{\eta} = -\boldsymbol{R}^{eq}_{n+1,j} \tag{5.80}$$

$$\boldsymbol{K}^{pu}_{n+1,j}\boldsymbol{d} + \boldsymbol{K}^{pp}_{n+1,j}\boldsymbol{\eta} = \boldsymbol{0} \tag{5.81}$$

Concentrating on (5.81), we can solve for the vector $\boldsymbol{\eta}$, in terms of the displacement degrees of freedom $\boldsymbol{d}$.

$$\boldsymbol{\eta} = -\left[\boldsymbol{K}^{pp}_{n+1,j}\right]^{-1}\boldsymbol{K}^{pu}_{n+1,j}\boldsymbol{d} \tag{5.82}$$

Now we can use the result of (5.82) by substitution into (5.80) to arrive at the following equation.

$$\left(\boldsymbol{K}^{uu}_{n+1,j} - \boldsymbol{K}^{up}_{n+1,j}\left[\boldsymbol{K}^{pp}_{n+1,j}\right]^{-1}\boldsymbol{K}^{pu}_{n+1,j}\right)\boldsymbol{d} = -\boldsymbol{R}^{eq}_{n+1,j} \tag{5.83}$$

The previous process is not unlike static condensation for a local field, however the matrix to be inverted in this case, $[\boldsymbol{K}^{pp}_{n+1,j}]$, is global by nature due to the interior facet terms, and cannot be reduced down to a matrix inversion at the element level. Nevertheless, manipulation of the system into (5.83) deserves attention and will be studied in future work.

CHAPTER 6

Numerical Results

In order to test the model formulation and implementation, a number of simulations were run. Specifically, this Chapter will focus on boundary value problems that illustrate the features of the gradient plasticity model. The first problem examined will be the cylinder under torsion discussed in Section2.3, mainly because the solution exhibits a spatially varying strain field which produces a gradient in the displacement gradient and in $\boldsymbol{H}^p$. These gradients activate pertinent features of the model that uniform strain fields do not. A comparative example will be given for uniaxial tension. Next, the plane strain compression problem from Section 2.3 will be studied for the effect of the gradient model on the localization phenomenon. The gradient hardening term in the model provides a length scale by which dissipation occurs, as opposed to any inherent mesh size.

6.1 Torsion

The implementation seen in Algorithm 5.1 for the DG IP formulation is first applied to the torsional boundary value problem. Please see Figure 2.6 to recall the scenario. The first set of simulations are intended to show that as the gradient modulus, k, is varied, a proportional increase in hardening is observed. To ensure that the mesh resolution is sufficient to resolve the gradients, three meshes are used for a constant domain size and constant hardening modulus. The number of elements

Mesh	Number of tets
Mesh 1	1031
Mesh 2	3882
Mesh 3	6826

Table 6.1: Number of elements per mesh for the DG torsion problem

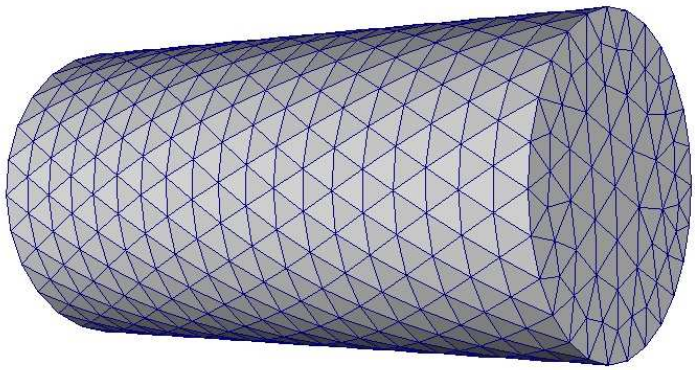

Figure 6.1: Picture of Mesh 3 for the DG torsion problem

in each mesh used can be seen in Table 6.1, and a picture of Mesh 3 can be seen in Figure 6.1. In Figure 6.2 the relative change between the torque curves is sufficiently small to justify the use of Mesh 3 for our studies. Ideally, mesh resolutions similar to those seen in Section 2.3.1 would be used in the comparison to the analytical solution for perfect plasticity would be used. However, additional computation cost introduced by the DG formulation place practical restrictions on the mesh size for the initial implementation of this model. Further refinement studies will follow more efficient implementations.

In Figure 6.3, k is varied from 0 (perfect plasticity) to 1000 [MPa-mm^2] using a constant domain size and Mesh 3 from Table 6.1. The response of the model shows increased hardening, in terms of the applied torque versus twist, as k is increased.

To illustrate that the torsion problem, or another similar boundary value prob-

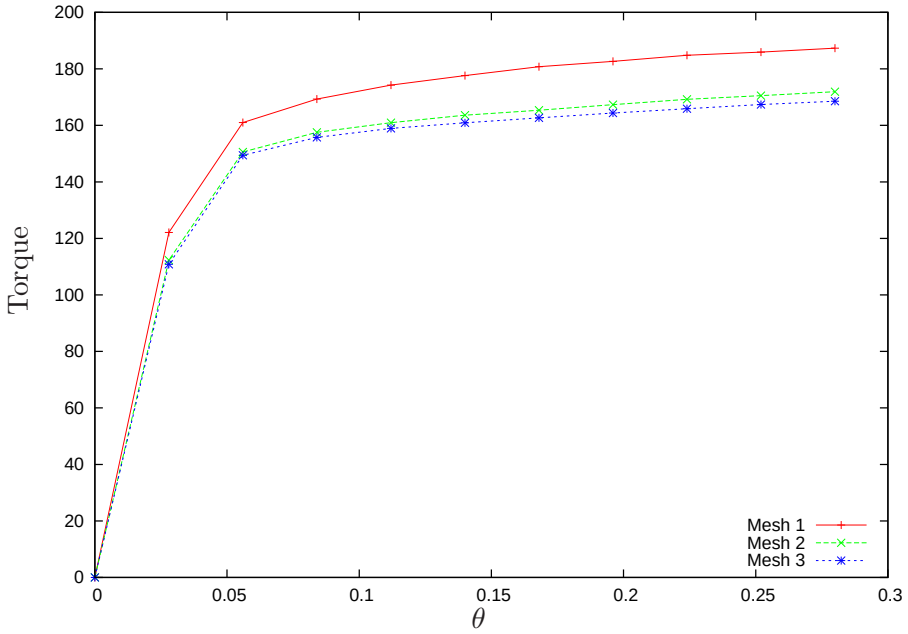

Figure 6.2: Hardening curve for various mesh densities

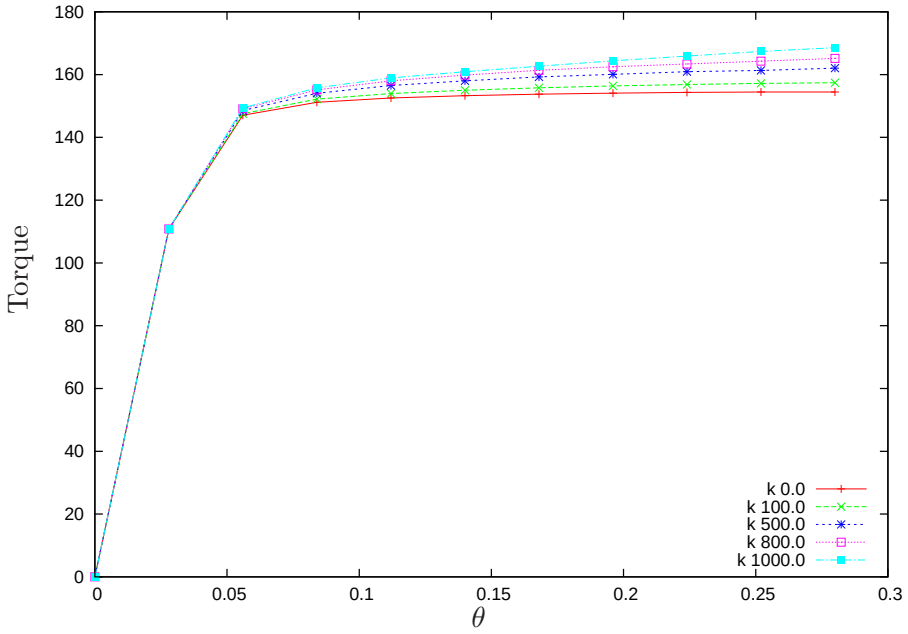

Figure 6.3: Influence of hardening modulus on torque versus twist

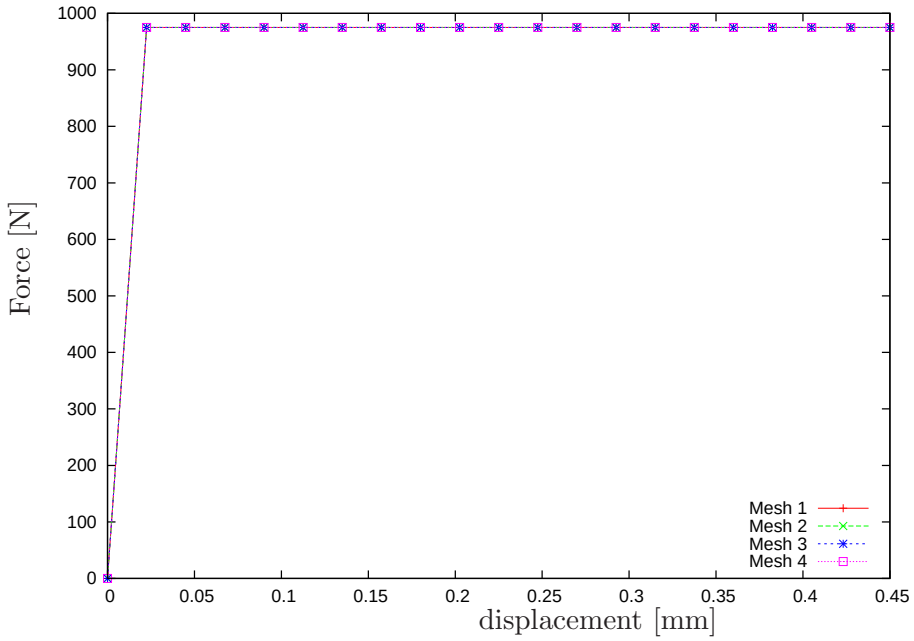

Figure 6.4: No hardening for model in tension

lem, is necessary to show the gradient dependence of the model, consider uniaxial tension. The solution will be a constant stress field throughout the domain, and the corresponding jump in $\boldsymbol{H}^p$ will be zero, with a net result of zero hardening in the model. It is worth noting that for this reason, the kinematic hardening introduced in this model is not a mechanism by which to model the Bauschinger effect, seen in Section 2.3.1 and discussed in Section 3.1, which can be observed in uniaxial cyclic loading. Figure 6.4 shows the lack of effect that the gradient term has on a uniaxial stress field with a gradient modulus $k = 1000.0$. In this case, since the hardening term is not activated, the response of the model is elastic-perfectly plastic. The number of elements for the meshes used in Figure 6.4 varied monotonically from 6 tetrahedral elements for Mesh 1 to 384 for Mesh 4 for a cubic geometry.

The first of our objectives in formulating the gradient model presented in this dissertation is the ability to model a size effect in a plastically deforming material. To accomplish this, a series of cylinders of various radius a, ranging from 1 mm to

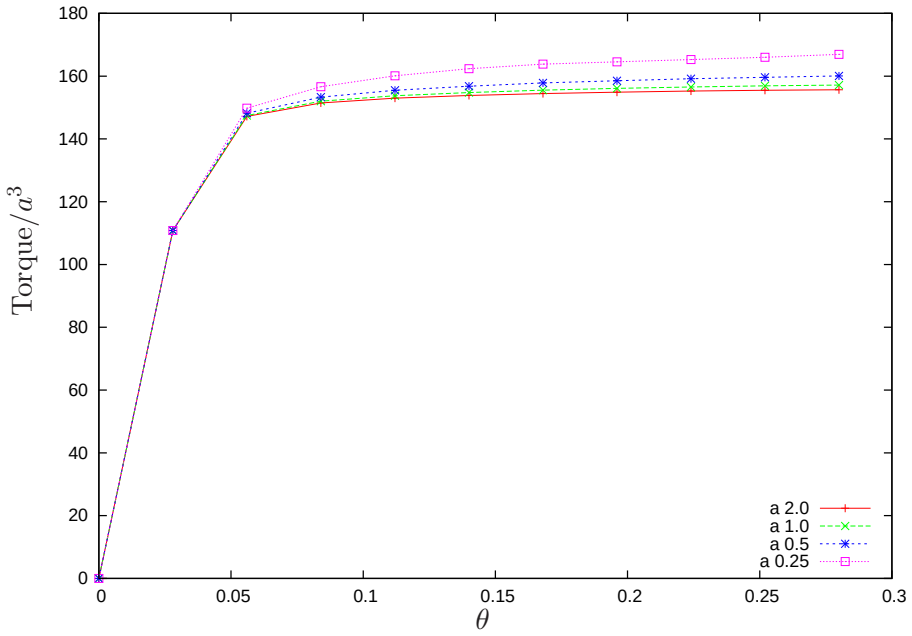

Figure 6.5: Size effect of varying the cylinder radius

0.125 mm, were meshed and subjected to the same torsional boundary conditions as previously discussed. Figure 6.5 shows that, for a constant gradient hardening modulus k=20, as the radius of the cylinder is decreased, the normalized hardening response increases, indicating an inverse relationship between size and hardening. The size effect cannot be captured by the classical theory, since it does not include an inherent length scale.

6.2 Localization

The second main objective of the gradient formulation is the ability to achieve mesh independent solutions for localization problems. As discussed earlier, the softening pathologies illustrated in Section 2.3.2 can be alleviated by the introduction of a length scale by which energy can be dissipated. To this end, linear isotropic hardening is added to the gradient plasticity model, following the procedures outlined in Chapter 2. The implementation, however, differs due to the fact that the primal

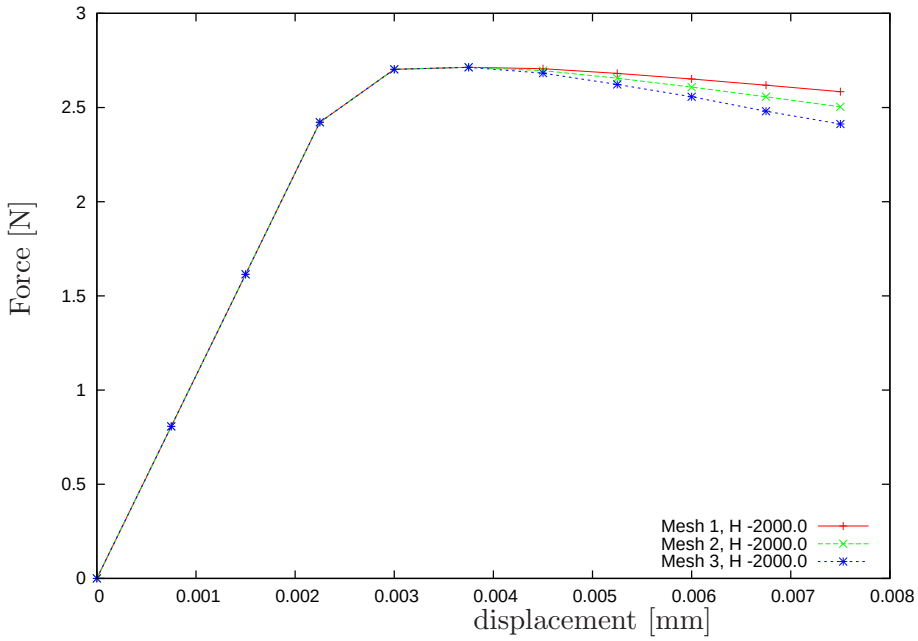

Figure 6.6: Mesh dependent softening

plastic field is now a global variable. Nevertheless, the main ideas remain the same. To show the impact that the gradient formulation has on a localization problem, we will revisit the plane strain compression problem, and apply the DG IP gradient plasticity formulation to it. See Figure 2.11 to recall the boundary value problem. The value of the linear isotropic hardening modulus used for this study is fixed at -2000 MPa.[1] To revisit the behavior of the model with a negative linear isotropic hardening modulus, simulations were run for three different meshes, and the results can be seen in Figure 6.6, which compares with the results from the classical implementation seen in Figure 2.12. The number of elements for Meshes 1-3 correspond to the values in Table 2.3.

Introduction of a non-zero gradient modulus has the effect of introducing a length scale that serves to define a finite volume over which energy can be dissipated. For

[1] As opposed to the exponential hardening law used in Section 2.3.2. The load displacement curves come out nearly the same in each case, and it should be clear that the pathology exists for both of these cases.

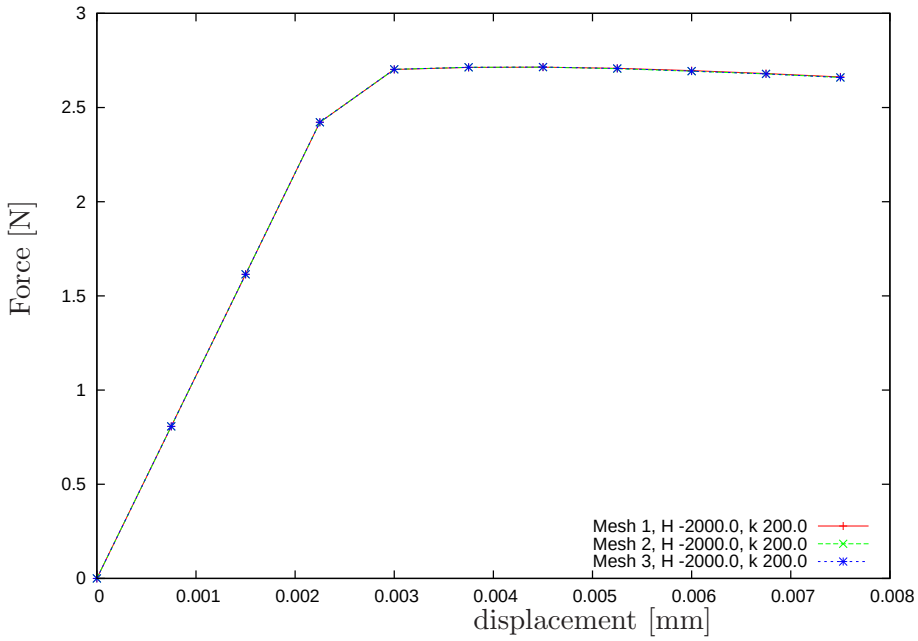

Figure 6.7: Mesh independent softening via the gradient model

the problem under question, a gradient modulus of 200 [MPa-m^2] is used. Figure 6.7 illustrates the effect that the gradient plasticity model has on the softening problem. The force versus displacement curves essentially lie on top of each other, providing evidence that the model does indeed alleviate the pathology associated with softening.

CHAPTER 7

Concluding Remarks

This dissertation presented a formulation of a gradient plasticity model cast in a discontinuous Galerkin framework. Attention was paid to the classical theory in order to illustrate the foundation of concepts central to the field of plasticity. Details regarding finite element implementation and example problems examining features of the classical theory were also presented. The principles behind discontinuous Galerkin methods were discussed along with an example of the DG variational formulation in the simple setting of linear elasticity. The relationship between dislocations and plasticity, specifically dislocation motion, was examined and used as a basis for a continuum theory of a gradient dependent constitutive model. Variational principles along with the DG machinery were employed to derive a variational statement of the gradient plasticity problem fit for implementation into a nonlinear finite element code. Numerical results were generated for a select number of boundary value problems that illustrated desirable features of the proposed model, namely the ability to predict a size effect for bodies undergoing plastic deformation, and the regularization of softening problems leading to mesh independent solutions.

The defining characteristic of this work was the utilization of the symmetric DG IP method in formulating the flow rule. This allowed for the use of piecewise discontinuous functions for $\boldsymbol{H}^p$. A novel investigation into the approximation of the back-stress term in the yield condition was undertaken, comparing a utilization of the

lifting operator approach to approximate the curl operator, versus an exploitation of the flow rule. Furthermore, the integration algorithm for the mixed system was investigated, the result being a staggered scheme that conceptually resembles the predictor-corrector strategy of the classical method.

Despite the published results justifying the effort of developing a gradient plasticity theory, the search for clean, reproducible experimental methods is ongoing because of the assumptions and difficulty in handling the specimen and loading conditions at such small scales. In particular for the microtorsion experiments presented in Fleck and Hutchinson (1993), another valid explanation for the hardening response could be constructed if the grain size in the copper wires also decreased with diameter, as grain size is a known influence on the ability of a material to harden. No characterization of the grain size was discussed, so the topic is still open for debate. Experiments at these scales are not straightforward. Good results, however, are necessary for a meaningful model validation exercise. Validation entails comparisons between numerical predictions and experimental data for the purpose of determining if the correct physics have been incorporated into the model. Comparison efforts can be focused both towards legacy data found in the literature and also at results of current work. At this time, the model presented in this dissertation would not sufficiently describe the hardening response of a material in a validation exercise. To make the model generally applicable, other well known hardening mechanisms would have to be incorporated into the theory, and any future extension of the model should incorporate other mechanisms of physically motivated isotropic and kinematic hardening.

As another direction of future research, more efficient implementation would facilitate a greater ability to study the behavior of the method, and should proceed in

a parallel finite element code. In terms of the constitutive model, the extension to finite deformation is necessary for applicability to a wider variety of problems, possibly coinciding with the inclusion of other hardening mechanisms. Further research on how to apply the DG methodology in the context of finite deformation should also follow. The lifting formulation for the proposed model should be investigated, since it adds the possibility of separating the hardening term away from the stabilization term. Other theories of gradient plasticity should be implemented as well to gauge a comparison between effectiveness and efficiency.

APPENDICES

APPENDIX A

Nonlinear Continuum Mechanics

The following section presents a short introduction to nonlinear continuum mehcanics. Familiarity with direct and indicial notation is assumed. Specific results are used in Chapter 2 in the discussion about classical theoretical plasticity. For more detailed expositions, refer to the cited continuum mechanics texts (Truesdell and Noll, 1965; Malvern, 1969; Holzapfel, 2000; Gurtin, 2003).

A.1 Kinematics

Kinematics is the study of motion and deformation in continuum bodies. We postulate the existence of a body, defined as an open subset of $\mathbb{R}^3$, as a collection of an infinite number of material points. The placement of all material points in the body at a given time is termed a *configuration*. The reference configuration of a body, Ω_0, with the material points in their reference positions, $\boldsymbol{X} \in \Omega_0$, is arbitrary, but for convenience is often chosen such that none of the points within the body have experienced any motion or deformation. The initial configuration of a body coincides with the placement of the body at the time $t = 0$. For simplicity, it is further assumed that the initial configuration and reference configuration are one and the same (which is certainly not necessary). At some time, $t > 0$, after experiencing

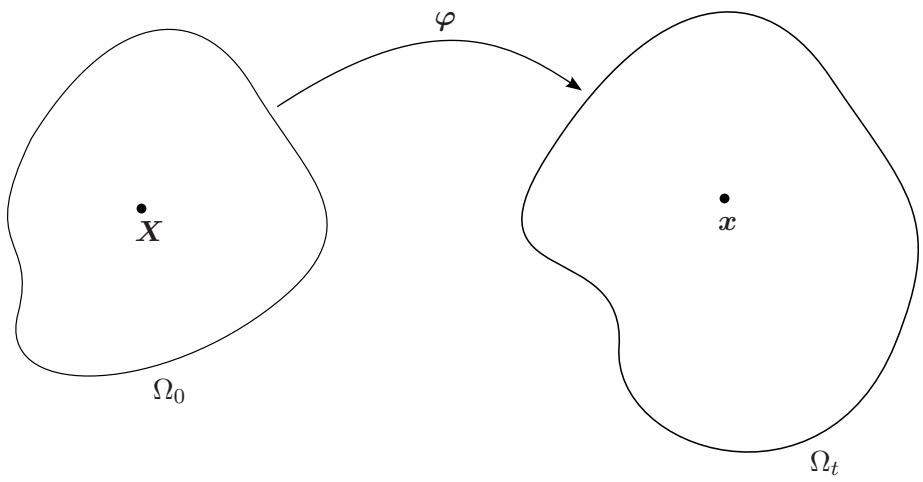

Figure A.1: Reference and current configuration, motion of a continuum body

loads in some manner, the body exists in its current, or deformed, configuration, Ω_t, with the material points at the current coordinates, $\boldsymbol{x}$. The motion of the body, $\boldsymbol{\varphi} : \overline{\Omega}_0 \times [0, T] \to \mathbb{R}^3$ is a mapping from the reference to the current configuration, as depicted in Figure A.1, where $\overline{\Omega}_0 := \overline{\Omega_0 \cup \partial\Omega_0}$; $\partial\Omega_0$ being the boundary of Ω_0. Quantites in the reference configuration will henceforth be termed *material* quantities, while those in the current configuration will be termed *spatial* quantities.

The spatial *displacement* of the body, $\boldsymbol{u}(\boldsymbol{x}, t)$, is a vector field that relates the placement of the material point in the current configuration to the position it had in the reference configuration.

$$\boldsymbol{u} = \boldsymbol{x} - \boldsymbol{X} \tag{A.1}$$

By this definition and because we have assumed that the initial and reference placements of the body coincide, the displacement vector vanishes in the reference configuration.

The *velocity* and *acceleration* are also defined for the body in both the reference and current configurations. The material versions of the velocity and acceleration

and the first are second time derivatives of the mapping.

$$\boldsymbol{V}(\boldsymbol{X},t)=\frac{\partial\boldsymbol{\varphi}}{\partial t},\ \boldsymbol{A}(\boldsymbol{X},t)=\frac{\partial^2\boldsymbol{\varphi}}{\partial t^2} \tag{A.2}$$

The spatial velocity field is determined from the material time derivative of the motion, or $\boldsymbol{v}=\frac{\partial\boldsymbol{x}}{\partial t}$. Finally, the spatial acceleration, determined from the material time derivative of the spatial velocity can be evaluated as follows.

$$\boldsymbol{a}=\dot{\boldsymbol{v}}=\frac{\partial\boldsymbol{v}}{\partial t}+\boldsymbol{\nabla v}\,\boldsymbol{v} \tag{A.3}$$

The *deformation gradient*, $\boldsymbol{F}$, is a tensor that is used to characterize the deformation of a body as it transforms from the reference configuration into the current configuration. A derivation of the deformation gradient can easily be accomplished by considering a material curve in the reference configuration, parametrized by ξ, $\boldsymbol{X}=\boldsymbol{\Gamma}(\xi)$. Recall that a material curve is undeformed and associated with the reference configuration, Ω_0. After imposition of a motion, or deformation mapping, $\boldsymbol{\varphi}$, the material curve deforms into a spatial curve, $\boldsymbol{x}=\boldsymbol{\gamma}(\xi,t)$ (spatial quantities will depend on time, whereas the material curve will not be a function of time). The spatial curve can then be described parametrically as

$$\boldsymbol{x}=\boldsymbol{\varphi}(\boldsymbol{\Gamma}(\xi),t), \tag{A.4}$$

which upon taking derivatives holding time fixed to determine the tangent to the spatial curve yields

$$\mathrm{d}\boldsymbol{x}=\frac{\partial\boldsymbol{\gamma}}{\partial\xi}\mathrm{d}\xi. \tag{A.5}$$

Similarly for the material curve

$$\mathrm{d}\boldsymbol{X}=\frac{\partial\boldsymbol{\Gamma}}{\partial\xi}\mathrm{d}\xi. \tag{A.6}$$

Now using the chain rule and (A.4) to define a relationship between the material curve and spatial curve tangent vector we arrive at

$$\mathrm{d}\boldsymbol{x} = \boldsymbol{F}(\boldsymbol{X}, t)\,\mathrm{d}\boldsymbol{X}, \tag{A.7}$$

where the formation gradient $\boldsymbol{F}$ is defined as

$$\boldsymbol{F}(\boldsymbol{X}, t) = \frac{\partial \boldsymbol{\varphi}}{\partial \boldsymbol{X}} = \frac{\partial \boldsymbol{x}}{\partial \boldsymbol{X}}. \tag{A.8}$$

The formation gradient is considered a *two point tensor* since one argument, $\boldsymbol{x}$, lives in the current configuration while the other, $\boldsymbol{X}$, lives in the reference configuration. $\boldsymbol{F}$ is generally a nonsingular or invertible, which implies that $\det\boldsymbol{F} \neq 0$. The determinant of $\boldsymbol{F}$ is an important quantity called the *jacobian determinant*, $\det\boldsymbol{F} = J$, and physical arguments, such as the impenetrability of matter, dictate that $J > 0$. In order to aid later discussion it is useful to show that $\boldsymbol{F}$ can be written in terms of the displacement vector, $\boldsymbol{u}$. By combining (A.1) and (A.8) we arrive at the following alternate expression for the deformation gradient, in terms of displacements, where $\mathbf{1}$ is the second-order identity tensor.

$$\boldsymbol{F} = \mathbf{1} + \frac{\partial \boldsymbol{u}}{\partial \boldsymbol{X}} \tag{A.9}$$

Various *strain* measures have been proposed, usually as functions of $\boldsymbol{F}$, which asssist in the characterization of the material response. One such strain measure will be introduced here, called the Green-Lagrange strain tensor, $\boldsymbol{E}$, which is a material tensor. To define $\boldsymbol{E}$ it is convenient to first define the right Cauchy-Green tensor, $\boldsymbol{C} = \boldsymbol{F}^{\mathrm{T}}\boldsymbol{F}$. Then the Green-Lagrange strain tensor follows, using $\mathbf{1}$ as the second-order identity tensor.

$$\boldsymbol{E} = \frac{1}{2}(\boldsymbol{C} - \mathbf{1}) = \frac{1}{2}(\boldsymbol{F}^{\mathrm{T}}\boldsymbol{F} - \mathbf{1}) \tag{A.10}$$

$\boldsymbol{E}$ is a nonlinear measure of strain which can be illustrated by expanding out (A.10) using the alternate definition of $\boldsymbol{F}$, (A.9).

$$\boldsymbol{E} = \frac{1}{2}\left((\mathbf{1}+\frac{\partial \boldsymbol{u}}{\partial \boldsymbol{X}})^{\mathrm{T}}(\mathbf{1}+\frac{\partial \boldsymbol{u}}{\partial \boldsymbol{X}})-\mathbf{1}\right) \tag{A.11}$$

$$= \frac{1}{2}\left(\frac{\partial \boldsymbol{u}}{\partial \boldsymbol{X}}+(\frac{\partial \boldsymbol{u}}{\partial \boldsymbol{X}})^{\mathrm{T}}+(\frac{\partial \boldsymbol{u}}{\partial \boldsymbol{X}})^{\mathrm{T}}\frac{\partial \boldsymbol{u}}{\partial \boldsymbol{X}}\right) \tag{A.12}$$

It is evident from (A.11) that $\boldsymbol{E}$ is quadratic in the displacements. A simple view of linearizing this theory that coincides with the classical small strain tensor, $\boldsymbol{\varepsilon}$, is to consider the quadratic term a higher-order term that can be omitted under the assumption of infinitesimal displacements. Then the classical symmetric strain tensor is recovered.

$$\boldsymbol{\varepsilon} = \frac{1}{2}\left(\frac{\partial \boldsymbol{u}}{\partial \boldsymbol{X}}+(\frac{\partial \boldsymbol{u}}{\partial \boldsymbol{X}})^{\mathrm{T}}\right) \tag{A.13}$$

A.1.1 Scaling Between the Reference and Current Configurations

It is useful to be able to express quantities in either the reference or current configuration. To accomplish this recall from (A.7) that for material and spatial curves the tangents of the curves are mapped via the deformation gradient. Next we can consider the relationship between surfaces in the reference and current configuration. Define a surface in Ω_0 parametrized using ξ_1 and ξ_2 as $\boldsymbol{R}(\xi_1,\xi_2)$. Similarly for the surface in Ω_t use $\boldsymbol{r}(\xi_1,\xi_2)$. Elemental areas for $\boldsymbol{R}$ and $\boldsymbol{r}$ are then cross products of the tangent vectors of each of the parametrized directions.

$$\frac{\mathrm{d}\boldsymbol{R}}{\mathrm{d}\xi_1}\times\frac{\mathrm{d}\boldsymbol{R}}{\mathrm{d}\xi_2} = \frac{\frac{\mathrm{d}\boldsymbol{R}}{\mathrm{d}\xi_1}\times\frac{\mathrm{d}\boldsymbol{R}}{\mathrm{d}\xi_2}}{\left\|\frac{\mathrm{d}\boldsymbol{R}}{\mathrm{d}\xi_1}\times\frac{\mathrm{d}\boldsymbol{R}}{\mathrm{d}\xi_2}\right\|}\left\|\frac{\mathrm{d}\boldsymbol{R}}{\mathrm{d}\xi_1}\times\frac{\mathrm{d}\boldsymbol{R}}{\mathrm{d}\xi_2}\right\| = \boldsymbol{N}\mathrm{dA} \tag{A.14}$$

$$\frac{\mathrm{d}\boldsymbol{r}}{\mathrm{d}\xi_1}\times\frac{\mathrm{d}\boldsymbol{r}}{\mathrm{d}\xi_2} = \frac{\frac{\mathrm{d}\boldsymbol{r}}{\mathrm{d}\xi_1}\times\frac{\mathrm{d}\boldsymbol{r}}{\mathrm{d}\xi_2}}{\left\|\frac{\mathrm{d}\boldsymbol{r}}{\mathrm{d}\xi_1}\times\frac{\mathrm{d}\boldsymbol{r}}{\mathrm{d}\xi_2}\right\|}\left\|\frac{\mathrm{d}\boldsymbol{r}}{\mathrm{d}\xi_1}\times\frac{\mathrm{d}\boldsymbol{r}}{\mathrm{d}\xi_2}\right\| = \boldsymbol{n}\mathrm{da} \tag{A.15}$$

Now we can note that the spatial elemental area can also be expressed using the deformation gradient to map the tangent vectors from the reference to the current

configuration.

$$\boldsymbol{n}\,\mathrm{da} = \left(\boldsymbol{F}\frac{\mathrm{d}\boldsymbol{R}}{\xi_1}\right) \times \left(\boldsymbol{F}\frac{\mathrm{d}\boldsymbol{R}}{\xi_2}\right) \tag{A.16}$$

Recalling A useful formula, Nanson's formula can be stated for $a, b \in \mathbb{R}^3$ and second-order tensor $\boldsymbol{A}$,

$$\boldsymbol{A}\boldsymbol{a} \times \boldsymbol{A}\boldsymbol{b} = \det(\boldsymbol{A})\boldsymbol{A}^{-\mathrm{T}}(\boldsymbol{a} \times \boldsymbol{b}). \tag{A.17}$$

Using (A.17) in (A.16) yield the important result.

$$\boldsymbol{n}\mathrm{da} = \det \boldsymbol{F}\, \boldsymbol{F}^{-\mathrm{T}}\, \boldsymbol{N}\mathrm{dA}. \tag{A.18}$$

Then consider an elemental volume, $\mathrm{d}\boldsymbol{V}$, parametrized by three vectors, $\boldsymbol{u}, \boldsymbol{v}, \boldsymbol{w}$.

$$\mathrm{d}\boldsymbol{V} = (\boldsymbol{u} \times \boldsymbol{v}) \cdot \boldsymbol{w} \tag{A.19}$$

The volume element in the current configuration can be written using the deformation gradient as

$$\mathrm{d}\boldsymbol{v} = (\boldsymbol{F}\boldsymbol{u} \times \boldsymbol{F}\boldsymbol{v}) \cdot \boldsymbol{F}\boldsymbol{w}. \tag{A.20}$$

Relating the two is a simple process involving the (A.17) and the transpose of a tensor and the result follows.

$$\mathrm{d}\boldsymbol{v} = \det \boldsymbol{F}\, \mathrm{d}\boldsymbol{V} = J\mathrm{d}\boldsymbol{V} \tag{A.21}$$

A.2 Stress

If we consider a deformable body, then a loading of that body produces interactions between neighboring material points. The concept of *stress* is a natural consequence of these interior interactions. Cutting an imaginary plane through our

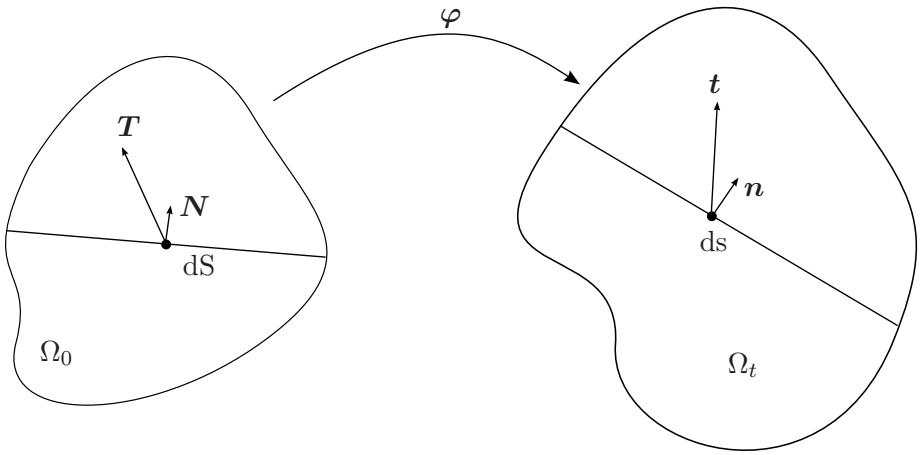

Figure A.2: Reference and current configuration, tractions on interior surfaces

two configurations in Figure A.1, an interior surfaces dS, in the reference configuration, and ds in the current configuration, are created. See Figure A.2 for a visual depiction of the quantities in the two configurations. The normal vectors of these new surfaces are $\boldsymbol{N}$ and $\boldsymbol{n}$ respectively. Now consider that forces are acting between the two portions of the body divided by the plane. With forces and surfaces we can define the notion of a traction vector, which has units of stress; force per unit area. The Cauchy traction vector follows as the force measured per unit surface area defined in the current configuration. Similarly, in the reference configuration, the first Piola-Kirchhoff traction vector is the force per unit surface area defined in the reference configuration. In differential form, the force can be related to the surface elements and tractions.

$$\mathrm{df} = \boldsymbol{t}\,\mathrm{ds} = \boldsymbol{T}\,\mathrm{dS} \tag{A.22}$$

A specific relationship between the tractions ($\boldsymbol{t}$ and $\boldsymbol{T}$) on a surface and the normals ($\boldsymbol{n}$ and $\boldsymbol{N}$) to that surface was proposed by Cauchy. He states that there is a linear relationship between the normal vector into the traction vector.

Cauchy's Stress Theorem There exist unique second-order tensor field $\boldsymbol{\sigma}$ and

$\boldsymbol{P}$ so that

$$\boldsymbol{t} = \boldsymbol{\sigma}\boldsymbol{n} \tag{A.23}$$

$$\boldsymbol{T} = \boldsymbol{P}\boldsymbol{N} \tag{A.24}$$

where $\boldsymbol{\sigma}$ is a spatial second-order tensor labeled the Cauchy, or true, stress, and $\boldsymbol{P}$ is a two point tensor, like $\boldsymbol{F}$, labeled the first Piola-Kirchhoff, or nominal, stress. A detailed proof of Cauchy's Theorem can be found in Gurtin (2003), and the result is so widely used it will not be reproduced here.

The relationship between the Cauchy stress and the first Piola-Kirchhoff stress can be discerned using Nanson's formula. First consider that since the material and spatial representation of the tractions are equivalent, we can equate them.

$$\boldsymbol{t}\,\mathrm{ds} = \boldsymbol{T}\,\mathrm{dS} \tag{A.25}$$

Next we can invoke Cauchy's stress theorem to rewrite (A.25) in terms of $\boldsymbol{\sigma}$ and $\boldsymbol{P}$.

$$\boldsymbol{\sigma}\boldsymbol{n}\,\mathrm{ds} = \boldsymbol{P}\boldsymbol{N}\,\mathrm{dS} \tag{A.26}$$

Now (A.18) can be used to write the spatial normal vector in terms of the material frame, and the result expresses the first Piola-Kirchhoff stress in term of the Cauchy stress.

$$\boldsymbol{P} = J\boldsymbol{\sigma}\boldsymbol{F}^{-\mathrm{T}} \tag{A.27}$$

It will be shown below in Section A.3.2 that the Cauchy stress in symmetric, which implies that $\boldsymbol{P}\boldsymbol{F}^{\mathrm{T}} = \boldsymbol{F}\boldsymbol{P}^{\mathrm{T}}$, and it follows that the first Piola-Kirchhoff stress is generally non-symmetric.

A.3 Balance Laws

The balance laws are fundamental concepts in continuum mechanics, meaning that they apply for any material. To make the same statement in a stronger fashion, the balance laws must be satisfied in a material for all time in order for the description of that material to fit within physical limitations as we understand them. The quantities that must remain in balance are mass, linear momentum, angular momentum, and energy. Each will be discussed subsequently.

A.3.1 Balance of Mass

If the restriction is made to the description of solid bodies that are neither losing nor gaining mass by any means of flux or source, then we can state the balance of mass as the *conservation of mass*. Define the reference density $\rho_0(\boldsymbol{X})$ as mass per unit volume, and integrating over the whole volume we can express the mass, m, in the reference configuration. Exploiting the notion that the mass is constant we can also define the spatial density, $\rho(\boldsymbol{x}, t)$, and integrate over Ω_t to arrive at the same mass.

$$m = \int_{\Omega_0} \rho_0(\boldsymbol{X}) \, \mathrm{d}V = \int_{\Omega_t} \rho(\boldsymbol{x}, t) \, \mathrm{d}v \tag{A.28}$$

Using (A.21), (A.28), and standard localization arguments, we can arrive at the *mass continuity equation*.

$$\rho_0 \boldsymbol{X} = \rho(\boldsymbol{x}, t) J(\boldsymbol{X}, t) \tag{A.29}$$

Since the mass is constant, we note that $\dot{\rho_0} = 0$, which implies from (A.29) that $\dot{\rho J} = 0$. Expanding this out using $\dot{J} = J \operatorname{div} \boldsymbol{v}$ gives the spatial form of the conservation of mass.

$$\dot{\rho J} = \dot{\rho} J + \rho \dot{J} = J(\dot{\rho} + \rho \operatorname{div} \boldsymbol{v}) = 0 \tag{A.30}$$

A.3.2 Balance of Momenta

Momentum balance principles are used to define the equations of motion for a body, and excluding polar continua, also result in a symmetric Cauchy stress tensor.

Linear Momentum

Elementary definition of linear momentum of a particle is simply its mass times its velocity. Generalization of this concept to a continuum body constitutes integrating the density multiplied by the velocity vector over the proper configuration.

$$\boldsymbol{L}(t) = \int_{\Omega_0} \rho_0 \boldsymbol{V} \, \mathrm{d}V = \int_{\Omega_t} \rho \boldsymbol{v} \, \mathrm{d}v \tag{A.31}$$

The rate of change of linear momentum is due to resultant forces, $\boldsymbol{F}_r(t)$, acting on the body, $\dot{\boldsymbol{L}}(t) = \boldsymbol{F}_r(t)$. Bodies satisfying this balance are in *equilibrium*. The resultant force vector can be decomposed into boundary terms (traction) and body force terms. First consider the spatial description.

$$\boldsymbol{F}_r(t) = \int_{\Omega_t} \boldsymbol{t} \, \mathrm{ds} + \int_{\partial\Omega_t} \boldsymbol{b} \, \mathrm{dv} \tag{A.32}$$

Now, we can employ Reynold's transport theorem to take the material time derivative of the spatial term in (A.31) and combining with (A.32) we arrive at

$$\int_{\Omega_t} \rho \dot{\boldsymbol{v}} \, \mathrm{dv} = \int_{\partial\Omega_t} \boldsymbol{t} \, \mathrm{ds} + \int_{\Omega_t} \boldsymbol{b} \, \mathrm{dv}. \tag{A.33}$$

Lastly, Cauchy's stress theorem is called upon again to write the tractions in term of a stress, $\boldsymbol{\sigma}$. Then the divergence theorem is used to convert the boundary integral into a domain integral.

$$\int_{\partial\Omega_t} \boldsymbol{t} \, \mathrm{ds} = \int_{\partial\Omega_t} \boldsymbol{\sigma}\boldsymbol{n} \, \mathrm{ds} = \int_{\Omega_t} \mathrm{div}\boldsymbol{\sigma} \, \mathrm{dv}. \tag{A.34}$$

What results, after localization, by combining (A.34) with (A.33) are the local equations of equilibrium.

$$\text{div}\boldsymbol{\sigma} + \boldsymbol{b} = \rho\dot{\boldsymbol{v}}, \quad \sigma_{ij,j} + b_i = \rho\dot{v}_i \tag{A.35}$$

Angular Momentum

Angular momentum relative to a fixed point, $\boldsymbol{r}$, is (not to be confused with J, the jacobian determinant) essentially $\boldsymbol{r} \times \boldsymbol{L}(t)$.

$$\boldsymbol{J}(t) = \int_{\Omega_0} \boldsymbol{r} \times \rho_0 \boldsymbol{V} \, \mathrm{d}V = \int_{\Omega_t} \boldsymbol{r} \times \rho \boldsymbol{v} \, \mathrm{d}v \tag{A.36}$$

Similar to the treatment above in Section A.3.2, we define a resultant moment equal to the rate of change of the angular momentum.

$$\dot{\boldsymbol{J}}(t) = \boldsymbol{M}(t) = \int_{\partial\Omega_t} \boldsymbol{r} \times \boldsymbol{t} \, \mathrm{ds} + \int_{\Omega_t} \boldsymbol{r} \times \boldsymbol{b} \, \mathrm{dv} \tag{A.37}$$

Again, we use Reynold's transport theorem to take the material time derivative of $\boldsymbol{J}(t)$ where we note that $\boldsymbol{r} \dot{\times} \boldsymbol{v} = \boldsymbol{r} \times \dot{\boldsymbol{v}}$.

$$\int_{\Omega_t} \boldsymbol{r} \times \rho\dot{\boldsymbol{v}} \, \mathrm{d}v = \int_{\partial\Omega_t} \boldsymbol{r} \times \boldsymbol{t} \, \mathrm{ds} + \int_{\Omega_t} \boldsymbol{r} \times \boldsymbol{b} \, \mathrm{dv} \tag{A.38}$$

Using Cauchy's stress theorem and the divergence theorem on the boundary traction term gives rise to two terms after the distribution of the derivative. In indicial notation

$$\int_{\partial\Omega_t} \varepsilon_{ijk} r_j t_k : \mathrm{ds} = \int_{\partial\Omega_t} \varepsilon_{ijk} r_j \sigma_{kl} n_l \, \mathrm{ds} = \int_{\Omega_t} (\varepsilon_{ijk} r_j \sigma_{kl,l} + \varepsilon_{ijk} \sigma_{kj}) \mathrm{dv}. \tag{A.39}$$

Now combining (A.39) with (A.38) and reorganizing terms, we have indicially

$$\int_{\Omega_t} \varepsilon_{ijk} r_j (\dot{v}_k - b_k - \sigma_{kl,l}) \, \mathrm{dv} = \int_{\Omega_t} \varepsilon_{ijk} \sigma_{kj} \, \mathrm{dv}. \tag{A.40}$$

Upon inspection of (A.40) note that the left hand side contains the local form of the balance of linear momentum, or equilibrium, (A.35). This must be satisfied for all time, which implies the following with the arbitrariness of the elemental volume

$$\varepsilon_{ijk}\sigma_{kj} = 0, \tag{A.41}$$

which can only be satisfied if

$$\sigma_{kj} = \sigma_{jk}. \tag{A.42}$$

This is the classical result dictating the symmetry of the Cauchy stress tensor.

A.4 Objectivity

The principal of objectivity is a fundamental concept in continuum mechanics, so much so that theories that do not abide by it are summarily dismissed out of hand. The basic intuitive idea behind it is that physics and physical laws should not be affected by the location of the observer, or similarly by a shift in the location of the observation. What this amounts to is a restriction on the functional forms of tensors used to describe material behavior.

A change is observer can be equivalently expressed as a rigid body motion of the current configuration. So given the current position of a body described by $\boldsymbol{x}$, we denote positions of a body that has undergone a superposed rigid body motion by $\boldsymbol{x}^+$. The relation between the two can be expressed as

$$\boldsymbol{x}^+ = \boldsymbol{c}(t) + \boldsymbol{Q}(t)\boldsymbol{x}. \tag{A.43}$$

Here, $\boldsymbol{c}(t)$ is an arbitrary translation, and thus only a function of time, and $\boldsymbol{Q}(t)$, is a proper orthogonal tensor, also only a function of time. It follows that the deformation gradient in the "+" configuration is $\boldsymbol{F}^+ = \boldsymbol{Q}(t)\boldsymbol{F}$. The requirement for

spatial tensors to be objective is that they transform according to the rule (for a tensor $\boldsymbol{\sigma}$),

$$\boldsymbol{\sigma}^{+} = \boldsymbol{Q}(t)\boldsymbol{\sigma}\boldsymbol{Q}^{\mathsf{T}}(t). \tag{A.44}$$

Tensors defined in the reference configuration, for example the right Cauchy-Green tensor $\boldsymbol{C} = \boldsymbol{F}^{\mathsf{T}}\boldsymbol{F}$, are invariant under superposed rigid body motions.

$$\boldsymbol{C}^{+} = \boldsymbol{F}^{+\mathsf{T}}\boldsymbol{F}^{+} = \boldsymbol{F}^{\mathsf{T}}\boldsymbol{Q}^{\mathsf{T}}(t)\boldsymbol{Q}(t)\boldsymbol{F} = \boldsymbol{C} \tag{A.45}$$

For a theory of constitutive behavior to have any physical significance, the tensor measures used to describe the behavior must behave objectively.

APPENDIX B

Supplementary Topics

B.1 Jump-Average Identity : I

We set out to prove the identity, for scalar fields f and g,

$$[\![fg]\!] = \langle f \rangle [\![g]\!] + [\![f]\!] \langle g \rangle.$$

To accomplish this we will begin with the right hand side and work back to the left hand side. Recalling the definitions of jump, (5.4), and the average, (5.5), we expand the right hand side of the assertion:

$$\begin{aligned}
& ave f [\![g]\!] + [\![f]\!] \langle g \rangle \\
= \; & \frac{1}{2}(f^+ + f^-)(g^+ - g^-) + (f^+ - f^-)\frac{1}{2}(g^+ + g^-) \\
= \; & \frac{1}{2}\left(f^+g^+ - f^+g^- + f^-g^+ - f^-g^- + f^+g^+ + f^+g^- - f^-g^+ - f^-g^-\right) \\
= \; & \frac{1}{2}\left(2f^+g^+ - 2f^-g^- + (f^+g^- - f^+g^-) + (f^-g^+ - f^-g^+)\right) \\
= \; & f^+g^+ - f^-g^- \\
= \; & [\![fg]\!]
\end{aligned}$$

And the proof is complete.

B.2 Curl Integration by Parts

We set to prove the following identity, with tensor fields $\boldsymbol{A}$ and $\boldsymbol{B}$ and unit normal $\boldsymbol{n}$ to boundary $\partial\Omega$.

$$-\int_{\partial\Omega}(\boldsymbol{n}\times\boldsymbol{A}):\boldsymbol{B}^{\mathsf{T}}\,\mathrm{d}S=\int_{\Omega}\left(\boldsymbol{A}:\mathsf{curl}\,\boldsymbol{B}-\boldsymbol{B}^{\mathsf{T}}:\mathsf{curl}\,(\boldsymbol{A}^{\mathsf{T}})\right)\,\mathrm{d}V$$

To accomplish this we will expand the left hand side in indicial notation and manipulate using integration by parts to obtain the right hand side.

$$\begin{aligned}-\int_{\partial\Omega}\varepsilon_{irp}n_rA_{pj}B_{ji}\,\mathrm{d}S &= -\int_{\Omega}\left(\varepsilon_{irp}A_{pj}B_{ji}\right),_r\,\mathrm{d}V\\ &= -\int_{\Omega}\left(\varepsilon_{irp}A_{pj}B_{ji,r}+\varepsilon_{irp}A_{pj,r}B_{ji}\right)\,\mathrm{d}V\\ &= \int_{\Omega}\left(A_{pj}\varepsilon_{pri}B_{ji,r}-B_{ji}\varepsilon_{irp}A_{pj,r}\right)\,\mathrm{d}V\end{aligned}$$

Here we have used the property of the alternating tensor, $\varepsilon_{pri}=-\varepsilon_{irp}$, and the fact that its gradient is zero.

B.3 Jump-Average Identity: II

We set out to prove the following identity, with tensor fields $\boldsymbol{A}$ and $\boldsymbol{B}$ and unit normal $\boldsymbol{n}$.

$$[\![\boldsymbol{A}(\boldsymbol{n}\times):\boldsymbol{B}]\!]=[\![\boldsymbol{A}(\boldsymbol{n}\times)]\!]:\langle\boldsymbol{B}\rangle+\langle\boldsymbol{A}\rangle:[\![\boldsymbol{B}(\boldsymbol{n}\times)^{\mathrm{T}}]\!]$$

To accomplish this we will start by expanding the right hand side and working

back to the left hand side.

$$
\begin{aligned}
&[\![\boldsymbol{A}(\boldsymbol{n}\times):\boldsymbol{B}]\!] \\
&= [\![\boldsymbol{A}(\boldsymbol{n}\times)]\!]:\langle\boldsymbol{B}\rangle + \langle\boldsymbol{A}\rangle:[\![\boldsymbol{B}(\boldsymbol{n}\times)^{\mathrm{T}}]\!] \\
&= (\boldsymbol{A}^{+}(\boldsymbol{n}^{+}\times)+\boldsymbol{A}^{-}(\boldsymbol{n}^{-}\times)):\left(\frac{\boldsymbol{B}^{+}+\boldsymbol{B}^{-}}{2}\right)+\left(\frac{\boldsymbol{A}^{+}+\boldsymbol{A}^{-}}{2}\right):(\boldsymbol{B}^{+}(\boldsymbol{n}^{+}\times)^{\mathrm{T}}+\boldsymbol{B}^{-}(\boldsymbol{n}^{-}\times)^{\mathrm{T}}) \\
&= \begin{array}{l}\boldsymbol{A}^{+}(\boldsymbol{n}^{+}):\dfrac{\boldsymbol{B}^{+}}{2}+\boldsymbol{A}^{+}(\boldsymbol{n}^{+}):\dfrac{\boldsymbol{B}^{-}}{2}+\boldsymbol{A}^{-}(\boldsymbol{n}^{-}):\dfrac{\boldsymbol{B}^{+}}{2}+\boldsymbol{A}^{-}(\boldsymbol{n}^{-}):\dfrac{\boldsymbol{B}^{-}}{2}+ \\ \dfrac{\boldsymbol{A}^{+}}{2}:\boldsymbol{B}^{+}(\boldsymbol{n}^{+}\times)^{\mathrm{T}}+\dfrac{\boldsymbol{A}^{+}}{2}:\boldsymbol{B}^{-}(\boldsymbol{n}^{-}\times)^{\mathrm{T}}+\dfrac{\boldsymbol{A}^{-}}{2}:\boldsymbol{B}^{+}(\boldsymbol{n}^{+}\times)^{\mathrm{T}}+\dfrac{\boldsymbol{A}^{-}}{2}:\boldsymbol{B}^{-}(\boldsymbol{n}^{-}\times)^{\mathrm{T}}\end{array} \\
&= \begin{array}{l}\boldsymbol{A}^{+}(\boldsymbol{n}^{+}):\boldsymbol{B}^{+}+\boldsymbol{A}^{-}(\boldsymbol{n}^{-}):\boldsymbol{B}^{-} \\ +\boldsymbol{A}^{+}(\boldsymbol{n}^{+}):\dfrac{\boldsymbol{B}^{-}}{2}-\boldsymbol{A}^{+}(\boldsymbol{n}^{+}):\dfrac{\boldsymbol{B}^{-}}{2}+\boldsymbol{A}^{-}(\boldsymbol{n}^{-}):\dfrac{\boldsymbol{B}^{+}}{2}-\boldsymbol{A}^{-}(\boldsymbol{n}^{-}):\dfrac{\boldsymbol{B}^{+}}{2}+\end{array} \\
&= \boldsymbol{A}^{+}(\boldsymbol{n}^{+}\times):\boldsymbol{B}^{+}+\boldsymbol{A}^{-}(\boldsymbol{n}^{-}\times):\boldsymbol{B}^{-} \\
&= [\![\boldsymbol{A}(\boldsymbol{n}\times):\boldsymbol{B}]\!]
\end{aligned}
$$

Where fact that $\boldsymbol{A}:\boldsymbol{B}(\boldsymbol{n}\times)^{\mathrm{T}}=\boldsymbol{A}(\boldsymbol{n}\times):\boldsymbol{B}$ and also that $(\boldsymbol{n}^{+}\times)=-(\boldsymbol{n}^{-}\times)$ were used extensively. This completes the proof.

B.4 Linearization of the Flow Rule

This section describes the linearization of the flow rule for the DG IP formulation for implementation in a Newton-Raphson iterative scheme. In order to linearize, it is necessary to define the algorithmic approximation of $\dot{\boldsymbol{H}}^{p}$,

$$\dot{\boldsymbol{H}}^{p}=\frac{\boldsymbol{H}^{p}_{n+1,k}-\boldsymbol{H}^{p}_{n}}{\Delta t}, \tag{B.1}$$

where $\boldsymbol{H}^{p}_{n}$ is the previous converged solution at time t_n, and $\boldsymbol{H}^{p}_{n+1,k}$ is the current solution at time t_{n+1} and iteration k. It is then convenient to define a term to simplify the writing of the forms,

$$\Delta\boldsymbol{H}^{p}=\boldsymbol{H}^{p}_{n+1,k}-\boldsymbol{H}^{p}_{n}. \tag{B.2}$$

Next we can state the approximation for the effective distortion rate, (4.22),

$$\widetilde{d^p}_{n+1} = \|\Delta \boldsymbol{H}^p_{n+1,k} - \boldsymbol{H}^p_n\|, \tag{B.3}$$

and recall the expression for the microstress, (5.61).

With these definitions in hand, we want to compute the directional derivative in the direction of an increment in $\boldsymbol{H}^p$, which we will denote as $\delta\boldsymbol{H}^p$. This leads us to the following substitution

$$\boldsymbol{H}^p_{n+1,k} = \boldsymbol{H}^p_{n+1,k} + \epsilon\, \delta\boldsymbol{H}^p, \tag{B.4}$$

for use in the directional derivation defined as

$$\mathrm{D}A = \frac{\mathrm{d}}{\mathrm{d}\epsilon} A\Big|_{\epsilon=0}. \tag{B.5}$$

We can then systematically insert the expressions previously derived for each term in the variational form, and take the directional derivative to obtain the desired linearization. Using the variations of $\boldsymbol{H}^p_{n+1,k}$, as in (B.4), we can define quantities that will need to be differentiated. First the increment in the plastic distortion.

$$\Delta\boldsymbol{H}^p(\epsilon) = \boldsymbol{H}^p_{n+1,k} + \epsilon\delta\boldsymbol{H}^p - \boldsymbol{H}^p_n = \Delta\boldsymbol{H}^p_{n+1,k} + \epsilon\delta\boldsymbol{H}^p \tag{B.6}$$

Then the plastic strain,

$$\boldsymbol{\varepsilon}^p(\epsilon) = \frac{1}{2}\left(\boldsymbol{H}^p_{n+1,k} + \epsilon\delta\boldsymbol{H}^p + (\boldsymbol{H}^p_{n+1,k} + \epsilon\delta\boldsymbol{H}^p)^{\mathrm{T}}\right) = \boldsymbol{\varepsilon}^p_{n+1,k} + \epsilon\,\mathrm{sym}\,\delta\boldsymbol{H}^p, \tag{B.7}$$

followed by the effective distortion rate.

$$\widetilde{d^p}(\epsilon) = \|\Delta\boldsymbol{H}^p(\epsilon)\| = \|\Delta\boldsymbol{H}^p_{n+1,k} + \epsilon\delta\boldsymbol{H}^p\| \tag{B.8}$$

Finally, the microstress, which incorporates both (B.6) and (B.8),

$$\boldsymbol{T}^p(\epsilon) = \frac{\sigma_y}{\widetilde{d^p}(\epsilon)}\Delta\boldsymbol{H}^p(\epsilon), \tag{B.9}$$

and the Cauchy stress. Note that for the Cauchy stress the total strain term has no iterate subscript, due to the fact that the displacement field is held constant during the solution of the flow rule.

$$\boldsymbol{\sigma}(\epsilon) = \mathbb{C} : (\boldsymbol{\nabla}^s \boldsymbol{u}_{n+1} - \boldsymbol{\varepsilon}^p(\epsilon)) = \mathbb{C} : \left(\boldsymbol{\nabla}^s \boldsymbol{u}_{n+1} - (\boldsymbol{\varepsilon}^p_{n+1,k} + \epsilon \,\mathrm{sym}\, \delta \boldsymbol{H}^p)\right) \tag{B.10}$$

It is necessary to employ the directional derivative on the variational form. Starting with (5.48), we can take derivatives of the domain integral, by first moving the scalar derivative inside of the integral.[1]

$$\frac{\mathrm{d}}{\mathrm{d}\epsilon}(\boldsymbol{V}, \boldsymbol{T}^p(\epsilon) - \boldsymbol{\sigma}(\epsilon))_\Omega \Big|_{\epsilon=0} = \left(\boldsymbol{V}, \frac{\mathrm{d}}{\mathrm{d}\epsilon}(\boldsymbol{T}^p(\epsilon)) - \frac{\mathrm{d}}{\mathrm{d}\epsilon}(\boldsymbol{\sigma}(\epsilon))\right)_\Omega \Big|_{\epsilon=0} \tag{B.11}$$

It follows that we need to evaluate the derivative of the two stress variation terms. Consider the directional derivative of the microstress,

$$\frac{\mathrm{d}}{\mathrm{d}\epsilon}(\boldsymbol{T}^p(\epsilon))\Big|_{\epsilon=0} = \frac{\mathrm{d}}{\mathrm{d}\epsilon}\left(\frac{\sigma_y}{\widetilde{d}^p(\epsilon)}(\Delta \boldsymbol{H}^p(\epsilon))\right)\Big|_{\epsilon=0}. \tag{B.12}$$

Using the product rule of differentiation, we can separate (B.12) in two terms.

$$\begin{aligned}\frac{\mathrm{d}}{\mathrm{d}\epsilon}(\boldsymbol{T}^p(\epsilon))\Big|_{\epsilon=0} =& \sigma_y \left(\frac{\mathrm{d}}{\mathrm{d}\epsilon}(\widetilde{d}^p(\epsilon))^{-1}\right)\Big|_{\epsilon=0} \Delta \boldsymbol{H}^p_{n+1,k} + \\ & \frac{\sigma_y}{\widetilde{d}^p{}_{n+1,k}} \left(\frac{\mathrm{d}}{\mathrm{d}\epsilon}\Delta \boldsymbol{H}^p(\epsilon)\right)\Big|_{\epsilon=0}\end{aligned} \tag{B.13}$$

To arrive at the last result we have used the fact that $\widetilde{d}^p(\epsilon)\Big|_{\epsilon=0} = \widetilde{d}^p{}_{n+1,k}$ and $\Delta \boldsymbol{H}^p(\epsilon)\Big|_{\epsilon=0} = \Delta \boldsymbol{H}^p_{n+1,k}$. Repeated use of the chain rule facilitates the evaluation of the first term on the right hand side of (B.13).

$$\sigma_y \left(\frac{\mathrm{d}}{\mathrm{d}\epsilon}(\widetilde{d}^p(\epsilon))^{-1}\right)\Big|_{\epsilon=0} \Delta \boldsymbol{H}^p_{n+1,k} = -\frac{\sigma_y}{\widetilde{d}^p{}^3_{n+1,k}} (\Delta \boldsymbol{H}^p_{n+1,k} \otimes \Delta \boldsymbol{H}^p_{n+1,k}) : \delta \boldsymbol{H}^p \tag{B.14}$$

Straight forward evaluation of the second term on the right hand side of (B.13) yields

$$\frac{\sigma_y}{\widetilde{d}^p{}_{n+1,k}} \left(\frac{\mathrm{d}}{\mathrm{d}\epsilon}\Delta \boldsymbol{H}^p(\epsilon)\right)\Big|_{\epsilon=0} = \frac{\sigma_y}{\widetilde{d}^p{}_{n+1,k}} \delta \boldsymbol{H}^p. \tag{B.15}$$

[1] We can do this because the variation of a definite integral is equal to the definite integral of the variation, see Lanczos (1970).

Next consider the Cauchy stress term, from (B.11), expanded out using (B.10).

$$\frac{\mathrm{d}}{\mathrm{d}\epsilon}(\boldsymbol{\sigma}(\epsilon))\Big|_{\epsilon=0} = -\mathbb{C} : (\operatorname{sym} \delta \boldsymbol{H}^p) \tag{B.16}$$

Inserting the expression in (B.14), (B.15), and (B.16) into the appropriate positions in (B.11), we have the complete linearization of the domain term in the flow rule.

$$\left(\boldsymbol{V}, \left[\frac{\sigma_y}{\widetilde{dp}_{n+1,k}} \mathbf{1} \otimes \mathbf{1} - \frac{\sigma_y}{\widetilde{dp}^3_{n+1,k}} \Delta \boldsymbol{H}^p_{n+1,k} \otimes \Delta \boldsymbol{H}^p_{n+1,k} + \mathbb{C} \right] : \delta \boldsymbol{H}^p \right)_\Omega \tag{B.17}$$

The remaining term in the DG IP formulation for the flow rule is linear in $\boldsymbol{H}^p$, and therefore can simply be stated.

$$\frac{\alpha k}{h} \left([\![\boldsymbol{V}(\boldsymbol{n}\times)]\!], [\![\delta \boldsymbol{H}^p(\boldsymbol{n}\times)]\!] \right)_{\widetilde{\Gamma}} \tag{B.18}$$

The combination of (B.17) and (B.18) yields the linearization of the flow rule and thus the tangent to be used in the iterative solution scheme.

APPENDIX C

FEniCS

The `FEniCS` project, Dupont et al. (2003), Logg (2007) (`www.fenics.org`), is an open source suite of codes with the goal of automating the solution of partial differential equations. To achieve this goal, the project consists of a number of component codes that handle a different step in the solution process. The core components of `FEniCS` consist of the following: 1) the variational form of the PDE written in a form language, 2) tabulation of finite element basis functions and quadrature rules for integration, 3) translation from the variational form into a common interface for finite element assembly, 4) a solver interface between the code generated from the variational form and the linear algebra library. Of particular interest to this dissertation were the expression of the PDEs describing equilibrium and the flow rule, and the solver interface.

The `FFC` (Kirby and Logg (2006), Kirby and Logg (2007), Ølgaard et al. (2008)) component is used to describe the variational equations in a form language and translate those into `C++` code. This python based code essentially reads in a variational form written in a form language, including specification of basis functions and element types, and translates it into a set of finite element specific methods. The ability of `FFC` to automatically generate code for the DG operators, jump and average, that

arise in the DG variational statement for the flow rule is a pertinent feature related to the subject of this dissertation. For the implementation presented in Section 5.5, an example of the flow rule written in the form language of `FFC` can be seen below.

$$\texttt{dot}(\texttt{V}, \texttt{Tp} - \texttt{s}) * \texttt{dx}+$$

$$\texttt{alpha}('+') * \texttt{k}('+')/\texttt{aveh}('+') * \texttt{dot}(\texttt{mult}(\texttt{jump}(\texttt{Hp}), \texttt{skwM}(\texttt{n}('+'))),$$

$$\texttt{mult}(\texttt{jump}(\texttt{V}), \texttt{skwM}(\texttt{n}('+')))) * \texttt{dS}$$

Here, for an example instance of the form language, the `*dx` operator indicates integration over the domain, and `*dS` indicates integration over the interior domain boundaries, (the analog of $\widetilde{\Gamma}$).

After the code generation of the variational forms, the Newton-Raphson solver algorithm is written in another core `FEniCS` component named `DOLFIN`, Logg and Wells (2009). `DOLFIN` includes support for meshes, i/o, interfaces to linear algebra libraries, and finite element assembly algorithms based on the code generated by `FFC`. It also includes a class for solving non-linear PDEs. To use this class, code is generated for the residual, or the linear form of the PDE. Similarly code is generated for the linearized tangent, or the bilinear form of the PDE, which is used to assemble the stiffness matrix. Then the stiffness matrix and residual vector are repeated called during the solution process.

BIBLIOGRAPHY

BIBLIOGRAPHY

Aifantis, E., 1987. The Physics of Plastic Deformation. International Journal of Plasticity 3 (3), 211–247. 4, 47, 75

Arnold, D., Brezzi, F., Cockburn, B., Marini, L., 2002. Unified Analysis of Discontinuous Galerkin Methods for Elliptic Problems. SIAM JOURNAL ON NUMERICAL ANALYSIS 39 (5), 1749–1779. 8, 67

Asaro, R., 1983. Crystal plasticity. Journal of applied mechanics 50 (4 B), 921–934. 57

Bassi, F., Rebay, S., 1997. A High-Order Accurate Discontinuous Finite Element Method for the Numerical Solution of the Compressible Navier-Stokes Equations. J. Comput. Phys. 131 (2), 267–279. 8, 67, 72

Bazant, Z., Pijaudier-Cabot, G., 1988. Nonlocal continuum damage, localization instability and convergence. Journal of Applied Mechanics 55 (2), 287–293. 5

Bazant, Z. P., Belytschko, T. B., Chang, T. P., 1984. Continuum Theory for Strain Softening. Journal of Engineering Mechanics 110, 1666–1691. 5, 47

Brezzi, F., 1990. A discourse on the stability conditions for mixed finite element formulations. Comp. Methods in Applied Mech. Engrg. 82 (1-3), 27–57. 7

Brezzi, F., Manzini, G., Marini, D., Pietra, P., Russo, A., 2000. Discontinuous Galerkin approximations for elliptic problems. Numerical Methods for Partial Differential Equations 16 (4), 365–378. 72, 73

Cermelli, P., Gurtin, M., 2001. On the characterization of geometrically necessary dislocations in finite plasticity. Journal of Mechanics and Physics of Solids 49 (7), 1539–1568. 5, 57

Cockburn, B., Shu, C., 1989. TVB Runge-Kutta local projection discontinuous Galerkin finite element method for conservation laws II: general framework. Mathematics of Computation , 411–435. 67

Coleman, B., Hodgdon, M., 1985. On shear bands in ductile materials. Archive for Rational Mechanics and Analysis 90 (3), 219–247. 3

Djoko, J., Ebobisse, F., McBride, A., Reddy, B., 2007a. A discontinuous galerkin formulation for classical and gradient plasticity - part 1: Formulation and analysis. Comp. Methods in Applied Mech. Engrg. 196, 3881–3897. 8

Djoko, J., Ebobisse, F., McBride, A., Reddy, B., 2007b. A discontinuous galerkin formulation for classical and gradient plasticity - part 2: Algorithms and numerical analysis. Comp. Methods in Applied Mech. Engrg. 197, 1–21. 8

Dupont, T., Hoffman, J., Johnson, C., Kirby, R. C., Larson, M. G., Logg, A., Scott, L. R., 2003. The FEniCS project. Tech. Rep. 2003–21, Chalmers Finite Element Center Preprint Series. 121

Engel, G., Garikipati, K., Hughes, T. J. R., Larson, M. G., Mazzei, L., Taylor, R. L., 2002. Continuous/Discontinuous Finite Element Approximations of Fourth-order Elliptic Problems in Structural and Continuum Mechanics with Applications to Thin Beams and Plates, and Strain Gradient Elasticity. Comp. Methods in Applied Mech. Engrg. 191 (34), 3669–3750. 8, 75

Fleck, N., Hutchinson, J., 2001. A reformulation of strain gradient plasticity. Journal of the Mechanics and Physics of Solids 49 (10), 2245–2271. 47

Fleck, N. A., Hutchinson, J. W., 1993. A Phenomenological Theory for Strain Gradient Effects in Plasticity. Journal of Mechanics and Physics of Solids 12, 1825–1857. 4, 6, 99

Fleck, N. A., Muller, G. M., Ashby, M. F., Hutchinson, J. W., 1994. Strain Gradient Plasticity: Theory and Experiment. Acta Metallurgica et Materialia 42, 475–487. 4

Gao, H., Huang, Y., Nix, W. D., 1999. Mechanism-based Strain Gradient Plasticity–I. Theory. Journal of Mechanics and Physics of Solids 47, 789–828. 5

Garikipati, K., Hughes, T., 1998. A study of strain localization in a multiple scale framework - the one-dimensional problem. Comp. Methods in Applied Mech. Engrg. 159 (3-4), 193–222. 46

Garikipati, K., Hughes, T., 2000. A variational multiscale approach to strain localization-formulation for multidimensional problems. Comp. Methods in Applied Mech. Engrg. 188 (1–3), 39–60. 47

Gurtin, M., 2003. An Introduction to Continuum Mechanics. Academic Press. 12, 102, 109

Gurtin, M., 2004. A gradient theory of small-deformation isotropic plasticity that accounts for the burgers vector and for dissipation due to plastic spin. Journal of Mechanics and Physics of Solids 52, 2545–2568. 5, 57, 60

Gurtin, M., 2005. A theory of strain-gradient plasticity for isotropic, plastically irrotational materials. part i: Small deformations. Journal of Mechanics and Physics of Solids 53, 1624–1649. 5

Hill, R., 1950. The Mathematical Theory of Plasticity. Oxford University Press. 2

Holzapfel, G., 2000. Nonlinear Solid Mechanics. John Wiley & Sons, Ltd. 12, 102

Huang, Y., Gao, H., Nix, W., Hutchinson, J., 2000. Mechanism-based strain gradient plasticity-II. Analysis. Journal of Mechanics and Physics of Solids 48 (1), 99–128. 5

Hughes, T., 1980. Generalization of selective integration procedures to anisotropic and nonlinear media. Int. J. Numer. Methods Engrg. 15, 1413–1418. 29

Hughes, T. J. R., 1987. The Finite Element Method. Prentice-Hall, Englewood-Cliffs, N. J. 2, 22, 25

Kachanov, L. M., 1971. Foundations of the Theory of Plasticity. North Holland Publishing Co. 2

Key, S. W., Krieg, R. D., 1982. On the numerical implementation of inelastic time dependent and time independent, finite strain constitutive equations in structural mechanics. Comp. Methods in Applied Mech. Engrg. 33 (1-3), 439 – 452. 3

Kirby, R. C., Logg, A., 2006. A compiler for variational forms. ACM Transactions on Mathematical Software 32 (3), 417–444. 121

Kirby, R. C., Logg, A., 2007. Efficient compilation of a class of variational forms. ACM Transactions on Mathematical Software 33 (3). 121

Krieg, R., Key, S., 1976. Implementation of a time independent plasticity theory into structural computer programs. Constitutive equations in viscoplasticity: Computational and engineering aspects , 125–137. 3

Kroner, E., Teodosiu, C., 1972. Lattice defect approach to plasticity and viscoplasticity. In: Sawczuk, A. (Ed.), Problems of Plasticity. Noordhoff. 57

Lanczos, C., 1970. The Variational Principles of Mechanics, 4th Edition. Dover Publications Inc., New York. 119

Lee, E. H., 1969. Elastic-Plastic Deformation at Finite Strains. J. Applied Mechanics 36, 1–6. 57

Lewandowski, J., Greer, A., 2005. Temperature rise at shear bands in metallic glasses. Nature Materials 5 (1), 15–18. 43

Logg, A., 2007. Automating the finite element method. Arch. Comput. Methods Eng. 14 (2), 93–138. 121

Logg, A., Wells, G. N., 2009. DOLFIN: Automated finite element computing. Submitted .
URL http://www.fenics.org/pub/documents/dolfin/papers/dolfin-2009.pdf 122

Lubliner, J., 1990. Plasticity Theory. Macmillan Publishing Co. 2

Ma, Q., Clarke, D., 1995. Size dependent hardness of silver single crystals. Journal of Materials Research 10 (4), 853–863. 6

Malvern, L. E., 1969. Introduction to the Mechanics of a Continuous Medium. Prentice Hall. 12, 102

Marsden, J. E., Hughes, T. J. R., 1994. Mathematical Foundations of Elasticity. Dover, New York. 14

McBride, A. T., 2008. Formulation, analysis and solution algorithms for a model of gradient plasticity within a discontinuous Galerkin framework. Ph.D. thesis, University of Cape Town. 8, 76

Meyers, M., Xu, Y., Xue, Q., Perez-Prado, M., McNelley, T., 2003. Microstructural evolution in adiabatic shear localization in stainless steel. Acta Materialia 51 (5), 1307–1325. 44

Molari, L., Wells, G. N., Garikipati, K., Ubertini, F., 2006. A discontinuous Galerkin method for strain gradient-dependent damage: Study of interpolations, convergence and two dimensional problems. Comp. Methods in Applied Mech. Engrg. 195, 1480–1498. 8

Muhlhaus, H., Aifantis, E., 1991. A variational principle for gradient plasticity. Int. J. Solids and Structures 28 (7), 845–857. 4

Nagtegaal, J., Parks, D., Rice, J., 1974. On numerical accurate finite element solutions in the fully plastic range. Comp. Methods in Applied Mech. Engrg. 4, 153–177. 29

Nitsche, J., 1971. Über ein Variationsprinzip zur Lösung von Dirichlet-Problemen bei Verwendung von Teilräumen, die keinen Randbedingungen unterworfen sind [On a variational principle for solving Dirichlet problems less boundary conditions using subspaces]. Abh. Math. Sem. Univ. Hamburg 36, 9–15. 7

Nix, W. D., Gao, H., 1998. Indentation Size Effects in Crystalline Materials: A Law for Strain Gradient Plasticity. Journal of Mechanics and Physics of Solids 46, 411–425. 5

Noels, L., Radovitzky, R., 2008. An explicit discontinuous galerkin method for non-linear solid dynamics: Formulation, parallel implementation and scalability properties. Int. J. Numer. Methods Engrg. 74, 1393–1420. 8

Ølgaard, K. B., Logg, A., Wells, G. N., 2008. Automated code generation for discontinuous galerkin methods. SIAM Journal on Scientific Computing 31 (2), 849–864.
URL http://dx.doi.org/10.1137/070710032 121

Ortiz, M., Simo, J., 1986. An analysis of a new class of integration algorithms for elastoplastic constitutive relations. Int. J. Numer. Methods Engrg. 23 (3). 3

Reed, W., Hill, T., 1973. Triangular mesh methods for the neutron transport equation. In: National topical meeting on mathematical models and computational techniques for analysis of nuclear systems. Vol. 8. 7, 67

Simo, J. C., 1988a. A Framework for Finite Strain Elastoplasticity based on Maximum Plastic Dissipation and the Multiplicative Decomposition: Part I. Continuum Formulation. Comp. Methods in Applied Mech. Engrg. 66, 199–219. 3

Simo, J. C., 1988b. A Framework for Finite Strain Elastoplasticity based on Maximum Plastic Dissipation and the Multiplicative Decomposition: Part II. Computational Aspects. Comp. Methods in Applied Mech. Engrg. 68, 1–31. 3

Simo, J. C., 1992. Algorithms for Multiplicative Plasticity that Preserve the form of the Return Mappings of the Infinitesimal Theory. Comp. Methods in Applied Mech. Engrg. 99, 41–104. 3

Simo, J. C., 1998. Numerical Analysis of Simulation of Plasticity. In: Ciarlet, P. G., Lions, J. L. (Eds.), Handbook of Numerical Analysis, Vol. VI. Elsevier, pp. 183–499. 3

Simo, J. C., Hughes, T. J. R., 1998. Computational Inelasticity. Springer Verlag. 3, 36, 37

Simo, J. C., Taylor, R. L., Pister, K. S., 1985. Variational and projection methods for the volume constraint in finite deformation elasto-plasticity. Comp. Methods in Applied Mech. Engrg. 51, 177–208. 29

Stölken, J., Evans, A., 1998. A microbend test method for measuring the plasticity length scale. Acta Materialia 46 (14), 5109–5115. 6

Taylor, G. I., 1938. Analysis of Plastic Strain in a Cubic Crystal. In: Lessels, J. M. (Ed.), Stephen Timoshenko. 60th Anniversary Volume. Macmillan, New York. 51

Truesdell, C. A., Noll, W., 1965. The Non-linear Field Theories (Handbuch der Physik, band III). Springer, Berlin. 12, 102

Wells, G., Dung, N., 2007. A c^0 discontinuous galerkin formulation for kirchhoff plates. Comp. Methods in Applied Mech. Engrg. 196, 3370–3380. 8, 75

Wells, G., Kuhl, E., Garikipati, K., 2006. A discontinuous galerkin method for the cahn-hilliard equation. J. Comput. Phys. 218, 860–877. 8, 74

Wells, G. N., Garikipati, K., Molari, L., 2004. A discontinuous Galerkin formulation for a strain gradient-dependent damage model. Comp. Methods in Applied Mech. Engrg. 193, 3633–3645. 8, 75

Wilkins, M., 1963. Calculation of elastic-plastic flow. UCRL–7322 (Rev. 1), California Univ., Livermore. Lawrence Radiation Lab. 3, 33

Zienkiewicz, O. C., Taylor, R. L., 1989. The Finite Element Method: Vol I and II. McGraw-Hill, London, New York. 2